

1127

CONCEPTUAL DESIGN AND NEUTRONICS ANALYSES OF  
A FUSION REACTOR BLANKET SIMULATION FACILITY

A Thesis  
Submitted to the Faculty

of

Purdue University

by

Denis Eugene Beller

In Partial Fulfillment of the  
Requirements for the Degree

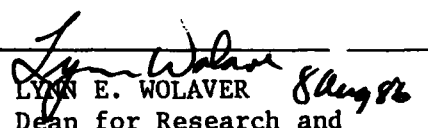
of

Doctor of Philosophy

May 1986

1

SECURITY CLASSIFICATION OF THIS PAGE (When Data Entered)

REPORT DOCUMENTATION PAGE		READ INSTRUCTIONS BEFORE COMPLETING FORM
1. REPORT NUMBER AFIT/CI/NR 86- 114D	2. GOVT ACCESSION NO.	3. RECIPIENT'S CATALOG NUMBER
4. TITLE (and Subtitle) Conceptual Design and Neutronics Analyses of a Fusion Reactor Blanket Simulation Facility		5. TYPE OF REPORT & PERIOD COVERED <b>THESIS/DISSERTATION</b>
		6. PERFORMING ORG. REPORT NUMBER
7. AUTHOR(s) Denis Eugene Beller		8. CONTRACT OR GRANT NUMBER(s)
9. PERFORMING ORGANIZATION NAME AND ADDRESS AFIT STUDENT AT: Purdue University		10. PROGRAM ELEMENT, PROJECT, TASK AREA & WORK UNIT NUMBERS
11. CONTROLLING OFFICE NAME AND ADDRESS AFIT/NR WPAFB OH 45433-6583		12. REPORT DATE 1986
		13. NUMBER OF PAGES 125
14. MONITORING AGENCY NAME & ADDRESS (if different from Controlling Office)		15. SECURITY CLASS. (of this report) UNCLAS
		15a. DECLASSIFICATION/DOWNGRADING SCHEDULE
16. DISTRIBUTION STATEMENT (of this Report) APPROVED FOR PUBLIC RELEASE; DISTRIBUTION UNLIMITED		
17. DISTRIBUTION STATEMENT (of the abstract entered in Block 20, if different from Report)  <b>B</b>		
18. SUPPLEMENTARY NOTES APPROVED FOR PUBLIC RELEASE: IAW AFR 190-1		  LYNN E. WOLAVER Dean for Research and Professional Development AFIT/NR
19. KEY WORDS (Continue on reverse side if necessary and identify by block number)		
20. ABSTRACT (Continue on reverse side if necessary and identify by block number)  ATTACHED.  <b>DTIC FILE COPY</b>		

## ABSTRACT

Beller, Denis Eugene, Capt, USAF.

Conceptual Design and Neutronics Analyses of a Fusion Reactor Blanket Simulation Facility.

183 pages, Ph.D., Purdue University, 1986. Major Professor: K.O. Ott.

A new conceptual design of a fusion reactor blanket simulation facility has been developed. This design follows the principles that have been successfully employed in the Purdue Fast Breeder Blanket Facility (FBBF), because experiments conducted in it have resulted in the discovery of deficiencies in neutronics prediction methods. With this design, discrepancies between calculation and experimental data can be fully attributed to calculation methods because design deficiencies which could affect results are insignificant. Inelastic scattering cross sections are identified as a major source of these discrepancies. The conceptual design of this FBBF-analog, the fusion reactor blanket facility (FRBF), is presented. Essential features are a cylindrical geometry and a distributed, cosine-shaped line source

of 14 MeV neutrons. This source can be created by sweeping a deuteron beam over an elongated titanium-tritide target. To demonstrate that the design of the FRBF will not contribute significant deviations in experimental results, neutronics analyses were performed: results of comparisons of 2-dimensional to 1-dimensional predictions are reported for two blanket compositions. Expected deviations from 1-D predictions which are due to source anisotropy and blanket asymmetry are minimal. Then 1-D calculations can be performed in fine detail to produce course-group constants for 2-D predictions. When these 2-D neutronics studies include the asymmetry and anisotropy, differences between prediction and experimental results caused by the design will be less than 1%. Thus, the design of the FRBF allows simple and straightforward interpretation of experimental results, without a need for course 3-D calculations.

FILE  
COPY  
INSPECT  
1

Accession For	
NTIS	<input checked="" type="checkbox"/>
DTIC	<input type="checkbox"/>
UNCLASSIFIED	<input type="checkbox"/>
JUL	
By	
E	
A	
Dist.	
A-1	

For my wife, Judy Ann, and for my sons, David and Timothy, who continue to support my every ambition, and who sacrificed as much as I did for this education.

## ACKNOWLEDGEMENTS

The author offers a sincere thank you to Professor Ott for his guidance and for what the author feels is the most valuable lesson learned at Purdue: to examine the validity of all work, especially one's own. The author also thanks the other members of his committee--Professors Clikeman, Choi, and Landolt--who each contributed in his own way. Much thanks also to Dr. Dilber for his assistance with cross section processing; to R. Rhoades and R. Roussin at ORNL for their assistance with the neutron transport code and group constants; and to R.A. Manning at CDC-Knoxville for the programming assistance she provided.

Finally, thank you to the citizens of this nation for providing the opportunity to obtain ever higher education; the author hopes his service justifies their investment.

## TABLE OF CONTENTS

	Page
LIST OF TABLES .....	vi
LIST OF FIGURES .....	vii
LIST OF ABBREVIATIONS .....	ix
ABSTRACT .....	x
I. INTRODUCTION .....	1
II. REVIEW OF FUSION REACTOR BLANKET EXPERIMENTS .....	10
III. OVERVIEW OF THE FBBF .....	20
III.1. Facility Description .....	20
III.2. Results of FBBF Experiments .....	22
IV. CONCEPTUAL DESIGN OF A FUSION REACTOR BLANKET FACILITY .....	24
IV.1. Objectives .....	24
IV.2. General Considerations for the Design .....	24
IV.3. Desired Features of a FRB Simulation Facility ..	26
IV.4. Scope of Research .....	27
IV.5. Blanket Design .....	27
IV.6. Neutron Sources .....	29
IV.7. Neutronics Analyses .....	45
V. NEUTRONICS ANALYSES OF TWO FRBF MODELS .....	48
V.1. DORT, a Transport Code .....	49
V.2. The Anisotropic Neutron Source .....	50
V.3. Cross Sections .....	54
V.4. Computational Models .....	61
VI. NEUTRONICS RESULTS .....	66
VI.1. Results of 2-D, R-Z Analyses .....	67
VI.2. Comparison of 1-D and 2-D R- $\theta$ Results .....	76
VI.3. Central Source vs Plasma Source Results .....	84

	Page
VII. ADVANTAGES OF THE FRBF .....	93
VII.1. Flexibility for Multiple Experiments .....	94
VII.2. Operational and Personnel Safety in the FRBF .	96
VII.3. Measurement Techniques and Accuracy .....	99
VII.4. Other Issues .....	102
VIII. CONCLUSION .....	103
VIII.1. Summary .....	104
VIII.2. Recommendations .....	105
LIST OF REFERENCES .....	108
APPENDICES	
Appendix A. Tables .....	112
Appendix B. Angle-energy Correlation Code .....	118
VITA .....	125

## LIST OF TABLES

Table	Page
II.1. A Summary of Tritium Breeding Experiments .....	11
II.2. Computational Methods in Tritium Breeding Experiments .....	12
IV.1. Angular Distribution of d-T Neutrons .....	35
IV.2. Angular Distribution of d- <sup>6</sup> Li Neutrons .....	37
V.1. Multi-group Angular Distribution of d-T Neutrons ..	52
V.2. Scattering Cross Sections for Fusion Reactor Materials .....	57
Appendix	
Table	Page
A.1. Material Compositions for Blanket HeC .....	113
A.2. Material Compositions for Blanket LLC .....	114
A.3. Fifty-group Structure (ORNL) .....	115
A.4. Forty-one-group Structure (Purdue) .....	117

## LIST OF FIGURES

Figure	Page
IV.1.A. Cross Section of the FRBF .....	30
IV.1.B. Radial Geometry of the FRBF .....	31
IV.2.A. 1-Dimensional Model of Blanket HeC .....	32
IV.2.B. 1-Dimensional Model of Blanket LLC .....	33
IV.3. Neutron Flux Due to Three d-T Sources .....	40
IV.4. Neutron Flux Due to Five d-T Sources .....	40
IV.5. Sketch of the Fusion Reactor Blanket Facility ....	44
V.1. Yield of d-T Neutron vs d-beam Current .....	53
V.2. Inelastic Scattering Cross Sections of Copper and Lead from 14 MeV Neutrons .....	58
V.3. Energy Loss in Blanket HeC Due to Scattering Reactions .....	60
V.4.A. Geometry of Blanket HeC, R- $\theta$ .....	63
V.4.B. Geometry of Blanket LLC, R- $\theta$ .....	64
VI.1.A. Axial Group-flux Profiles in Blanket HeC .....	68
VI.1.B. Axial Group-flux Profiles in Blanket LLC .....	69
VI.2.A. Neutron Spectra in Blanket HeC, R-Z .....	71
VI.2.B. Neutron Spectra in Blanket LLC, R-Z .....	72
VI.3.A. Radial Group-flux Profiles in Blanket HeC, R-Z .	73
VI.3.B. Radial Group-flux Profiles in Blanket LLC, R-Z .	74
VI.4. Radial Tritium Production at the Mid-plane, R-Z ..	75

Figure	Page
VI.5.A. Azimuthal Group-Flux Ratios in Blanket HeC, 1-D vs 2-D R- $\theta$ .....	77
VI.5.B. Azimuthal Group-Flux Ratios in Blanket LLC, 1-D vs 2-D R- $\theta$ .....	78
VI.6.A. Radial Group-flux Profiles in Blanket HeC, 1-D vs 2-D R- $\theta$ .....	79
VI.6.B. Radial Group-flux Profiles in Blanket LLC, 1-D vs 2-D R- $\theta$ .....	80
VI.7.A. Radial Tritium Production in Blanket HeC, 1-D vs 2-D R- $\theta$ .....	82
VI.7.B. Radial Tritium Production in Blanket LLC, 1-D vs 2-D R- $\theta$ .....	83
VI.8.A. Central vs Plasma Source: Neutron Spectra in Blanket HeC .....	85
VI.8.B. Central vs Plasma Source: Neutron Spectra in Blanket LLC .....	86
VI.9.A. Central vs Plasma Source: Flux Differences in Blanket HeC .....	87
VI.9.B. Central vs Plasma Source: Flux Differences in Blanket LLC .....	88
VI.10.A. Central vs Plasma Source: Radial Tritium Production in Blanket HeC .....	90
VI.10.B. Central vs Plasma Source: Radial Tritium Production in Blanket LLC .....	91

## LIST OF ABBREVIATIONS

ANL	Argonne National Laboratory
BNL	Brookhaven National Laboratory
C/E	Calculation to Experiment Ratio
DT	Deuterium/Tritium Gas or Plasma
FBBF	Purdue Fast Breeder Blanket Facility
FRBF	The Fusion Reactor Blanket Facility
JAERI	Japan Atomic Energy Research Institute
LBM	Lithium Blanket Module
LANL	Los Alamos National Laboratory (LASL)
LLNL	Lawrence Livermore National Laboratory (LLL)
ORNL	Oak Ridge National Laboratory
PPPL	Princeton Plasma Physics Laboratory
RSIC	Reactor Shielding Information Center (at ORNL)
SS	Stainless Steel
SSTD	Solid State Track Detector
TFTR	Princeton Tokamak Fusion Test Reactor
TLD	Thermoluminescent Dosimeter
${}^n\text{Li}$	Natural Lithium
$T_6$	Production Rate of Tritium from ${}^6\text{Li}(d,T)\alpha$
$T_7$	Production Rate of Tritium from ${}^7\text{Li}(d,T)\alpha$
$T_n$	Production Rate of Tritium from ${}^n\text{Li}$
$T_T$	Total Production Rate of Tritium

## ABSTRACT

Beller, Denis Eugene. Ph.D., Purdue University, May 1988. Conceptual Design and Neutronics Analyses of a Fusion Reactor Blanket Simulation Facility. Major Professor: K.O. Ott.

A new conceptual design of a fusion reactor blanket simulation facility has been developed. This design follows the principles that have been successfully employed in the Purdue Fast Breeder Blanket Facility (FBBF), because experiments conducted in it have resulted in the discovery of deficiencies in neutronics prediction methods. With this design, discrepancies between calculation and experimental data can be fully attributed to calculation methods because design deficiencies which could affect results are insignificant. Inelastic scattering cross sections are identified as a major source of these discrepancies. The conceptual design of this FBBF-analog, the fusion reactor blanket facility (FRBF), is presented. Essential features are a cylindrical geometry and a distributed, cosine-shaped line source of 14 MeV neutrons. This source can be created by sweeping a deuteron beam over an elongated titanium-tritide target. To demonstrate that the design of the FRBF will not contribute significant deviations in experimental results, neutronics analyses were performed: results of comparisons of 2-dimensional to 1-dimensional predictions

are reported for two blanket compositions. Expected deviations from 1-D predictions which are due to source anisotropy and blanket asymmetry are minimal. Then 1-D calculations can be performed in fine detail to produce course-group constants for 2-D predictions. When these 2-D neutronics studies include the asymmetry and anisotropy, differences between prediction and experimental results caused by the design will be less than 1%. Thus, the design of the FRBF allows simple and straightforward interpretation of experimental results, without a need for course 3-D calculations.

## I. INTRODUCTION

Past work in fusion reactor blanket neutronics indicates a strong need for an inexpensive, flexible, properly designed experimental facility. This is pointed out by the FINESSE study<sup>1</sup>, a recent report on future requirements and plans for fusion reactor blanket and materials testing. It expresses the importance of accurately predicting, within at least 5%, neutron transport and tritium breeding rates. The reasons why accurate prediction of the transport of neutrons through the first wall, blanket, and shielding is of such great importance in future designs of fusion reactors is because in DT-fueled reactors 1) the neutrons carry 80 percent of the reaction energy away from the plasma, 2) they cause damage to and activation of reactor materials, and 3) they must provide new fuel through breeding reactions. A major source of error in these predictions will be from current uncertainties in inelastic scattering matrices in cross section libraries. Approximately 75-90% of the 14 MeV of DT-neutron energy is deposited as a result of inelastic scattering reactions. (see section V.3, Cross Sections) Thus, errors in inelastic data can cause significant errors in predicting both the location and amount of neutron-

induced energy (gamma and other products) deposition in proposed fusion reactor designs.

However, the few experiments which were done to compare to transport predictions in simulated fusion reactor blankets have not produced data which validates the neutronics methods or the data libraries. The facilities which had a "clean" design were inflexible; thus they could not produce multiple experiments to compare to a given neutronics method. More experiments would require construction of a new system, at great expense. Generally, the results of these individual experiments deviated from predictions by 20 to 40%.<sup>2-5</sup> The results of experiments done in flexible facilities deviated up to 50% from calculations. In only a few, one-of-a-kind experiments were results produced which compared favorably (about 10% deviations) to one of a number of prediction methods.

Transport codes are generally used in fusion reactor design studies to evaluate tritium breeding, heat deposition, and neutron leakage to field magnets; and design decisions are based upon these evaluations. Confidence in the results of these studies can only be achieved by improving the transport codes and group constants used to predict neutron behavior and by experimental validation of these codes. Generally, determination of the causes of errors in past transport predictions has been very difficult because of the system geometries and the neutron sources

used in the experiments. These "deficiencies" of the set-ups clearly affect the validation of codes and high-energy cross sections. Eliminating the interpretation problems due to deficiencies in the design of the fusion reactor blanket simulation facilities is the subject of this research.

Qualitatively, the effects of the deficiencies in these experimental set-ups should be considerably less than the acceptable deviations between eventual experimental results and theoretical predictions. This is a guideline which can be used during evaluation of conceptual designs of these facilities; however, this guideline has not been met for past fusion reactor blanket neutronics evaluations.

Fusion reactor blanket experiments are conducted to determine the space and energy dependence of neutron flux and reaction rates. Because of the computing time and expense required for a theoretical three-dimensional (3-D) description of flux spectra, attempts are made to reduce the space dependencies (or to simplify their description in one or two dimensions). If an appropriate geometry and incident neutron flux is used, the space dependency can essentially be reduced to one dimension. A slightly less advantageous, but still very useful technique, is to use a geometry and a source that allow separation of the flux function into a spatial dependency in one dimension and a space/energy dependency in the other dimension. Then the lateral transport can be approximated analytically while the space

and energy variation can be treated in one dimension using sophisticated codes. While not exact, this separability is a very good approximation, and the resulting differences are less than the deviations being investigated. However, previous fusion reactor blanket experiments have not provided the geometry and source necessary to permit these simplified computations without introducing corrections which were greater than the effects being investigated.

Past simulated fusion reactor blanket experiments have been designed with parallelepiped (slab), spherical, or cylindrical geometries.<sup>6-26</sup> These set-ups have been deficient in various ways:

- 1) An infinite slab with a plane-wave neutron source is the ideal geometry for 1-D neutronics analysis. However, the thick parallelepiped slabs used in experiments do not approximate infinite slabs, and the neutron flux from a small target is not a plane-wave source (nor does it impose the proper boundary condition for a non-infinite slab). Lateral leakage dominates the transport in these slabs; it is accounted for by including a buckling term in the neutronics codes or by approximating the lateral transport in radial geometry. Errors in buckling corrections can overshadow other errors in the neutronics calculations, and a square slab cannot be modelled in radial geometry.

- 2) A system with spherical geometry and a centered isotropic point source can also be modelled in 1-D geometry.

However, a DT-neutron generator which produces ~14 MeV neutrons was used for these experiments. These neutron sources are anisotropic in energy and yield, which eliminates the advantage of the spherical geometry (although the system does retain azimuthal symmetry). Two other major disadvantages of this geometry are its total lack of flexibility to modify the blanket composition and the requirement to bore asymmetric holes for experiments and measurements inside the blanket.

3) Another geometry which allows 1-D analysis is an infinite cylinder with an axial line source. Alternately, a finite-length cylinder with a cosine-shaped source distribution as a boundary condition in the center axis can be analyzed with 1-D calculations in good approximation. However, the past experiments which used cylindrical geometry used anisotropic point sources at the center of the mid-plane. Again the lateral flux adjustment and leakage-differences in this geometry strongly affect the transport, which makes this set-up inappropriate for validation of codes. These deficiencies in the design of the experiments and other problems resulted, almost without exception, in overestimation of tritium breeding and incorrect spectral predictions, with discrepancies from 5 percent to 50 percent.

These fusion reactor blanket simulation facilities can be contrasted with the Purdue Fast Breeder Blanket Facility

(FBBF), which allows very clean experiments.<sup>31</sup> Many different kinds of measurements have been made in the FBBF, and all consistently show the same trends. Although the neutronics problems are milder, due to lower-energy fission neutrons, discrepancies have also been found with FBBF experiments. Unlike the fusion reactor blanket experiments, these differences can be fully attributed to deficiencies in the computational methods and cross sections, and not to deficiencies in the configuration of the experimental facility. This is because the cylindrical facility has a distributed neutron source in the axis with a cosine-shaped flux distribution. Axial flux curvature which develops in the cylindrical blanket is already imposed by the source; thus little adjustment is required. Therefore, radial transport can be studied while errors due to axial leakage are minimized. Two other features contribute to the improved treatment of the neutron flux: the FBBF has complete azimuthal symmetry, and the ratio of height to radius is great enough that the flux curvature is minimal. Thus, there is no azimuthal dependence and almost no axial dependence of the flux at the mid-plane of the blanket. These features have allowed researchers working with the FBBF to determine the magnitudes of errors in neutron transport predictions with unprecedented accuracy, and to determine indications of their causes. It has also permitted them to discover differences between measurement techniques and to determine the sources of errors in some of

them. The same should be expected of a fusion reactor blanket simulation facility based on the same principles.

The research reported in this paper examines the conceptual design of a cylindrical facility similar to the FBBF: the Fusion Reactor Blanket Facility. This special facility will be referred to henceforth in this report as the FRBF. The FRBF will have the same general purpose as the FBBF, ".....to allow a direct comparison of measurements with design code calculations in a realistic geometrical structure."<sup>31</sup> The FRBF will be cylindrical, to simulate a section of the blanket of a toroidal or mirror reactor and to take advantage of simplified geometry; it will be flexible, to allow simulation of various blanket configurations and materials; it will have a cosine-shaped axially distributed neutron source, to greatly increase the accuracy of a buckling correction; it will take advantage of previously developed and thoroughly tested neutronics and reaction rate measurement techniques used in the FBBF; and it will take advantage of a faculty and staff experienced in the measurement of high-energy neutrons, theoretical transport predictions, and experiments in breeder blankets. Studies conducted in the FRBF will greatly enhance the expanding body of methodologies for fusion reactor blanket design, and will add confidence to studies leading to future fusion reactor design decisions.

The remainder of this paper begins with a review of fusion reactor blanket research in Chapter II, specifically a review of past blanket experiments and comparisons of experimental results to calculations. An overview of the FBBF is presented in Chapter III, including a brief description of the facility and results of FBBF experiments. Then, the design of the FRBF itself is described in Chapter IV, including discussions of the basis for selecting the blankets to be studied, of the anisotropy of the neutron source, and of the requirements for analysis of the design. Chapter V includes a discussion of the transport code (DORT) used to examine neutron transport, tritium breeding, and leakage; it includes a discussion of the modelling of the blankets (1-D, symmetric 2-D, and asymmetric 2-D); and it includes a discussion of the treatment of neutron sources (isotropic point, anisotropic boundary, and distributed plasma sources). The results of the transport computations are presented in Chapter VI. It includes comparisons of spectra; radial, axial, and azimuthal group-flux profiles; and tritium production rates in the different blanket models. Advantages of constructing the FRBF at Purdue and of the use of this facility to produce more and better fusion reactor blanket neutronics and tritium breeding experimental data are discussed in chapter VII. This chapter discusses safety issues, predicted measurement precision and accuracy, applicability of this design to the more complicated geometries of fusion reactors, and

flexibility for multiple and inexpensive benchmark experiments. Finally, the research is summarized in Chapter VIII, and recommendations for further research are presented.

## II. REVIEW OF FUSION REACTOR BLANKET EXPERIMENTS

Few actual fusion blanket experiments have been conducted. Leonard reviewed the blanket experiments up to 1975<sup>2</sup>, and Maynard reviewed essentially the same experiments at the BNL cross sections meeting in 1977.<sup>3</sup> L. Green then reviewed the experiments reported up to 1980.<sup>4</sup> In 1984 Woodruff summarized Green's paper and reviewed the fusion blanket experiments up to that time.<sup>5</sup> These experiments are summarized in Table II.1, and the corresponding computational methods are summarized in Table II.2. All the experiments except LOTUS and the LBM used a neutron source produced by directing a deuteron beam on a metal (Cu or Ti) target with tritium imbedded in it. However, different researchers treat the source differently in their measurements and calculations. Measurements have included local tritium production rates ( $T_n$  is the tritium production rate in natural lithium, tritons/cm<sup>3</sup>-source neutron,  $T_6$  from <sup>6</sup>Li,  $T_7$  from <sup>7</sup>Li), neutron and gamma-ray spectra (including angular flux), and fission rates. A brief discussion of the reported experiments, in chronological order, follows the tables.

Table II.1. A Summary of Tritium Breeding Experiments.

Ref.	Year	Place	Geometry	Materials
6	1954	LANL	60 cm sphere	$^6\text{LiD}$
7-9	1974-77	Karlsruhe	1 m sphere	$^6\text{Li}$ , SS
10&11	1974-75	Julich	120 cm cyl	$^6\text{Li}$ , SS
12	1978	Julich	120 cm cyl	$^6\text{Li}$ , SS
13-17	1975-78	JAERI	pseudo-sphere	$^6\text{Li}$ , U, C, $^6\text{Li}_2\text{O}$
18	1978	JAERI	pseudo-sphere	$^6\text{Li}_2\text{O}$ , C
19	1978	LANL	60 cm sphere	$^6\text{LiD}$
20	1979	Osaka U.	slabs	$^6\text{Li}$ or C
21	1980	Tokyo U.	slab	$^6\text{LiF}$
22	1981	U. Birm., England	1.25 m sphere	$^6\text{LiF}$ powder, Al
23	1981	ORNL	slabs	LiH, Pb-LiH
24	1980-81	UCSB	88 cm cyl	$^6\text{Li}$ , SS
25	1983	JAERI	pseudo-cyl slab	$^6\text{Li}_2\text{O}$
26	1983	JAERI	pseudo-cyl slab	$^6\text{Li}_2\text{O}$
27-29	1984-?	Lausanne	LOTUS	Fusion- fission
30	1986-?	PPPL-TFTR	LBM	$^6\text{Li}_2\text{O}$ , SS

Table II.2. Computational Methods in Tritium Breeding Experiments.

Ref.	Codes	Cross Sections	Source Treatment
6	DTF-IV (Sn)	ENDF/B-III	isotropic
7-9	DTK (Sn)	ENDF/B-III KEDAK3 (Fe)	meas'd spectrum anisotropic
10&11	ANISN, DOT-II MORSE	ENDF/B-III	same as 7
12	ANISN, MORSE DOT-II	ENDF/B-III	isotropic, 1 gp
13-17	ANISN	ENDF/B-III	isotropic, 1 gp
18	ANISN	ENDF/B-IV	isotropic
19	MCN (Monte Carlo)	ENDF/B-III 67 UK-LASL	E/ $\theta$ correlation anisotropic
20	ANISN, NITRAN NIMOS	ENDF/B-IV	measured, 14.8 MeV
21	ANISN	ENDF/B-III&IV	measured, 14 MeV
22	MORSE, ANISN	ENDF/B-IV	anisotropic, meas'd spectrum
23	DOT	ENDF/B-IV	E/ $\theta$ correlation anisotropic
24	MORSE-L	ENDF/B-IV	disc, 1 group, isotropic
25	BERMUDA-2DN	ENDF/B-IV	meas'd spectrum
26	same as 25		
27-29	ANISN, MCNP	DLC-2, SINEX	anisotropic, collided MCNP
30	Monte Carlo	?	plasma

The first documented tritium breeding integral experiment was conducted at LANL in 1954, but the neutronics analysis wasn't performed until 1972 by Muir and Wyman.<sup>6</sup> The 60-cm-diameter natural lithium deuteride ( ${}^6\text{LiD}$ ) sphere with a neutron source at the center produced  $T_7$  and  $T_n$  data. These data were compared to 1-dimensional breeding predictions, and discrepancies ranged from a few to  $\sim 35\%$ , depending upon isotope and radius. They argued that the  ${}^7\text{Li}(n,n'\alpha)\text{T}$  cross sections were too great, but not enough to explain the magnitudes of errors in the data.

Another experiment was conducted in Great Britain in 1964, but information on this experiment is difficult to obtain (report AWRE NR-4/64 is supposed to have information on this experiment). Maynard listed this cylindrical  ${}^6\text{Li}$  experiment in his table in Ref. 3, but gave no comparison of results to calculations.

Various transport codes were compared to the results of experiments in a 1-m-diameter  ${}^6\text{Li}$  sphere with a stainless steel shell from 1974 through 1977.<sup>7-9</sup> Bachmann et al. found that  $T_n$  was overpredicted by  $\sim 35\%$  throughout the blanket, and neutron flux was greatly overpredicted between 3 and 11 MeV. The neutron source in this experiment was strongly anisotropic, so it was measured and the measured spectrum was used as the source in their codes.

Herzing et al. performed experiments in a cylindrical blanket model of  ${}^6\text{Li}$  at Julich in 1975.<sup>10,11</sup> They measured  $T_7$ ,  $T_8$ , and  $T_n$  and spectra using solid state track detectors. They used various 1, 2, and 3-dimensional codes and assumed an isotropic neutron source. They found that the results of Monte Carlo predictions matched the  $T_n$  data except at the boundaries. Since others have determined that the  ${}^7\text{Li}(n,n'\alpha)\text{T}$  cross sections are ~15% too large and the scattering cross sections are quite inaccurate in ENDF/B-III;<sup>5,6,7</sup> they should have found discrepancies. Additionally, they determined  $T_7$  was overpredicted throughout the blanket by about 15-20%. Only the Monte Carlo method gave them what they considered acceptable results. This experiment was repeated in 1976 with a 15-cm-thick graphite blanket added.<sup>12</sup> Again  $T_n$ ,  $T_8$ , and  $T_7$  were measured. Generally good agreement was obtained in the outer region of the blanket, but  $T_n$  was underpredicted toward the center (~12%) and at the outer regions of the reflector (~16%), and overpredicted within 5 cm of the blanket/reflector interface (~8%). Additionally,  $T_8$  was greatly overpredicted (~45%) at the inner wall. Again, ENDF/B-III cross sections were used, and  $T_7$  should have been overpredicted.

A series of experiments were conducted at JAERI between 1975 and 1979.<sup>13-18</sup> Pseudo-spherical blankets were formed by assembling rectangular blocks of various materials (Li,

U, C, Li<sub>2</sub>O). Fission rates were measured in miniature fission chambers containing <sup>235</sup>U, <sup>238</sup>U, <sup>232</sup>Th, and <sup>237</sup>Np. Discrepancies between ANISN calculations and measurements depended on blanket material, fission isotope, and depth; they ranged from +15% to -15%, sometimes with strong transitions through the blanket. Angular flux spectra were compared to predictions in the last experiment; results indicated that C/E was a strong function of angle, with differences up to 30%.<sup>17</sup> Maekawa et al. attributed discrepancies to inadequate cross section libraries and to non-spherical interfaces due to the use of the blocks.

Another 60-cm-diameter spherical assembly was tested at LANL in 1978.<sup>18</sup> It contained <sup>6</sup>LiD (95.6% <sup>6</sup>Li), and breeding was measured. T<sub>6</sub> and T<sub>7</sub> were measured and compared to 3-dimensional Monte Carlo predictions (using ENDF/B-III). The source was treated with an angle-energy correlation and anisotropic yield. T<sub>6</sub> was generally very close to the predictions (except at boundaries), but T<sub>7</sub> was again overpredicted by about 10% (except at the outer boundary).

Yamamoto et al. measured angular spectra from various thicknesses of Li or graphite slabs in 1979.<sup>20</sup> They compared the measurements with various codes, using a monochromatic 14.8 MeV source. Transverse leakage was blamed for a large part of the 20-30% discrepancies in the spectra at low energies. The spectra were much softer than predicted, especially below 8 MeV for the Li slabs. ANISN

results were totally unacceptable.

Another slab, this time of natural LiF, was tested at the University of Tokyo in 1980.<sup>21</sup> Neutron spectra and  $T_n$  were measured and compared to ANISN predictions, which were found to be good to no better than 20-30%.

LiF was also tested in a spherical blanket model in 1980.<sup>22</sup> However, in this experiment a 1.25-m-diameter aluminum sphere was filled with a powder--variable packing density may have affected the results. An anisotropic, measured spectrum was used as the source in various codes. Great attention to detail in this experiment did not seem to ensure better results. Some measured spectra were much softer than predicted, others were much harder. Woodruff was concerned with this because of the quality of the effort and results which he considered opposite to those of Profio et al. (see Ref. 24 below).

Experiments were conducted on slabs of LiH with and without 5 cm of Pb at ORNL in 1981.<sup>23</sup> Santoro et al. measured neutron and  $\gamma$ -ray leakage spectra and compared their results to DOT predictions. They used a first collision source produced by a code which used an angle-energy-yield correlation for neutron production in the target. Results were good between 6 and 10 MeV, but spectra were underpredicted above and below that range. This may be due to an error in the source correlation in the forward

direction (toward the slab).<sup>22</sup>

Profio et al. experimented with a cylindrical  ${}^6\text{Li}$  blanket at UCSB in 1980.<sup>24</sup> This system was unique due to the radial rather than axial orientation of the d-beam tube. They measured fast scalar flux along the axis of the cylinder, rather than radially. Monte Carlo calculations using ENDF/B-IV significantly underpredicted the penetration of fast neutrons, by 50-100% for some spectral peaks.

Maekawa et al. measured the leakage spectra from pseudo-cylindrical slabs of  $\text{Li}_2\text{O}$  by time-of-flight methods in 1983.<sup>25,26</sup> They used a 2-dimensional transport code with ENDF/B-IV cross sections to predict the high-energy angular neutron flux. Measurement errors were 1-20% depending on slab thickness and angle. Spectral shapes were reproduced, but calculated spectra were softer than measured spectra, and some spectral peaks were overpredicted by ~50%. Aside from the past experiments which were previously discussed, and despite the obvious requirement for further research, only two new projects are currently in progress.

One new project for testing conceptual designs for fusion and fusion-fission hybrid blankets is being conducted at Lausanne, Switzerland.<sup>27</sup> It is called the LOTUS project and uses a higher intensity neutron source than most other blanket experiments. Sitaraman et al. did a Monte Carlo analysis of its HAEFELY mixed-beam DT-neutron generator.<sup>28</sup>

They determined that the neutron source for LOTUS would be highly anisotropic, and noted only 37% of the neutrons would be emitted toward the blanket; of those, only 67% would be uncollided neutrons. Initial experiments were scheduled for 1985, and the neutronics predictions have been completed. Sahin and Kumar have predicted that lateral leakage will be a major source of discrepancies.<sup>29</sup> Experimental results have not appeared in the open literature.

Another planned experiment will be the Lithium Blanket Module (LBM) to be placed in the TFTR at PPPL. Jassby et al. describe the program, including design, manufacturing techniques, neutronics analyses, and experiment plans.<sup>30</sup> The LBM will be a segment 81 cm x 76.7 cm x 86.5 cm, with  $\text{Li}_2\text{O}$  pellets contained in steel rods and with a steel reflector. Tritium production and neutron current are predicted to be flat across the LBM to within ~5% except within 8 cm of the sides (probably due to neutron leakage from the surrounding structure). When the TFTR burns deuterium fuel within the next few years, the fusion community will have its first real fusion reactor blanket data.

The above experiments suffer from many deficiencies: complicated geometries, problems with anisotropy of the DT-neutron source, inadequate measurement techniques, and designs which were not flexible. Only the JAERI, ORNL, and LOTUS experiments allow changes in blanket composition; the

ORNL system and LOTUS are thick slabs, and JAERI used non-smooth boundaries. Thus, many of Leonard's, Maynard's, Green's, and Woodruff's conclusions are still valid:  $T_7$  cannot be predicted accurately, measurement techniques need refinement in both accuracy and sensitivity, cross section libraries and transport codes need improvements, and integral experiments are needed on prototypic fusion reactor blanket designs to validate the codes and the designs. The lack of fusion reactor blanket experiments since 1984 should cause concern, since the past research has not yielded data which validated transport codes or cross sections for tritium breeding and neutronics predictions.

The deficiencies previously discussed have contributed to the deviations between experimental results and theory sufficiently to prevent validation (or invalidation) of neutronics codes. A new fusion reactor blanket simulation facility without the deficiencies in design of the past experiments will provide data which can be used to inexpensively validate those codes and the cross section libraries for a variety of fusion reactor blankets. The following chapter describes how the FBBF was designed for this same purpose (for fast reactor neutronics), and it summarizes the highly successful results.

### III. OVERVIEW OF THE FBBF

#### III.1. Facility Description

Ott, Clikeman, and Harms describe the FBBF in Ref. 31, and present a summary and analysis of the many experiments conducted in it. The facility includes a heavily shielded room, which contains the cylindrical blanket simulation system, and an exterior control and instrumentation room. The experimental system itself consists of an axial neutron source of  $^{252}\text{Cf}$  of about  $10^9$  n/s, a two-region spectrum modifier with an outer radius of 22 cm, a breeding blanket with an outer radius of 73 cm (51 cm thick), and a NaCl and SS reflector with an outer radius of 89 cm (16 cm thick). Four pellets of Cf are distributed on the axis to create the desired neutron source; they are fixed in a moveable rod (lowered into underground shielding while changing experiments, etc.), and their intensities and locations are such that a cosine-shaped source results after some distance. The inner region contains 4.8%-enriched, close packed  $\text{UO}_2$  fuel rods clad in SS, with the gaps between rods filled with  $\text{B}_4\text{C}$  powder; the outer modifier contains the same fuel rods, but with wider spacing, and the gaps contain Na-filled SS tubes. These regions modify the neutron spectrum

from the Cf source to approximate the leakage spectrum entering the blanket from a typical 1000-MWe fast reactor core. They also smooth the flux from the four sources so that the axial flux distribution at the modifier/blanket interface closely matches that which would be produced by a continuously distributed chopped-cosine-shaped source (as in a critical fast reactor).

The blanket region contains natural  $UO_2$  fuel pellets clad with Al, then placed in Al or SS secondary cladding. The rods are placed in a uniform hexagonal array with the correct pitch between fuel rods, and no other materials are used (voids contain only air). All experiments are placed between fuel pellets or in a vacancy created by removing an experimental rod. Thus, measurements can be made throughout the blanket in axial, azimuthal, or radial traverses with negligible perturbations of the flux. Since Al has about the same macroscopic cross section and slowing down power as Na, it plays the role of the Na coolant in a fast reactor. These features allow the FBBF to simulate very closely the blanket of a full-scale fast breeder reactor--in geometry, in source spectrum and current, and in materials.

A new blanket is now being constructed with the fuel rods arranged in hexagonal arrays (assemblies). Additionally, initial plans are being formulated for fabricating several thousand metal fuel rods for use in the FBBF for testing the neutronic characteristics of the Integral Fast Reactor. The

outstanding results obtained in past FBBF experiments, discussed in the following section, should also be found with these new blanket configurations.

### III.2. Results of FBBF Experiments.

Measurements in the FBBF have included neutron capture rates in  $^{238}\text{U}$  and  $^{232}\text{Th}$ ; fission rates in  $^{235}\text{U}$ ,  $^{238}\text{U}$ ,  $^{232}\text{Th}$ , and  $^{239}\text{Pu}$  by solid state track detector (SSTD) measurements; resonance neutron capture rates in  $^{286}\text{W}$ ,  $^{55}\text{Mn}$ , and  $^{197}\text{Au}$ ; helium- and proton-recoil neutron spectrometry; and gamma-ray energy deposition rates in thermo-luminescent dosimeters (TLD). These measurements have been compared to diffusion calculations based on standard 50-group cross sections. The results of these comparisons are expressed as ratios of calculation to experiment (C/E values, C is based on absolute neutron-source strength, E on absolute measurements). The general trend in these C/E values is to begin at  $\sim 1$  at the transformer/blanket interface, then to decrease linearly with increasing radius to  $\sim 0.65$  at the outer circumference of the blanket. The cause of this trend has not been determined, but is suspected to be due to a gross (bulk) neutron effect, which should appear in all C/E results. Exceptions to this trend should be examined carefully for errors in measurement technique or interpretation, or in neutronics calculation. This careful examination has led to the identification of many problems

in blanket neutronics: faulty measurement techniques, errors in treating resonance self-shielding of detection isotopes in group constant production codes, shielding of resonance absorption in low-concentration materials by high-concentration materials, and short-range deformations of reaction rates (due to spectrum transition and its effect on self-shielding).

The consistency of the results of the various measurement techniques employed in the FBBF experiments lends great credibility to the results. The careful design of the FBBF insured these outstanding results. The conclusion of Ott et al. in Ref. 31 that some of the trends should be relevant to fusion reactor blankets came from a careful analysis and synthesis of the varied measurement results. They predicted that one result will be especially applicable to fusion reactor neutron transport: the difficulties in describing the transitory neutron fluxes in the FBBF blanket should be more severe, due to the wider range of neutron energy in a fusion blanket. Thus, the idea for the FRBF was born naturally from the results of FBBF investigations. However, the feasibility of constructing the FRBF and using it to produce more and better test data remains to be demonstrated; that demonstration follows in the next four chapters of this thesis.

#### IV. CONCEPTUAL DESIGN OF A FUSION REACTOR BLANKET FACILITY

##### IV.1. Objectives

The general objectives of the research reported herein were threefold:

1.a) to demonstrate the advantages of constructing a fusion reactor blanket testing facility (the FRBF) which is an analog of the FBBF, and

b) to show the feasibility of constructing the FRBF at Purdue University;

2) to demonstrate the new facility will produce more and better data and results than are (or will be) available elsewhere; and

3) to show the results are applicable to fusion reactors although neither the geometry nor the source are exactly duplicated.

##### IV.2. General Considerations for the Design

Before beginning the design of the FRBF, the requirements of a fusion reactor blanket simulation facility must be analyzed. Then, convincing arguments must be made which prove that the FRBF can be built as an FBBF-analog which

will satisfy these requirements. In Chapter II the multiple problems with past experiments, current facilities, and planned experiments were demonstrated. Those problems can be summarized as:

- severe source anisotropy,
- inappropriate geometry,
- ray effects due to point sources,
- short measurement times due to finite lifetime of targets, and
- inflexible designs.

To show that experiments conducted in the FRBF will contribute to the advancement of fusion reactor technology, this research needs only to demonstrate that and how those problems are eliminated, reduced, or ameliorated. Although the blanket model is neither toroidally shaped (as in a Tokamak) nor semi-infinitely long (as in a large mirror), nor is the source a "tube" of neutron-producing reactions, the results must be applicable to those geometries. Once precise data are produced which lead to improved transport codes and validation of data libraries, then confidence in these codes to predict transport in real blankets will have been obtained.

The results of the research reported in this paper will simultaneously satisfy the three objectives previously mentioned. The remainder of this chapter will present the desired properties of a fusion reactor blanket experiment,

and then will describe how these properties can be supplied by the appropriate design.

#### IV.3. Desired Features of a FRB Simulation Facility

The facility for fusion reactor blanket simulation experiments must have certain properties so that it will produce improved data. This new data must be more meaningful than that which has been produced in the past; or it must be data which might not otherwise be produced in the future, due to the high cost of one-of-a-kind simulations or fusion reactor experiments. The required properties include:

- simple geometry and an easily modelled source for improved analysis;
- flexibility for changing blanket materials or composition at moderate cost;
- long measurement times for greater accuracy and precision;
- multiple measurement techniques for verification of results and broader comparisons;
- low cost of changes in composition or blanket structure for many experiments; and
- low cost of initial construction and operation.

These properties are synergistic--geometry affects analysis, cost, and flexibility; source affects analysis and measurement statistics; cost affects number and variety of experiments and analyses; etc. Therefore, proper selection of the geometry and source can lead to an experimental

system which can yield better data quickly, accurately, and cheaply.

#### IV.4. Scope of Research

The research which needed completion prior to a decision to proceed with engineering design of the FRBF and its source was to develop a preliminary conceptual design; then to analyze that design to determine if it meets the guideline previously set forth. That is, does it have a geometry and a source that can be analyzed by standard methods without significant deviations due to inadequate representability? The steps to be followed were set forth as:

- 1) select a blanket design,
- 2) select a source arrangement, and
- 3) perform neutronics analyses.

These three efforts are discussed thoroughly in the following three sections.

#### IV.5. Blanket Design

The overall blanket geometry for the FRBF has already been selected due to the success of the FBBF. The non-availability of appropriate neutron sources for slab (plane-wave) or spherical (isotropic) geometries also leads to the selection of cylindrical geometry, as does the requirement

for flexibility. Additionally, others have performed optimization studies which have shown the FBBF blanket is about the correct size for fusion blanket research.<sup>10-12</sup> The final blanket design includes an inner source region and vacuum tube, a first wall of variable thickness, a blanket region, a reflector or plenum region, and a steel shield. The blanket designs are based on both the design of the present FBBF and on the primary candidates selected in the Blanket Comparison and Selection Study (BCSS), which was managed by ANL for the U.S. Fusion Power Program (FPP).<sup>1</sup> The thicknesses of blanket regions are the order of those reported for fusion reactor models (based on Tokamak or large mirror reactors) in the FINESSE study: but the radius of the plasma region is reduced by about an order of magnitude, and the reflector/shield region is decreased in thickness. The FRBF will actually be about the same dimensions as the proposed fusion test system, also described in FINESSE. This system will be placed in the center of the MFTF-B at LLNL, where tremendous magnetic fields will confine the test plasma inside the test blanket (at a probable cost of millions of dollars per test). Of the blanket candidates selected by the BCSS, only two were selected for analysis in this study.

Four blankets were selected as primary candidates by the BCSS group; two of those were selected for this research. They are:

- Blanket HeC--a helium-cooled solid blanket design, with natural lithium composition; and

- Blanket LLC--a liquid-metal-cooled liquid blanket design, with neutron multiplication and enriched lithium.

These two models offer totally different neutronic environments for studying the effects of asymmetries and anisotropic sources; thus helping insure that the conclusions reached from comparing the results of computations are not blanket-design or composition dependent. The general FRBF blanket geometric design is shown in Figures IV.1.A and IV.1.B. One dimensional representations of the complete blanket designs, including materials and densities, are shown in Figures IV.2.A and IV.2.B. The blanket inner radius and outer radius are 22 and 100 cm respectively, the height of the blanket is 100 cm, and it is capped by a 20 cm thick steel reflector/shield. Number densities of the components of the blanket materials are listed in Appendix A. The blanket will be constructed as a hollow annulus, with removable azimuthal and axial segments to allow flexibility in design of experiments. The source which will be created in the center of the blanket is a critical element; its conceptual design is described in the next section.

#### IV.6. Neutron Sources

A neutron source arrangement for the FRBF was investigated by Aparcedo in an earlier paper.<sup>33</sup> He studied

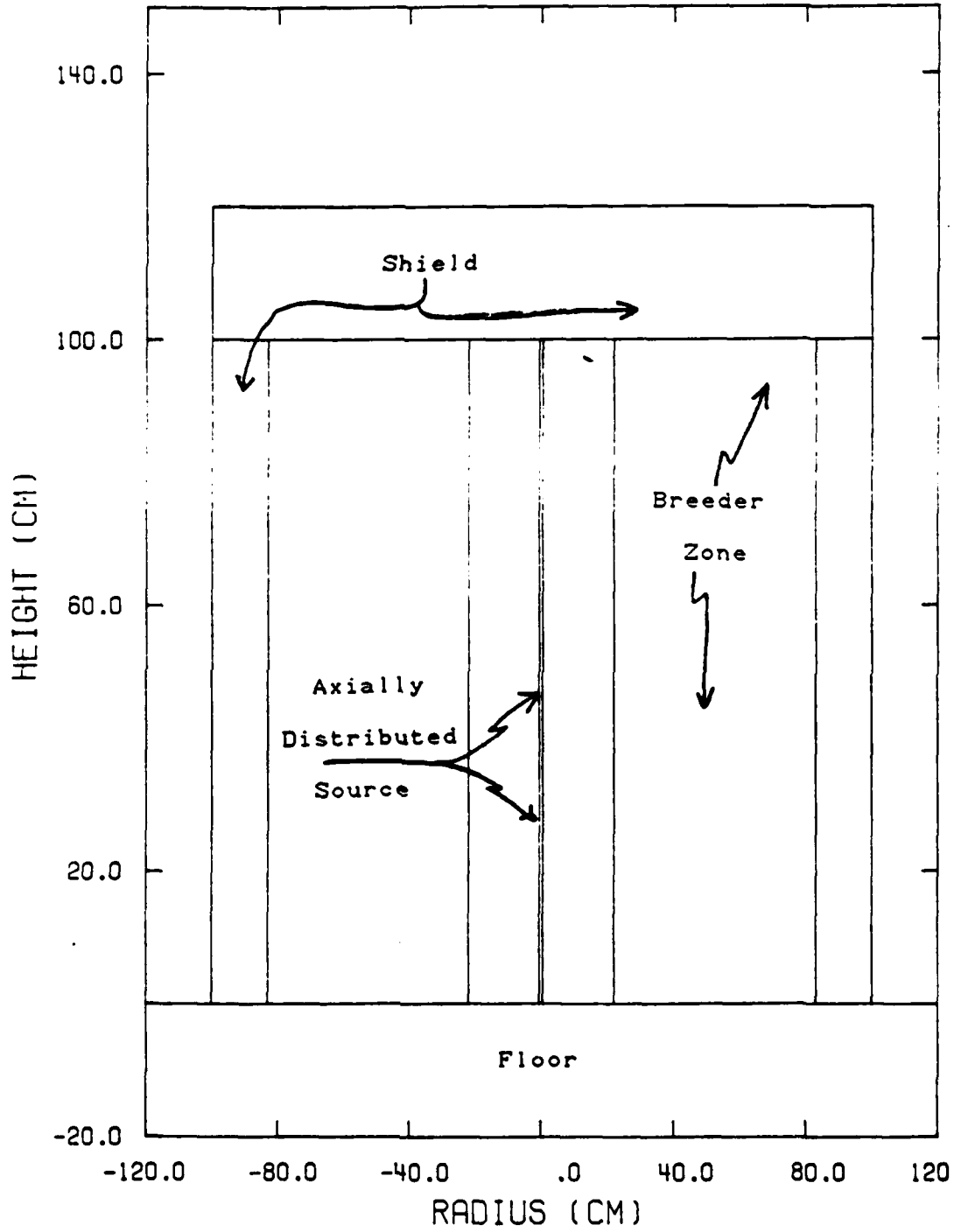


Figure IV.1.A. Cross Section of the FRBF.

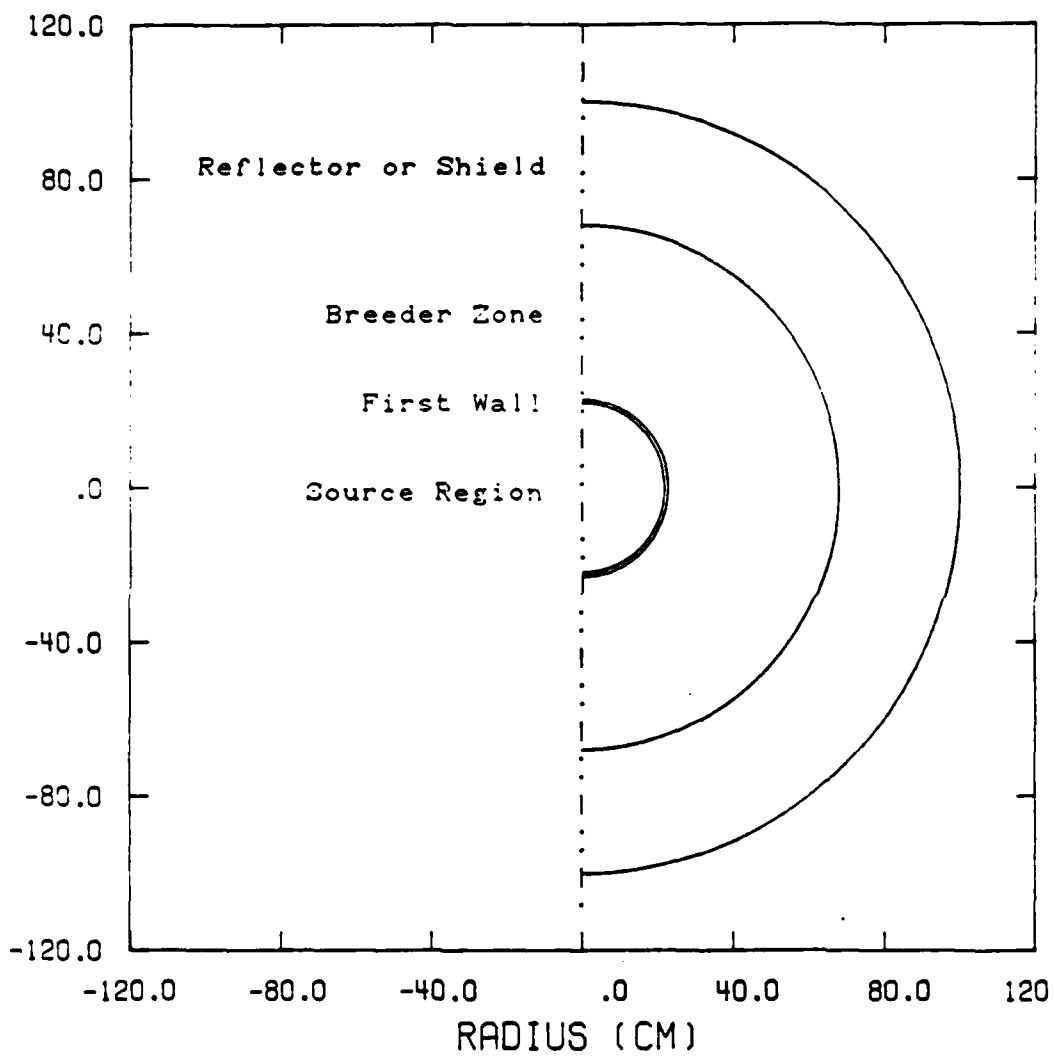


Figure IV.1.B. Radial Geometry of the FRBF. Note the shield inner-radius does not equal that of the previous figure, to indicate the designed-in flexibility.

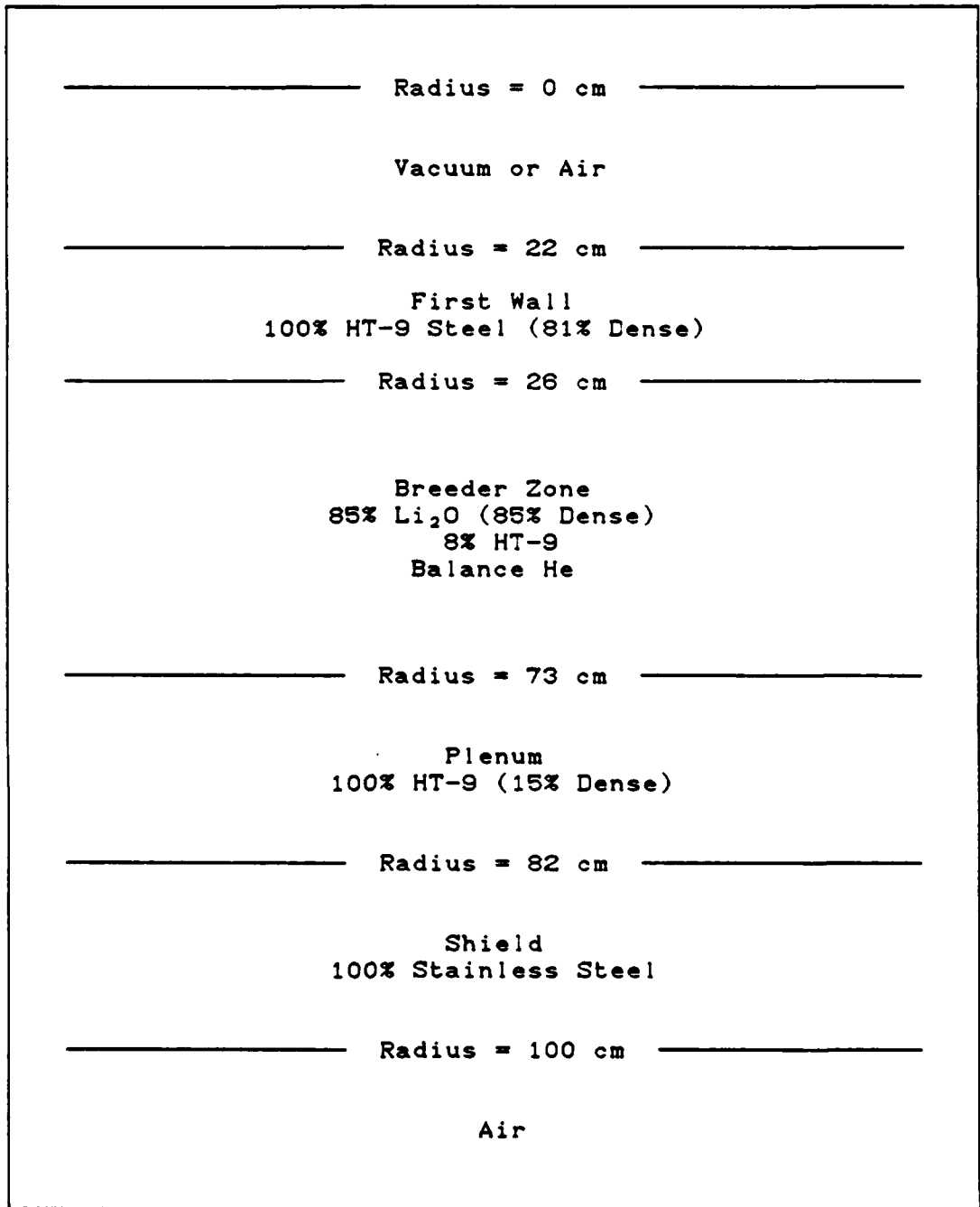


Figure IV.2.A. 1-Dimensional Model of Blanket HeC. He-cooled blanket with steel structure.

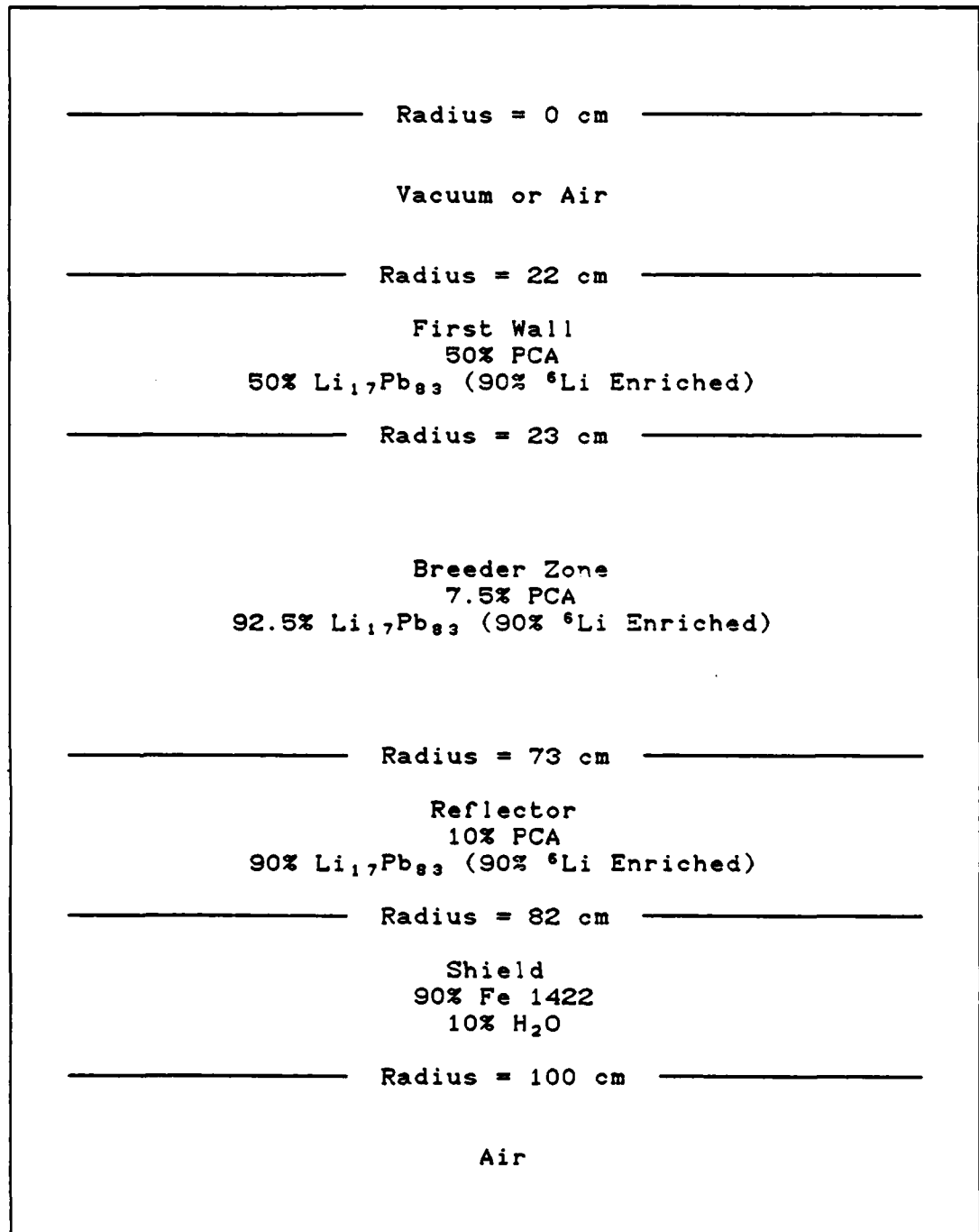


Figure IV.2.B. 1-Dimensional Model of Blanket LLC.  
 $\text{Li}_{17}\text{Pb}_{83}$  self-cooled with Primary Candidate Alloy structure.

a multi-target arrangement along the axis of a cylinder which would produce an approximately cosine-shaped total-flux distribution at the inner wall. In this preliminary investigation, he used an isotropic emission of  $T(d,n)\alpha$  neutrons from flat annular TiT targets; the result was a distribution of point sources which was symmetric about the mid-plane of the cylinder. In fact, the neutrons emitted from such targets are anisotropic in both energy and yield.<sup>32</sup>

A kinematic treatment of the two-body reaction, using conservation of momentum and energy in the center-of-mass (COM) reference frame, yields the energy-angle relationship for the  $T(d,n)\alpha$  reaction:

$$E_n(\theta) = BE_T(\cos\theta + (D/B - \sin^2\theta)^{1/2})^2, \quad (4.1)$$

where

$$E_n(\theta) = \text{energy of the neutron at the angle } \theta \text{ from the d-beam,}$$

$$E_T = E_d + Q \quad (Q = 17.59 \text{ MeV}), \text{ and}$$

$$E_d = \text{d-beam energy.}$$

The solid angle ratio for conversion of the COM reaction cross section to the laboratory cross section is

$$S_r(\theta) = E_n(\theta)/E_T(AC)^{1/2}(D/B - \sin^2\theta)^{1/2}. \quad (4.2)$$

The dimensionless constants A, B, C, and D are determined from the masses and energies of the interacting species.

For the  $T(d,n)\alpha$  reaction, they are given by

$$A = \mu_r M_d M_\alpha (E_d/E_T),$$

$$B = \mu_r M_d M_n (E_d/E_T),$$

$$C = \mu_r M_d M_n (1 + M_d Q / M_t E_T), \text{ and}$$

$$D = \mu_r M_d M_\alpha (1 + M_d Q / M_t E_T),$$

where

$$\mu_r = 1 / (M_d + M_t)(M_n + M_\alpha). \text{ Note that the product of } \mu_r \text{ with two masses is dimensionless also.}$$

When equations 4.1 and 4.2 are used to determine the energy and yield of neutrons emitted from a deuteron incident on a TiT target, the result is an angle-energy correlation of neutron emission. Table IV.1 lists the angle-energy correlation for a 150 KeV deuteron.

Table IV.1. Angular Distribution of d-T Neutrons.

	Angle of Emission (degrees)						
	0.0	10.0	45.0	90.0	135.0	170.0	180.0
$E_n(\theta)$	14.96	14.95	14.70	14.11	13.54	13.32	13.31
$E_\alpha(\theta)$	2.780	2.793	3.034	3.631	4.203	4.421	4.433
$S_f(\theta)$	1.059	1.058	1.042	1.000	0.959	0.943	0.942

The energy of neutrons and alpha particles in the table is in MeV. Note that the sum of  $E_n$  and  $E_\alpha$  is 17.74 MeV, which is the sum of the reaction energy,  $Q$ , and the deuteron energy,  $E_d$ , at each angle. Based on the solid angle ratios listed, the neutron production rate is about 12% greater in

the forward direction than in the backward direction.

The treatment which determines this distribution is incomplete for a deuteron beam, however. Due to slowing down and scattering of the beam in the target material, the reaction energy is not equal to the beam energy for most deuterons; in fact, the majority of reactions occur at the resonance energy of 109 KeV for the  $T(d,n)\alpha$  reaction. Therefore, the angle-energy correlation must be determined as a function of the slowing down; it has been evaluated and reported with respect to this loss of energy before reaction.<sup>32</sup> The implementation of this angle-energy-slowng down relationship will be presented in Chapter V. Since there is a distribution of energy and yield from the d-t-neutron source, and because of concerns of tritium leakage from the system, other high-energy neutron sources were considered.

Other reactions which yield high-energy neutrons were also evaluated, e.g., the  $d-{}^6\text{Li}$  and  $d-{}^7\text{Be}$  reactions were considered. These reactions have even stronger variations in energy and yield than the d-T reaction, because they require extremely high beam energy for acceptable neutron production rates. For example, the energy and solid angle ratios for the  ${}^6\text{Li}(d,n){}^7\text{Be}$  reaction ( $Q = 3.38$  MeV) for a 15 MeV deuteron are shown below in Table IV.2. Neutron energy is also in MeV in this table.

Table IV.2. Angular Distribution of d-<sup>6</sup>Li Neutrons.

	Angle of Emission (degrees)						
	0.0	10.0	45.0	90.0	135.0	170.0	180.0
$E_n(\theta)$	18.17	18.07	16.23	12.31	9.34	8.39	8.34
$S_r(\theta)$	1.422	1.414	1.281	0.981	0.737	0.656	0.652

Because they produce stronger anisotropy (due to energies of several MeV) and have wider distributions of energy (due to continuous slowing down from much greater energy); these types of reactions were eliminated as a possible source for the FRBF.

Due to the anisotropy previously demonstrated, the axially-symmetric source distribution determined by Aparcedo required re-evaluation with respect to the anisotropy in yield. The correlations above were used in a computer program to determine optimum positions for multiple anisotropic sources aligned axially in the FRBF to produce a chopped-cosine direct-flux distribution. The position of source "j" is  $Z_j$  and its strength is  $S_j$ , while "z" is the axial variable. To reduce the free variables in the search strategy, source positions were restrained such that the integrated flux at the first wall above and below the mid-plane were equal. This was done by requiring

$$\sum_i z_i \phi_i \delta z_i = 0. \quad (4.3)$$

where  $z_i$  is the axial position at the first wall ( $z = 0$  at the mid-plane),  $\phi_i$  is the flux (a function of  $Z_j$  and  $S_j$  and of  $z_i$ ), and all  $\delta z_i$ 's are equal. The result of this search for the central source position was  $Z_3 = -1.2$  cm (offset toward the beam). Two additional source positions ( $Z_2$  and  $Z_4$ ) were added, and another constraint was imposed:

$$\sum_i \sum_j z_i \phi_{i,j} \delta z_i = 0, \quad \text{and} \quad (4.4)$$

$$\Delta Z_2 = \Delta Z_3, \quad (4.5)$$

where  $\Delta Z_j = Z_{j+1} - Z_j$ , the separation between the sources. The result of this search showed that the position of the central source,  $Z_3$ , was very weakly dependent upon the source separation,  $\Delta Z$  ( $\pm 0.02\%$  over a range of  $\Delta Z = 0$  to 30 cm).

To find the optimum positions for three sources, a least-squares-error routine was used to minimize the difference between the flux profile and the chopped-cosine function. The error routine minimized  $\epsilon^2$ , where

$$\epsilon^2 = \sum_i (\phi_i - \cos(z_i^*))^2 \cos^2(z_i^*), \quad \text{and} \quad (4.6)$$

$$z_i^* = \pi z_i / H'.$$

$H'$ , the extrapolated height, was based upon the reflector savings of the FBBF. The summation interval ignored 10 cm at each end of the cylinder, since slight errors there will have a minimal effect at the midplane, where measurements will be concentrated. The extra  $\cos^2$  term in equation 4.6 is a weighting factor which tends to improve the fit around

the mid-plane. The results of this search are illustrated in Figure IV.3 (along with the flux profile produced by a single anisotropic point source). The y-coordinate of the octagons represents the relative strengths of the three sources. The RMS error over the central 80% of the cylinder is about 1%. Although it appears that three sources may be adequate, considering the projected accuracy of measurements, the cosine approximation becomes poor about 30 cm away from the mid-plane. More sources are needed for a smoother axial flux profile on the first wall of a cylindrical facility.

A similar search was performed for five point sources to determine if this would be enough for a smooth flux profile. Positions  $Z_1$  and  $Z_5$  were added, the search was improved as better fits were obtained, and constraints were successively loosened. The constraints were

- 1)  $\Delta Z_1 = \Delta Z_2 = \Delta Z_3 = \Delta Z_4$ ,  $S_1 = S_2 = S_3 = S_4 = S_5$ ,
- 2)  $\Delta Z_1 = \Delta Z_4 \neq \Delta Z_2 = \Delta Z_3$ ,  $S_1 = S_2 = S_3 = S_4 = S_5$ ,
- 3)  $\Delta Z_1 = \Delta Z_4 \neq \Delta Z_2 = \Delta Z_3$ ,  $S_1 = S_5 \neq S_2 = S_3 = S_4$ ,
- 4)  $\Delta Z_1 = \Delta Z_4 \neq \Delta Z_2 = \Delta Z_3$ ,  $S_1 = S_5 \neq S_3 \neq S_3 = S_4$ , and finally
- 5) interactive, making slight adjustments in any source strength or position.

The result of this search is shown in Figure IV.4; the flux profile from five sources is obviously a very close approximation to a chopped-cosine distributed source.

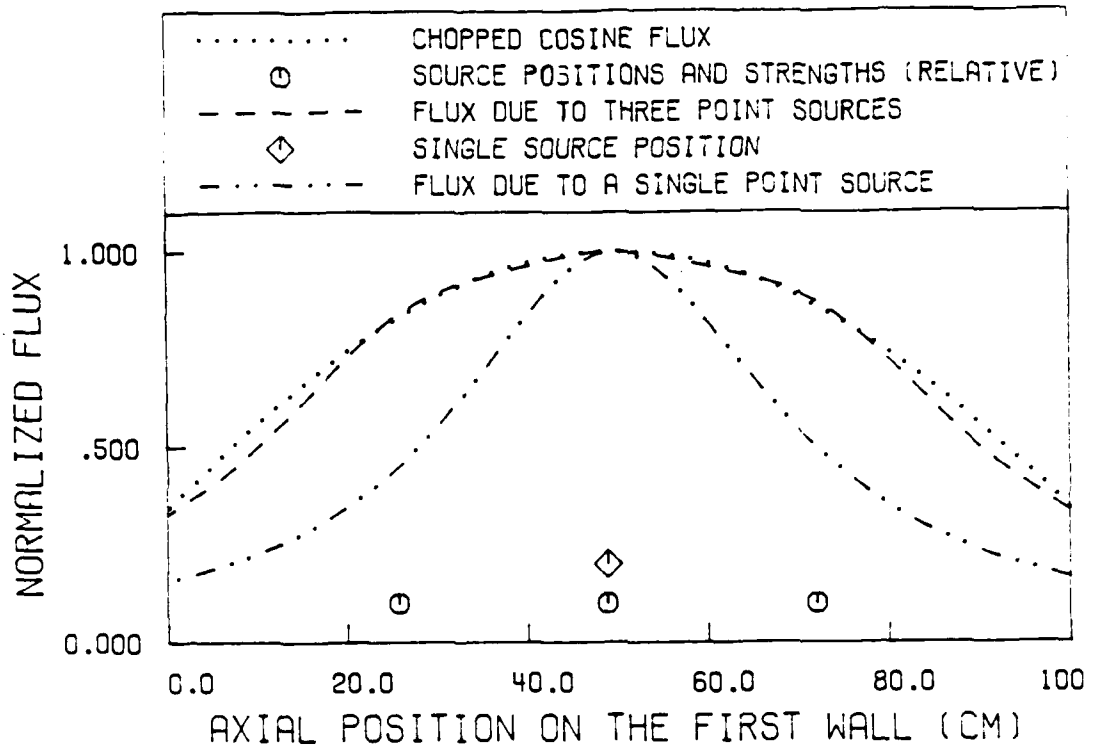


Figure IV.3. Neutron Flux Due to Three d-T Sources.

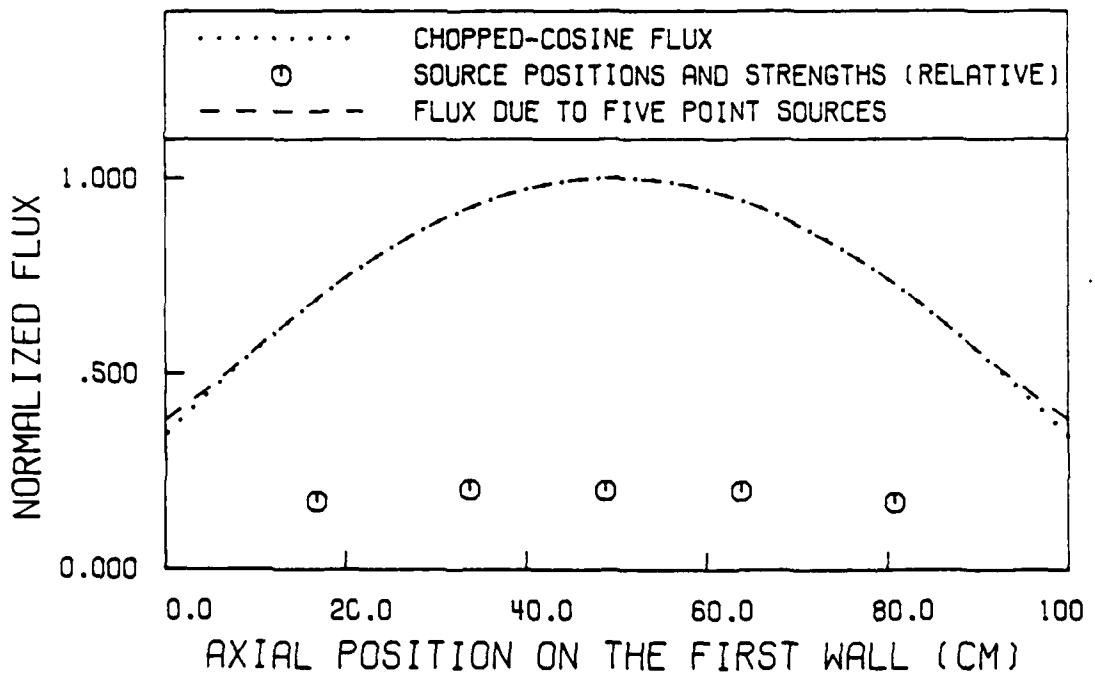


Figure IV.4. Neutron Flux Due to Five d-T Sources.

The RMS error for this search was less than 0.1% for the central 80% of the wall. Except for the energy variation axially, this set-up could produce outstanding experimental results.

Neutrons from an axially aligned d-beam would produce flux profiles which would still be unsymmetric in energy, with the average value in the lower end of the blanket about 1.5 MeV (~10%) greater than in the upper end. The effect of this variation was not investigated, but it would tend to cause very small energy-related differences in measurement results. Another detrimental effect of using few sources is ray-effects in neutron transport calculations.<sup>34</sup> The unattenuated neutrons striking any portion of the blanket would have three discrete incoming angles, which has been shown to produce erroneous results in most transport codes. These ray effects can be easily treated by the use of codes which calculate a first-scatter and unscattered neutron source throughout the blanket. Nevertheless, the combination of ray effects, large energy transition from top to bottom, difficulty of alignment of three or more targets with a charged particle beam, unpredictable transport of a charged particle beam past multiple conducting targets, and necessary bulky cooling structure make the prospect of any "point source" combination unattractive.

Thus, there is a need to find a better alternative. The most desirable alternative is to create an appropriate

source system which will produce a continuous flux distribution on the first wall. The solution to this is addressed in the following.

Since the distance from the axis of the blanket to the first wall is short, and due to the long mean-free-paths of the source neutrons, smoothing of the neutron flux on the first wall by scattering would be difficult (but not impossible) in the proposed FRBF. Also, too much scattering would alter the flux spectrum so it would not represent that incident on the first wall of a real fusion reactor blanket. The solution to this dilemma is to create an actual line source, which has never been done for a fusion reactor blanket experiment. A 14 MeV line source could be created by using an axial strip of TiT and a modulated deuteron beam. The d-beam would then have to come in the side of the cylindrical blanket, requiring a gap in the structure (as in Ref. 24). Studies conducted with the FBBF have shown that the neutron flux is unaffected by a discontinuity approximately 30 degrees in azimuth away from measurement location. An experiment to validate this prediction for a vacuum discontinuity in the FBBF will be performed during the unloading of the current blanket. If effects away from a discontinuity are also absent from the FRBF with a "slice" removed from the side, even at an acceptably greater azimuth, a greatly improved concept for fusion reactor blanket neutronics evaluations will have been developed. To

produce this line source, the d-beam will be directed along the target by a modulating electric or magnetic field, such that it produces a nearly exact chopped-cosine flux distribution in the center, at the first wall, and in the blanket. Figure IV.5 is a sketch of this configuration, including the source region, blanket components, and d-beam generator system. The advantages of this configuration will be many: no axial or radial ray effects, only very gradual variation of energy axially, much longer lifetime of the target, no problem with axial alignment of multiple targets in the path of a single beam, and most important, a source profile which matches the axial flux shape in the blanket. However, there will still be an energy and yield variation azimuthally; their effects on transport predictions require analysis. Although nearly-constant-density, long, thin tritium targets can be produced,<sup>35</sup> line targets could be constructed of short sections of TiT-plated copper. The tritium density of these targets can easily be measured by detection of Bremsstrahlung, which will ensure a consistent source strength.

The neutron source scheme described above requires evaluation of neutron transport. It also requires engineering design to determine d-beam production and control methods, source strength determination methods (a bank of recoil-alpha detectors), vacuum system requirements, and beam sweeping and control requirements; that evaluation

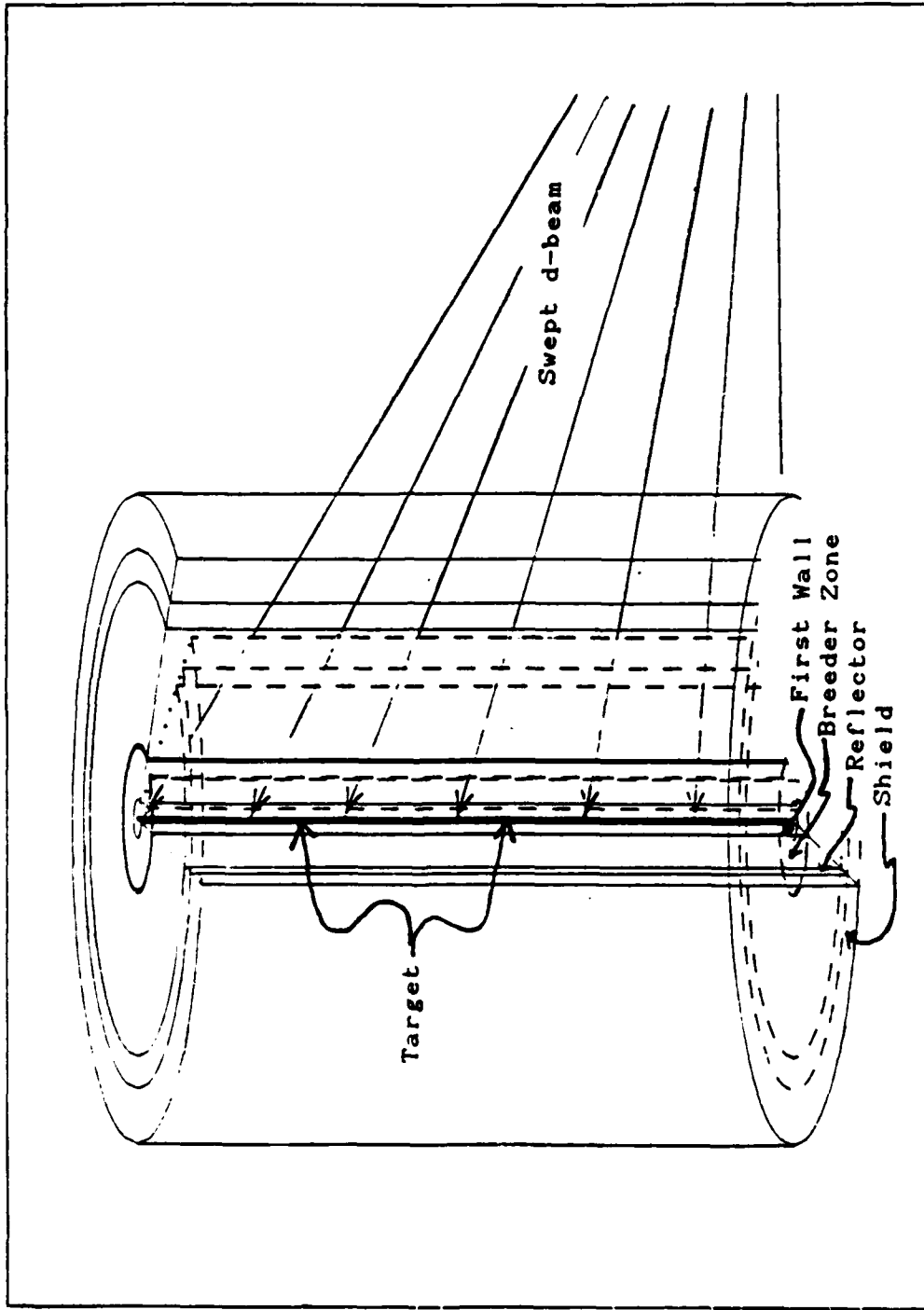


Figure IV.5. Sketch of the Fusion Reactor Blanket Facility.

is left to others. The presentation of the requirements for analysis of neutron transport in this proposed fusion reactor blanket simulation facility follows.

#### IV.7. Neutronics Analyses

The blanket design and source arrangement previously described will affect the transport of neutrons into, through, and out of the FRBF. Conversely, the transport of neutrons in the FRBF is the major factor defining the selection of the blanket design and the source arrangement. Therefore, the critical portion of the research reported in this paper involves neutronics analysis of the blanket/source configuration. The following should be considered:

- transport in the target support structure,
- effect of removing part of the azimuth,
- effect of azimuthal energy and yield variation.

Transport through the structure surrounding the actual target design (backing, coolant channels, support, etc.) should be evaluated to determine its effect on the neutron flux and spectrum throughout the system. Any adverse effect must be minimized to reduce perturbations which cannot be treated exactly in 2-dimensional transport codes. However, the construction of the source in a long target will reduce the thermal flux (per unit area) by about two orders of magnitude, thus reducing the requirement for extensive

cooling structure. The almost symmetric vacuum tube located a distance from the source also eliminates some of the asymmetry of previous sources caused by support and cooling structure. Additionally, the target can be constructed so that it is convex, thus offering no long, straight path for neutron attenuation in the radial direction. Then, absorption and scattering of the source neutrons will be almost negligible, and will not contribute significantly to asymmetry of flux distributions in the blanket. Therefore, the source region can be treated as a symmetric target, and extensive neutronics analyses of the target system are not required for this research, although these analyses must be done for the evaluation of experiments in a final system.

The effect of removing part of the blanket for the d-beam port must be analyzed to determine if it severely affects the flux or spectrum many mean-free-paths from the discontinuity. An azimuthal segment without large flux deviations spanning only  $45^\circ$  to  $135^\circ$  from the asymmetry will allow an experimental arc of about 40 to 100 cm in the breeding zone and 150 cm at the outer edge of the shield. To reduce the costs of multiple evaluations, the effect of the asymmetry also must be minimized to maintain approximately 1-dimensional geometry. Finally, the effect of the azimuthal asymmetry of flux and spectrum, due to the anisotropic neutron source, must be determined.

The previously mentioned effects were determined by comparing 1-D transport predictions (symmetric blanket with isotropic source) to 2-D predictions (asymmetric blanket with anisotropic source). The method used to make those predictions and comparisons is presented in the following chapter.

## V. NEUTRONICS ANALYSES OF TWO FRBF MODELS

The preceding chapters explained the requirements for more and better fusion blanket experiments, and described a proposed new facility, the FRBF, for conducting those experiments. To insure a new experiment or facility will yield improved data, it should be analyzed to help eliminate design deficiencies. This chapter describes the analysis of neutron transport through the two models which were selected for analyzing the FRBF design. To perform such an analysis, a neutron transport code is required. The code requires a correct source description for input, an appropriate set of group constants to describe the materials' transport characteristics, and correct modeling of the system geometries. The neutron transport code used for this analysis is discussed first, followed by a description of the method used to generate the isotropic and anisotropic source files for input to the code. Then, the source and production of the group constants used in this analysis is discussed, along with a presentation of the importance of inelastic scattering reactions in fusion materials. Finally, the use of the different models for analyzing transport through the FRBF is described. The order of

investigation of the transport is presented with a discussion of the output data, which was used to produce the information presented in Chapter VI, Neutronics Results.

#### V.1. DORT, A Transport Code

A new discrete ordinates theory (D.O.T.) code was used to analyze effects on neutron transport predictions due to the proposed geometry and source configuration of the FRBF. The code, DORT 1.0, was produced by the Reactor Shielding Information Center (RSIC) at ORNL. This code is an upgraded version of DOT 5.1, which was the next generation of the DOT series.<sup>36</sup> The previous version, DOT 4.3, is in wide use at many laboratories and industries, and was used by the BCSS for blanket design and selection studies and by RSIC for deep penetration (shielding) problems. Prior to this research, no version of DOT was available at Purdue University. RSIC gave this DORT package to Purdue for modification and validation; it was converted for this research to run on the Cyber 205 vector supercomputer, and it was thoroughly tested with documented sample problems prior to use for FRBF analyses. The sample problems included those supplied with the DOT 4.3 and DORT code packages, and two problems using EPRI-Cell cross sections. In most cases, the Purdue University version of DORT produced results which were identical (effective  $k$  and flux values) to the reference (Cray) cases from RSIC. Using the

EPRI-Cell benchmark cross sections, DORT produced almost identical results (differences  $\sim 0.01\%$ ) compared to TWODANT<sup>27</sup> (D.O.T.) and 2DB<sup>28</sup> (diffusion theory) results computed at Purdue.

The DORT code is a multi-capability program offering many alternatives for input, output, source types, mesh spacing, quadrature sets, etc. It allows variable mesh spacing and quadrature, and accepts a variety of sources (alone or combined); internal and/or external boundary sources, distributed source, first-collision source, etc. An additional feature is a capability for removing negative fluxes which result from truncation of a polynomial expansion of the scattering term in the D.O.T. treatment. This function is especially useful where there are large void regions. Another extremely useful feature is the capability to save flux, flux moment, and boundary source files; then to use those as input or re-start data for subsequent problems. This feature was used for investigations of R-Z and R- $\theta$  geometries, with either a distributed or a boundary source. The generation of these sources is explained in the following section.

## V.2. The Anisotropic Neutron Source

Production of neutrons by the  $T(d,n)\alpha$  reaction was described earlier as being dependent on the energy of the

deuteron beam. Slowing down of the beam ions in the target causes a distribution of neutron energies at any angle of emission. The treatment of this was described clearly in Ref. 32, which includes tables of the energy-angle correlation. The Fortran program included in Ref. 32 was modified for this research, and is listed in Appendix B. It employs the slowing down and energy-angle correlation to produce a table of neutron emission probabilities as a function of energy group and angle interval. However, the angular treatment was improved for a better approximation to the integral over emission angle in the forward and backward directions (near  $0^\circ$  and  $180^\circ$ ). Table V.1 is one result of this program, with the distribution computed for a beam energy of 150 KeV. Note that the isotropic probability between 0 and  $20^\circ$  would be 0.03015, while the anisotropic probability is 0.03155 (~5% difference). This program also predicts the theoretical emission rate of neutrons per milliamp deuteron-beam current; Figure V.1 is an illustration of this relationship. These values are in good agreement with others,<sup>39</sup> as are the probabilities versus angle and energy, which were used to generate sources for the neutronics evaluations.

The results in Table V.1 were used in two ways for input to the transport calculations. For 1-D predictions, the probabilities for each energy group were summed over all directions, so the input spectrum (at the bottom of Table

Table V.1. Multi-group Angular Distribution of d-T Neutrons.

Emission Interval (degrees)	Energy group and energy interval (MeV)					Total Prob.
	1 14.6-15.7	2 14.2-14.6	3 13.8-14.2	4 13.5-13.8	5 12.5-13.6	
0-20	2.953e-2*	2.024e-3	8.638e-9	0.000e-0	0.000e-0	3.155e-2
20-30	3.450e-2	3.922e-3	2.425e-8	0.000e-0	0.000e-0	3.842e-2
30-40	4.237e-2	9.564e-3	1.726e-7	0.000e-0	0.000e-0	5.193e-2
40-50	3.791e-2	2.577e-2	7.582e-7	0.000e-0	0.000e-0	6.368e-2
50-60	1.206e-2	6.125e-2	8.717e-6	0.000e-0	0.000e-0	7.332e-2
60-70	0.000e-0	8.036e-2	1.899e-4	0.000e-0	0.000e-0	8.055e-2
70-80	0.000e-0	7.909e-2	6.097e-3	0.000e-0	0.000e-0	8.519e-2
80-90	0.000e-0	1.449e-2	7.266e-2	0.000e-0	0.000e-0	8.715e-2
90-100	0.000e-0	0.000e-0	8.644e-2	0.000e-0	0.000e-0	8.644e-2
100-110	0.000e-0	0.000e-0	8.314e-2	0.000e-0	0.000e-0	8.314e-2
110-120	0.000e-0	0.000e-0	1.863e-2	5.878e-2	0.000e-0	7.741e-2
120-130	0.000e-0	0.000e-0	1.003e-3	6.846e-2	0.000e-0	6.946e-2
130-140	0.000e-0	0.000e-0	9.929e-5	5.949e-2	0.000e-0	5.959e-2
140-150	0.000e-0	0.000e-0	1.796e-5	3.603e-2	1.203e-2	4.808e-2
150-160	0.000e-0	0.000e-0	3.834e-6	1.586e-2	1.941e-2	3.527e-2
160-180	0.000e-0	0.000e-0	1.310e-6	8.413e-3	2.037e-2	2.878e-2
Spectrum	1.564e-1	2.765e-1	2.683e-1	2.470e-1	5.181e-2	1.000e-0

\*Read 1.000e-2 as  $1.000 \cdot 10^{-10}$ , values are probability of emission of a d-T neutron into the solid-angle interval and energy group. Sums of the columns gives the spectrum, while sum of a row gives the total probability of emission of a neutron into a solid-angle interval.

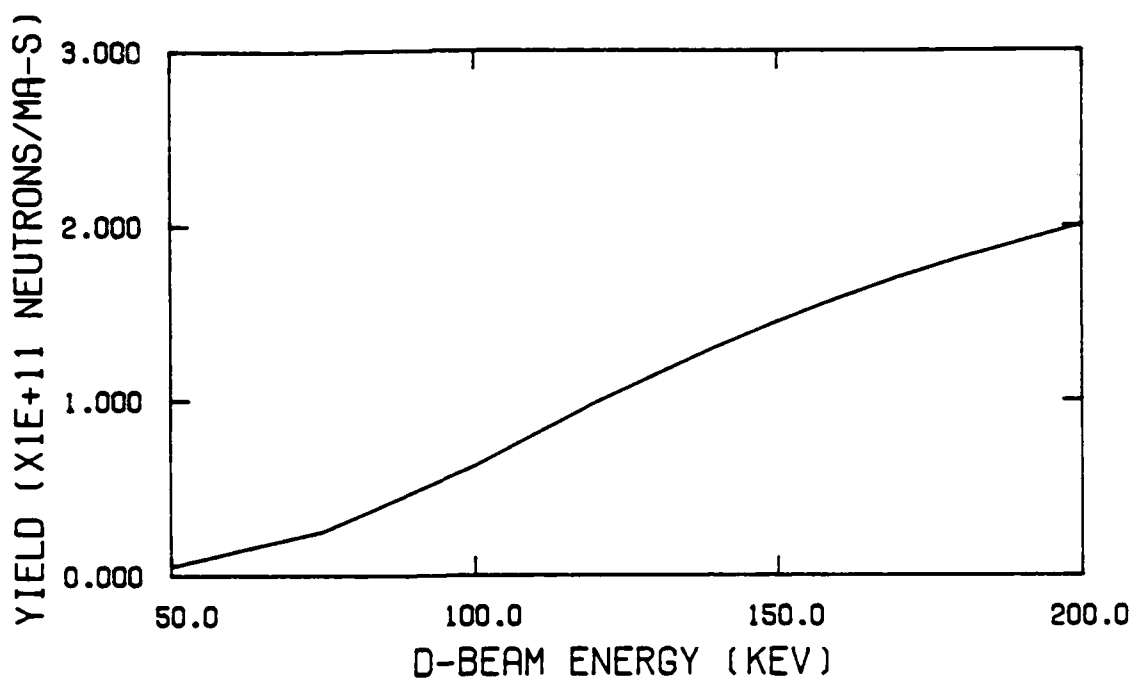


Figure V.1. Yield of d-T Neutrons vs d-beam Current. Based on numerical integration of the slowing down equation for deuterons in  $TiT_2$ , assuming the  $TiT$  layer is thick enough to stop the deuterons.

V.1 was an isotropic distribution of those five groups. For the 2-D, asymmetric blanket analyses, a second Fortran program was written which correlated the direction cosine of the face of a mesh space ( $\cos\phi$ ) and the direction cosines of the quadrature set ( $\mu$  and  $\eta$ ) with the angle of emission of the neutron from the target ( $\theta$ ). The equation which relates these angles and directions is

$$\cos \theta = \mu \cdot \cos\phi - \eta \cdot \sin\phi. \quad (5.1)$$

The direction cosine with respect to the radial direction is  $\mu$ , and the direction cosine with respect to the azimuthal direction is  $\eta$ . The program selects from the table a

relative probability corresponding to  $\theta$ ; then it assigns that value to the source for that mesh point, direction, and energy group (there are 5 groups times 96 directions for an  $S_{12}$  direction set, or 480 source values per boundary space mesh). This code was used to produce a multi-group anisotropic source for 2-D investigations.

Neutron transport in similar blankets with a plasma source in the center, rather than the boundary source, was also predicted. The source spectrum used for this prediction was taken from VITAMIN-E, which is a 174-neutron-group library taken from ENDF/B-V cross sections.<sup>40</sup> This source is based on a DT plasma at 25 KeV, with a Maxwellian velocity distribution. This plasma spectrum was also used to collapse the cross section library to a set of working group constants for this research. The isotropic source spectrum described previously and the fusion spectrum are listed along with the energy group structure and lethargies in Appendix A. These sources can then be used with the correct geometric models in the DORT calculations, after the transport cross sections are determined. A description of the production of those group constants follows.

### V.3. Cross Sections

So that the results of this study could be compared with future research, the most up-to-date cross sections were

obtained for the transport computations. The group constant library used to begin the transport investigation was produced by R. Roussin at RSIC from the VITAMIN-E (ENDF/B-V) library. He used a series of programs to select the fifteen isotopes and to collapse the 174-neutron-group data base to 50 groups, with a  $P_3$  scattering expansion. Upscatter was not included, and no neutron production cross sections were included. Tritium production cross sections were also not provided with this data set. The energy bounds and lethargy widths are listed in Appendix A. The collapsed (but unmixed) library was transmitted on a tape for use at Purdue University. A second library, including the same isotopes, but also including tritium breeding constants, was generated by I. Dilber from the MARS/VITAMIN-E package recently activated on the Purdue University computer system. The final transport calculations were completed using this forty-one-group library, after checking for consistency with the RSIC-supplied constants. However, the constants from either source required mixing and manipulation prior to input to DORT.

The cross sections were prepared for input to the DORT code by processing them through GIP, another program in the DORT package of codes. GIP accepts isotope-ordered cross sections, combines them in accordance with an input mixing table, and its output is a group-ordered library of mixed constants suitable for use by DORT, ANISN, DOT 3, or DOT 4.

GIP was used to prepare the material constants by using the number densities listed in Appendix A. Additionally, pure  ${}^6\text{Li}$  and  ${}^7\text{Li}$  constants were supplied for Blanket HeC to compute reaction rates for tritium breeding comparisons. In Blanket LLC, because  $T_2$  contributes only 0.2% to the breeding,<sup>1</sup> tritium breeding was not computed for the individual isotopes, only for the total material. The macroscopic constants which were produced by GIP were then used for the transport predictions with the models described in the following section.

This is an appropriate place to emphasize the importance of the inelastic reaction to neutronics in fusion reactor materials. Table V.2 lists elastic and inelastic scattering cross sections for a few important isotopes in fusion reactor blankets, shields, first walls, and magnets. The two types of reactions occur on the same order of magnitude. However, the energy loss in the two reactions is very different. Figure V.2 illustrates the energy loss due to inelastic reactions for lead and copper. These cross sections were taken from LIB-IV.<sup>41</sup> On the average, in a single collision, a 14 MeV neutron loses 12.1 MeV in Pb (86%); in contrast, only 0.2% is lost in an elastic collision. The energy which is lost in these inelastic collisions is deposited locally due to short-range gamma-rays emitted in the decay of excited nuclei. Thus, a large part of the power density in fusion reactor materials is due

Table V.2. Scattering Cross Sections for Fusion Reactor Materials

Isotope	Energy (MeV)	Elastic Scatter	Inelastic Scatter	Energy Left
<sup>6</sup> Li	14	0.97*	0.372	0.936
	10	1.25	0.589	0.888
	1	1.05	0.000	0.769
<sup>7</sup> Li	14	1.01	0.370	0.929
	10	1.41	0.538	0.885
	1	1.38	0.179	0.763
Fe	14	1.23	0.782	0.992
	10	1.98	1.47	0.993
	1	2.13	0.325	0.997
Cu	14	1.39	0.894	0.995
	10	2.10	1.56	0.994
	1	2.92	0.269	0.974
Pb	14	2.91	0.359	0.998
	10	3.36	2.32	0.997
	1	4.82	0.223	0.992

\*Cross section in barns. Energy left is the average of the neutron's original energy which remains after one elastic collision. This can be contrasted to the much lesser fraction remaining (0.05 to 0.20) after one inelastic collision.

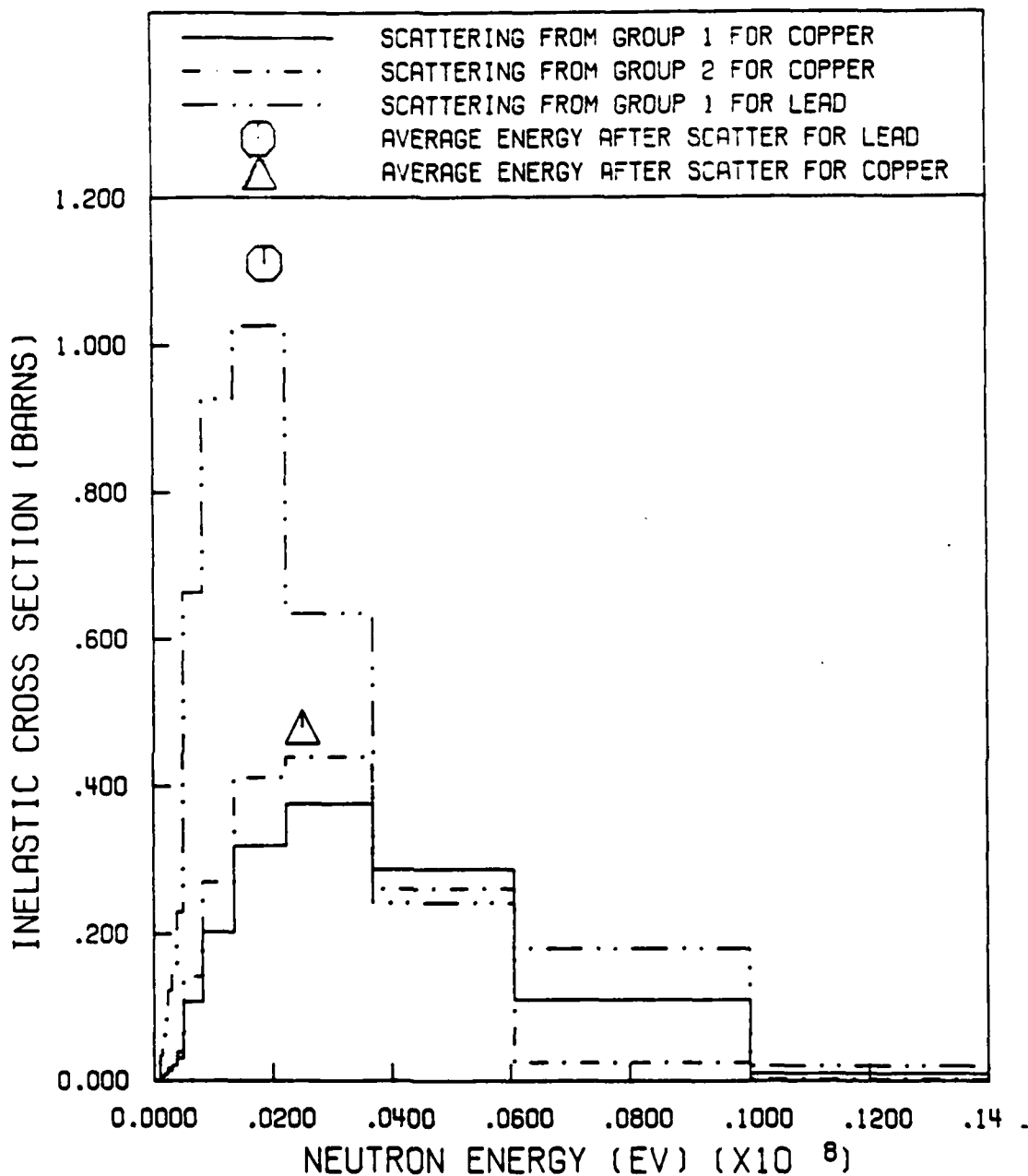


Figure V.2. Inelastic Scattering Cross Sections of Copper and Lead from 14 MeV Neutrons.<sup>41</sup> This figure demonstrates the large energy losses due to inelastic scattering of 14 MeV neutrons in lead and copper, and of 6-10 MeV neutrons in copper. The average energy of the neutron following the scatter is indicated. Thus, the average 14 MeV neutron scattered inelastically in lead deposits 12.1 MeV (86%) of its energy in the lead nucleus. This energy is dissipated locally as decay products.

to the inelastic scattering process. Another demonstration of the importance of this reaction is shown in Figure V.3, which compares the energy loss due to elastic scattering with the loss due to inelastic scattering in one FRBF model. This figure represents the product of the isotopic reaction rate with the average energy loss rate for the inelastic or elastic reaction (based on results from Chapter VI). It demonstrates that the power density due to inelastic scattering will be a factor of ten greater than that due to elastic scattering in a fusion reactor.

The important conclusion to be drawn from this is that knowledge of inelastic cross sections is critical for predicting the location and density of energy deposition in a fusion reactor system. However, accurate determination of these cross sections is very difficult due to the high-energy sources required, the multitude of competing reactions, and the spread of energy and direction of neutrons emitted in the various reactions. Therefore, these complicated scattering kernels or two-dimensional matrices of inelastic reactions are not accurately determined. Neither can the power distribution in a fusion reactor be accurately predicted, based on available cross section information and current computational methods. As this knowledge is critical for accurate prediction of neutronics and heat production for fusion reactor design, experimental studies are required to increase confidence in the data and

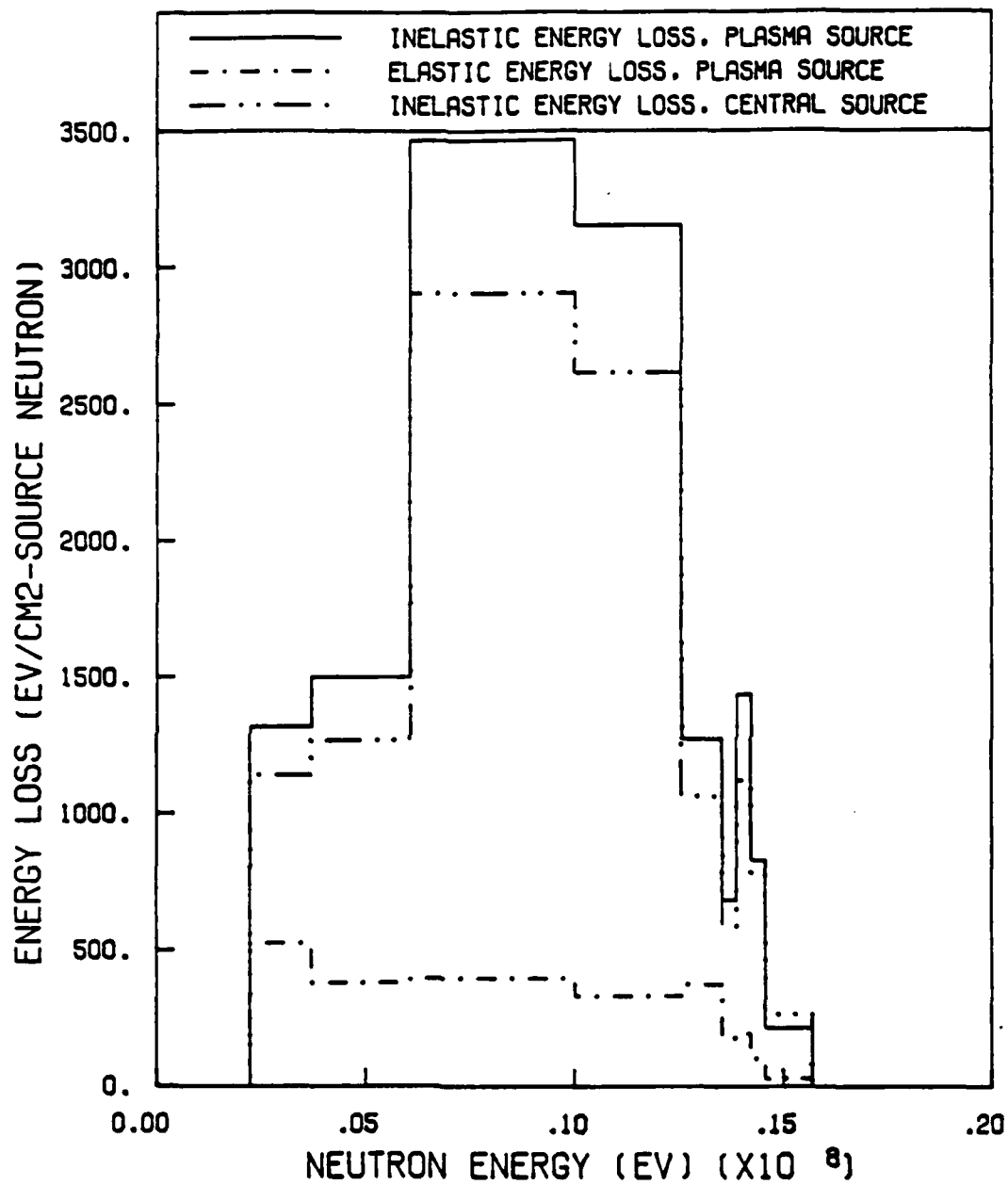


Figure V.3. Energy Loss in Blanket HeC Due to Scattering Reactions.

capability to accurately compute this information.

#### V.4. Computational FRBF Models

Four different models were required for the evaluations for this research. First, an R-Z, 2-D calculation was done using a  $P_3$  expansion of the scattering cross sections and an  $S_{16}$  quadrature set. The results of this calculation were used to estimate  $DB^2$  leakage for input to the R- $\theta$  computations, and for demonstrating the benefits of proper source selection (shape). The blanket was divided on the plane and axis of symmetry; it was treated only from the mid-plane up and the axis out, with axial mesh spacing every 5 cm (about 1/2 mean-free-path for fusion-energy neutrons). The bottom and left (center) boundary conditions were reflective, while the top and right (outer) boundary conditions were void.

The radial geometries of the R-Z and R- $\theta$  computations were identical; the spacing was given in Figures IV.2.A and B. The breeder zones were divided into 5 cm spacing (again  $\sim 1/2$  MFP), while the reflector or plenum and the shield were of slightly coarser mesh. The azimuthal intervals were  $10^\circ$ , with only one-half azimuth of the blanket modeled (18 intervals). The boundary conditions for the azimuthal surfaces were reflective, the left (center) boundary condition was cylindrical, and the right (outer) boundary condition was void.

The  $DB^2$  leakage from the R-Z computation was then used in a 1-D calculation to determine the flux and tritium production for a symmetric system with an isotropic distributed source. These results could then be compared to the results from a computation with an asymmetric model. The model for this 2-D computation included a  $10^\circ$  segment which contained a vacuum (air at  $10^{-3}$  atm). Also included was a SS wall in the next  $10^\circ$  segment between the vacuum tube and the first wall. The vacuum region simulated the section removed from the blanket for the incoming d-beam, and the SS wall represented the containment necessary to maintain a vacuum for the neutron generating system. The radially outermost mesh space of the first azimuthal interval contained shield material, rather than vacuum, to represent the closure of the vacuum system and shielding and instrumentation which will be required for the neutron generating system. Figures V.4.A and B illustrate the radial zone boundaries and the asymmetry for the blanket models. The  $10^\circ$  intervals represent a SS wall 3.8 cm thick at the first wall, a 7.7 cm vacuum gap (2 times the half-geometry) at the first wall, and a 35 cm section at the outer radius of the shield. These large dimensions can be considered upper limits on the expected asymmetries; they should produce maximum deviations in the results.

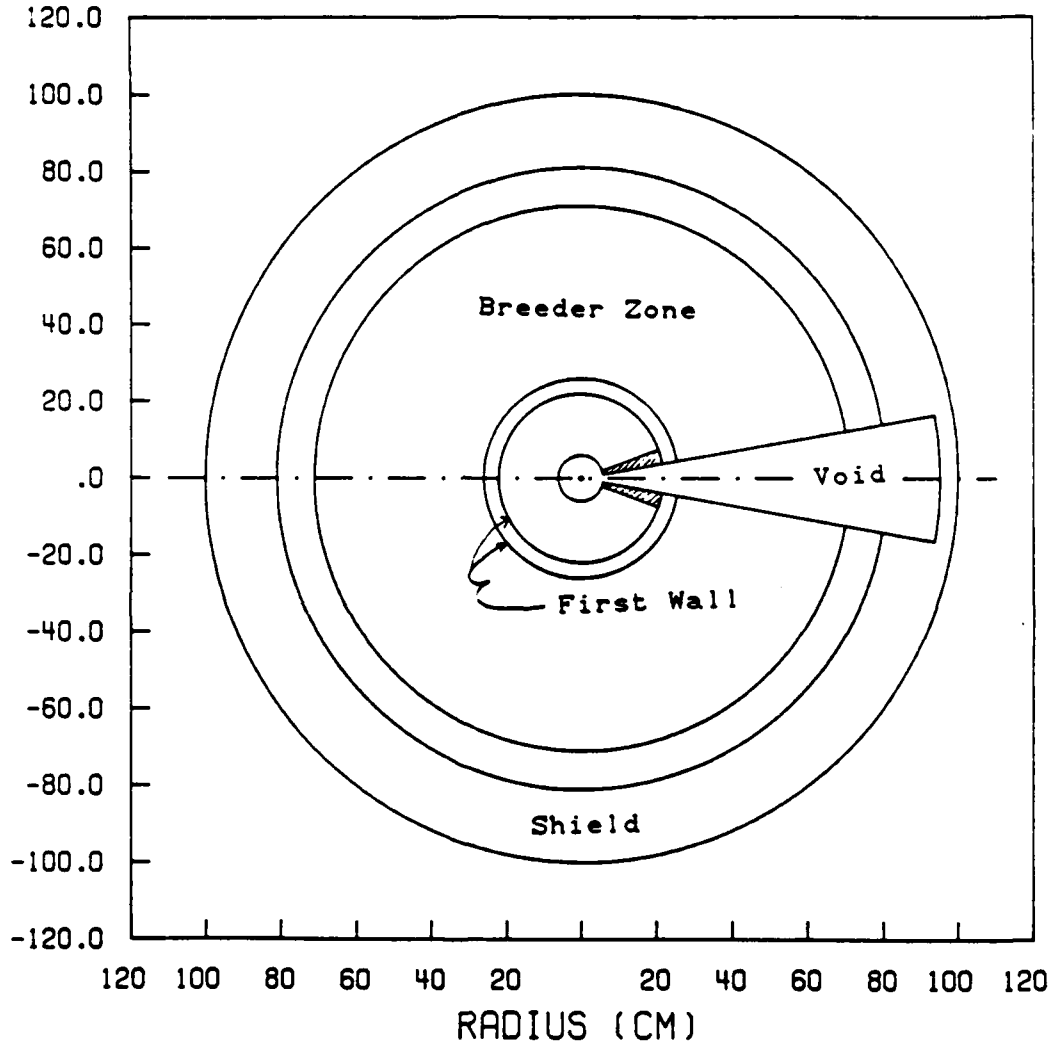


Figure V.4.A. Geometry of Blanket HeC, R- $\theta$ .

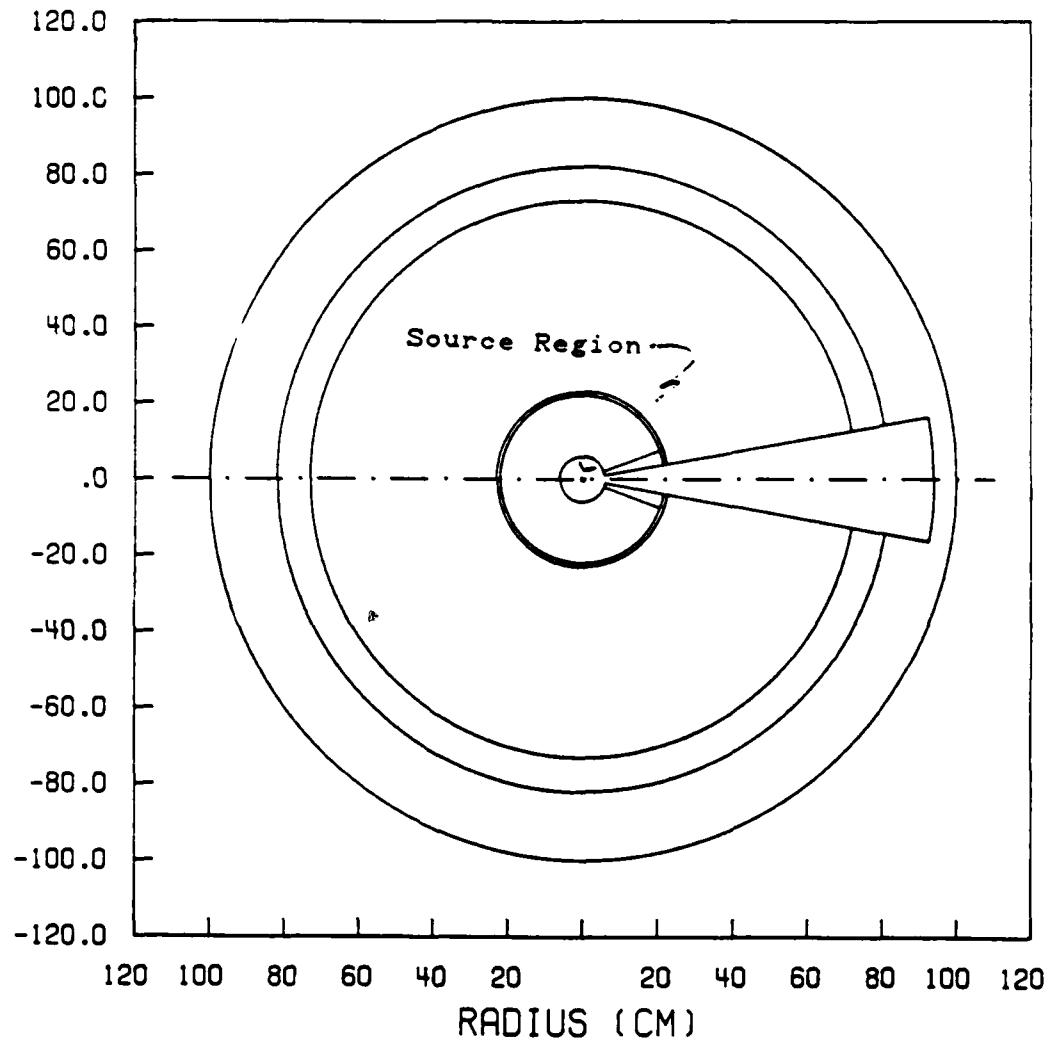


Figure V.4.B. Geometry of Blanket LLC, R- $\theta$ .

Two more models were used to estimate the differences between experimentally validated blanket physics and actual fusion reactor physics. The first was similar to the 1-D model discussed previously; however, the axial leakage was zero (as in an infinite system or the center of a long system). The second model was also 1-D with zero leakage, but instead of a source distributed in a thin target in the center, a plasma source was distributed in a 16-cm-radius vacuum region. These two models were used for both blanket compositions to determine flux profiles and tritium production rates. These four models were used to predict neutron transport through both Blankets HeC and LLC; the results are displayed in the following chapter.

## VI. NEUTRONICS RESULTS

The preceding chapters discussed the requirement for a new facility for testing neutron transport in fusion reactor blankets, a conceptual design for a facility which will meet that need, and the theory behind the design of that facility--the FRBF. Chapter V described a neutronics code to analyze that proposed design, the models and sources necessary for the analysis, and the group constants which could be used to predict the transport of neutrons. This chapter presents and compares the results of that neutronics evaluation. The results are presented in graphical and tabular forms as flux calculations and tritium breeding results from the various computations. This chapter discusses the neutronics results in the same order as the calculations were discussed in section V.5: R-Z, 1-D R- $\theta$  versus 2-D R- $\theta$  with asymmetry, and 1-D R- $\theta$  central source versus 1-D R- $\theta$  plasma source. The results of each model are presented as the appropriate flux comparison, tritium breeding comparison, etc. All results have been normalized to a per-source-neutron basis for each model. Each result for Blanket HeC is followed immediately by the result for Blanket LLC in each section. An attempt is made to present

the results in the most informative manner for the aspect to be demonstrated, as group-flux profiles, position-dependent spectra, flux ratios, or tritium production profiles. Since the R-Z analysis was required for buckling corrections for input to the R- $\theta$  predictions, and to demonstrate the adequacy of the cosine-shaped axial source, it is presented first.

#### VI.1. Results of 2-D, R-Z Analyses

The R-Z computations were completed to satisfy three separate needs:

- buckling corrections were needed for the R- $\theta$  geometries, to obtain more realistic transport results;
- axial source and group-flux profiles were needed to demonstrate the suitability of the cosine-shaped line source; and
- leakage fluxes were needed to calculate dose rates in the FRBF and surrounding areas.

The buckling coefficients which were obtained for Blankets HeC and LLC were used as input to the R- $\theta$  predictions. No presentation of those values is given here, as they would demonstrate nothing significant. However, the axial flux profiles, which develop due to a chopped-cosine-shaped line source, are extremely important, as this is the basis of one of the major advantages of the FRBF. Normalized axial flux profiles, which should approximately match the source profile, are shown in Figures VI.1.A and B. These figures

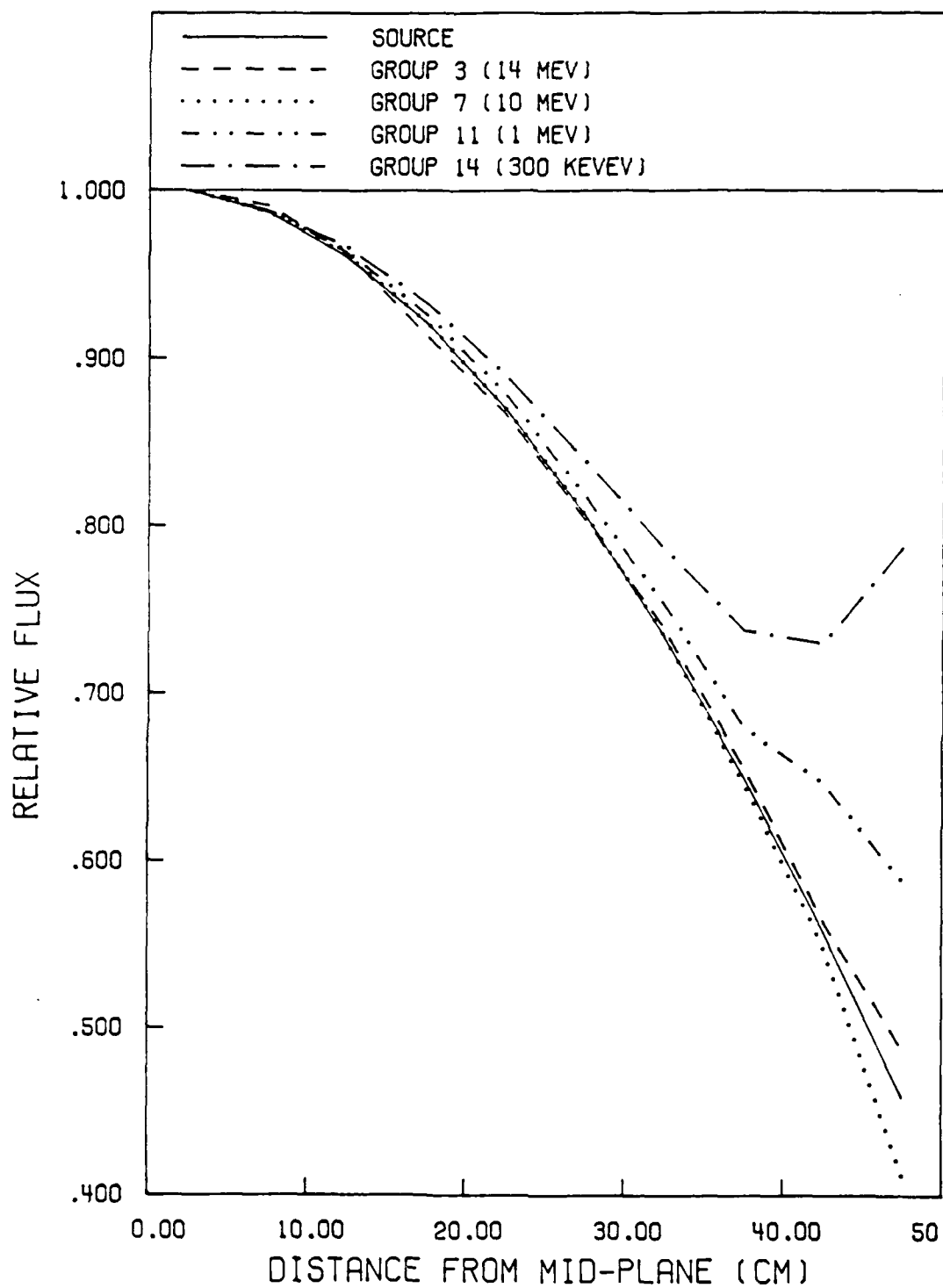


Figure VI.1.A. Axial Group-flux Profiles in Blanket HeC.

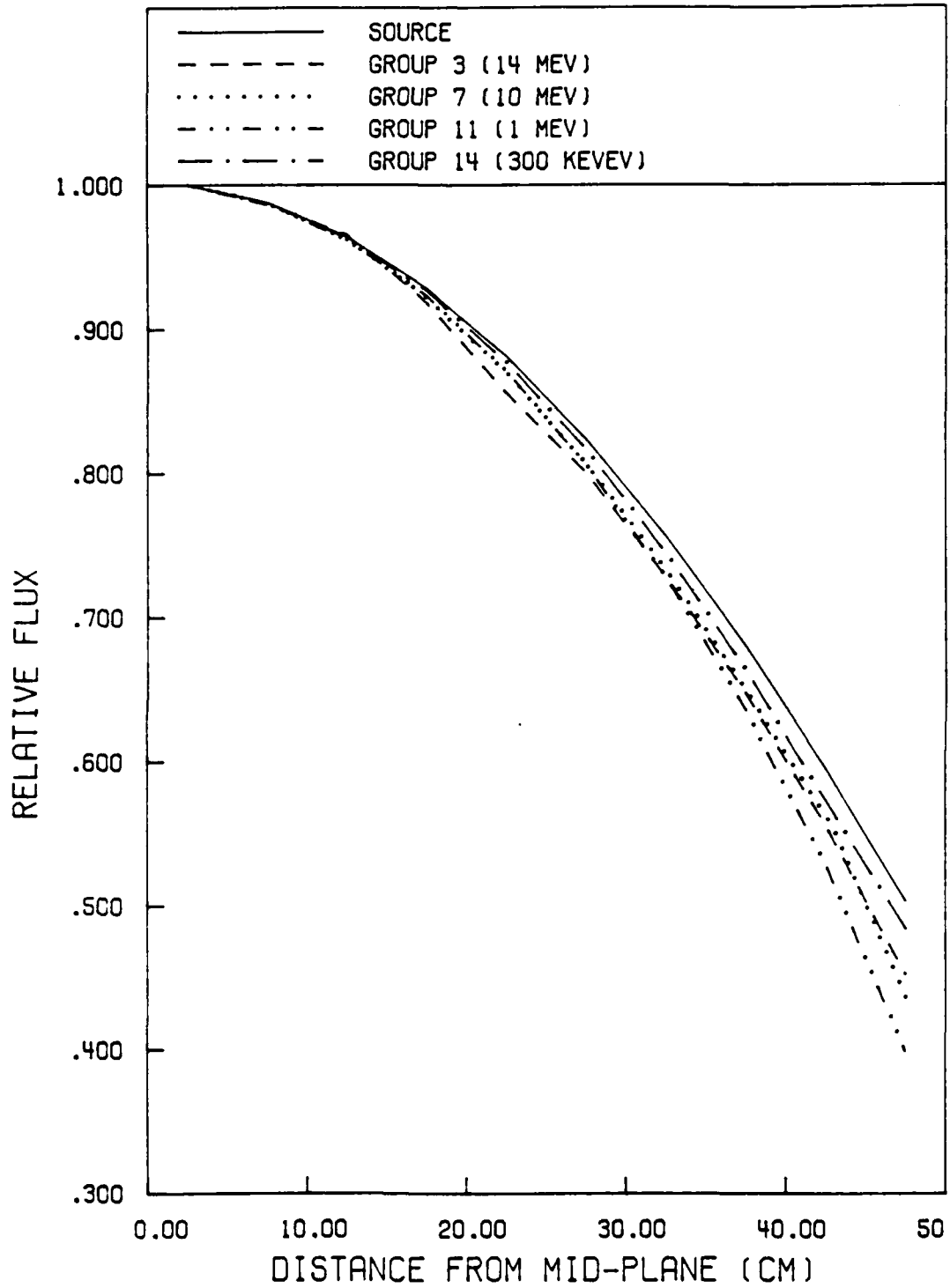


Figure VI.1.B. Axial Group-flux Profiles in Blanket LLC.

also include the source profile, which is a chopped-cosine function in the axial dimension (same for all source groups). The approximate equality of the flux profiles with the source profile demonstrates the suitability of the cosine-shaped line source to this geometry (Figure IV.3 showed how a point source, which is a delta function at the mid-plane, transitions to a gaussian at the first wall; the flux profile does not match the source profile). The variation of flux profile from the cosine distribution at the top (and bottom) of blanket HeC, near the shield, is from isotropic, elastic scattering of lower-energy neutrons in the top shield. This strongly supports the previously stated belief that spectrum transition will be a large factor in a fusion blanket. Figures VI.2.A and B show the spectra in various regions of the blankets, and Figures VI.3.A and B present the radial flux profiles for groups 3 (~14 MeV), 7 (~10 MeV), 11 (~1 MeV), and 14 (~300 KeV). These two figures also help demonstrate the flux transition within the blanket. The neutron spectrum gets 'softer' as the flux travels through the blanket (due to downscattering). However, Figures VI.2.A and B demonstrate that the spectral shapes are almost identical axially; there is no axial energy dependence of the flux. Finally, the axial tritium production predicted for the blankets is illustrated in Figure VI.4.

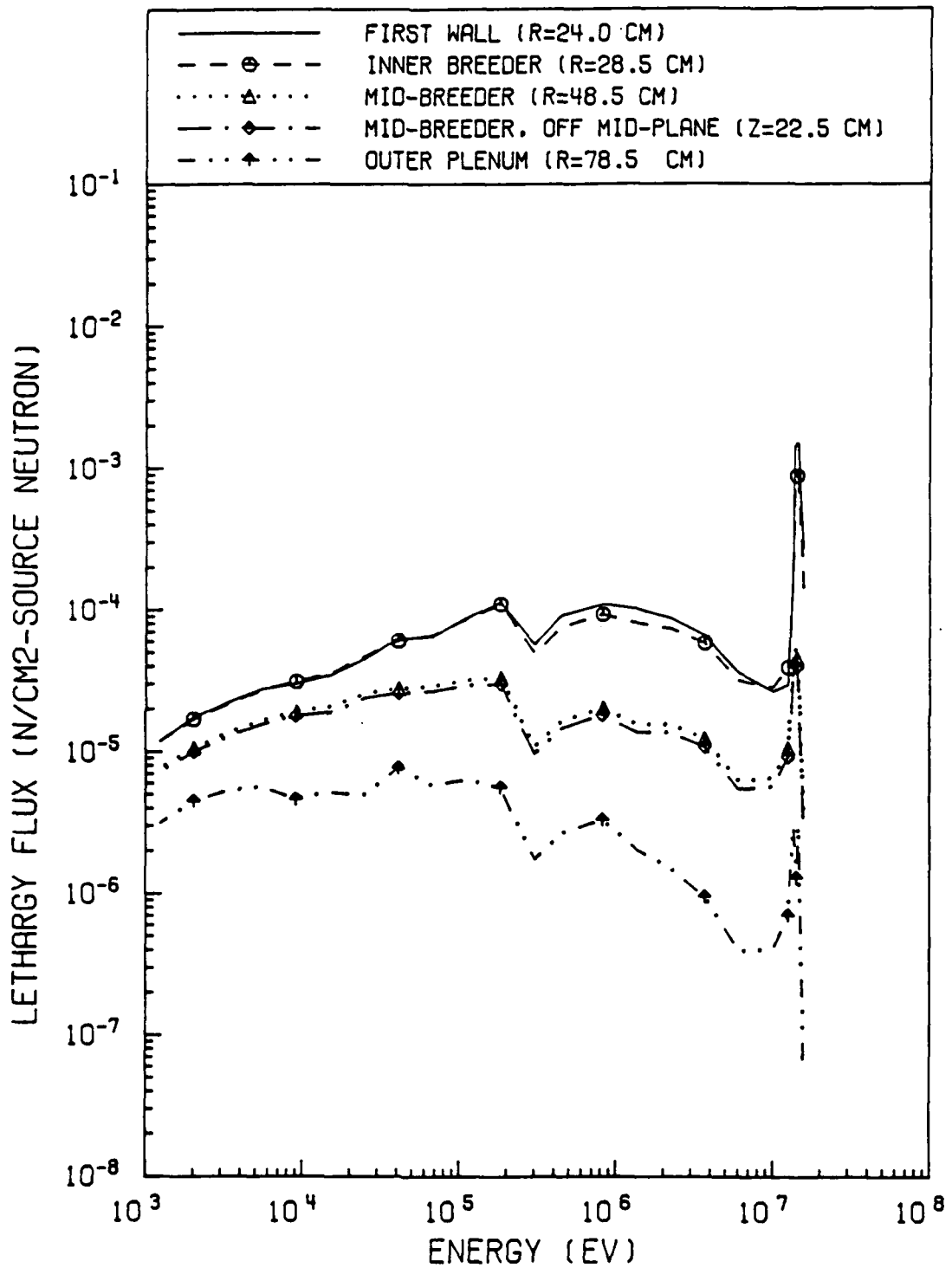


Figure VI.2.A. Neutron Spectra in Blanket HeC, R-Z.

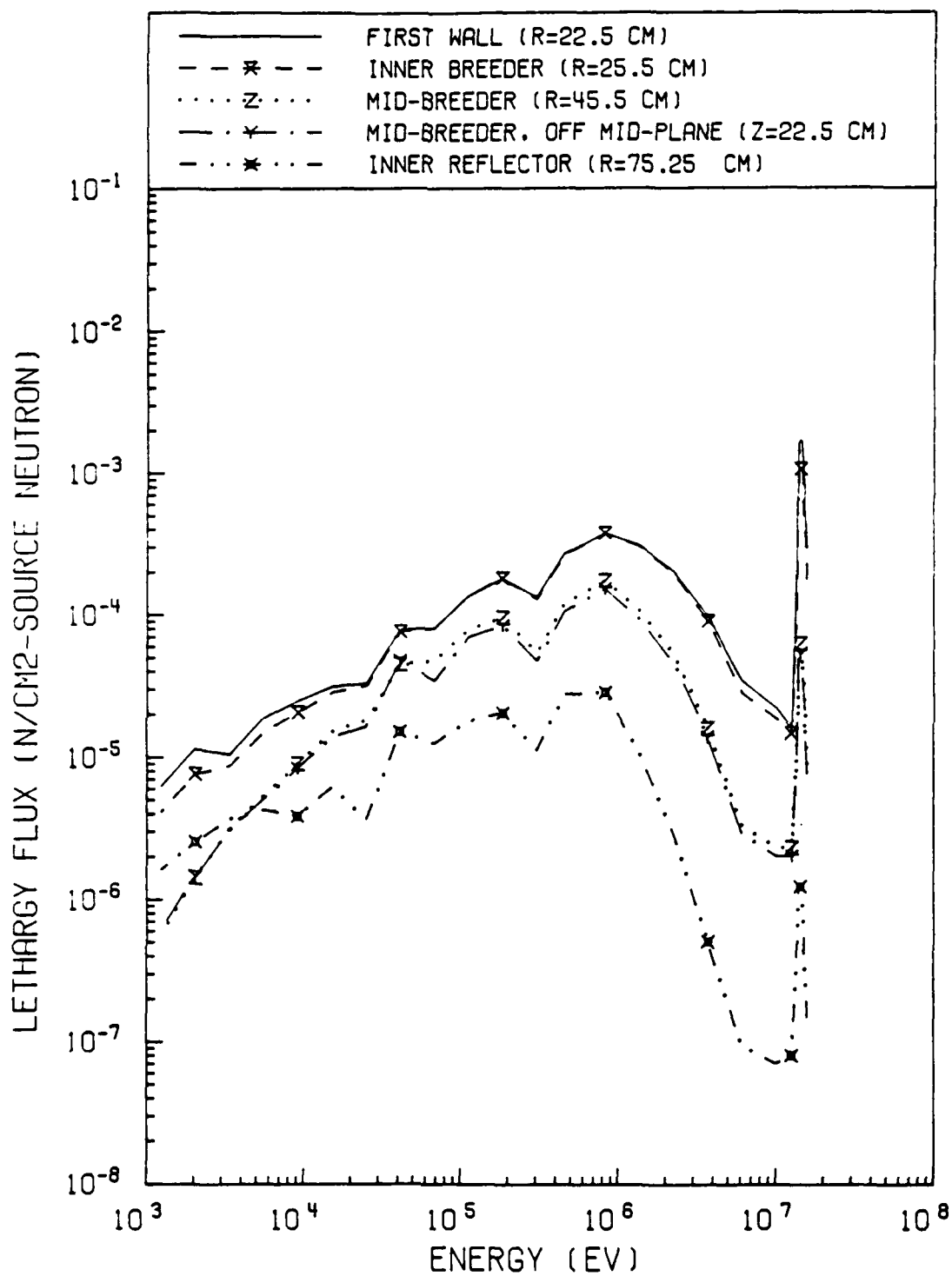


Figure VI.2.B. Neutron Spectra in Blanket LLC, R-Z.

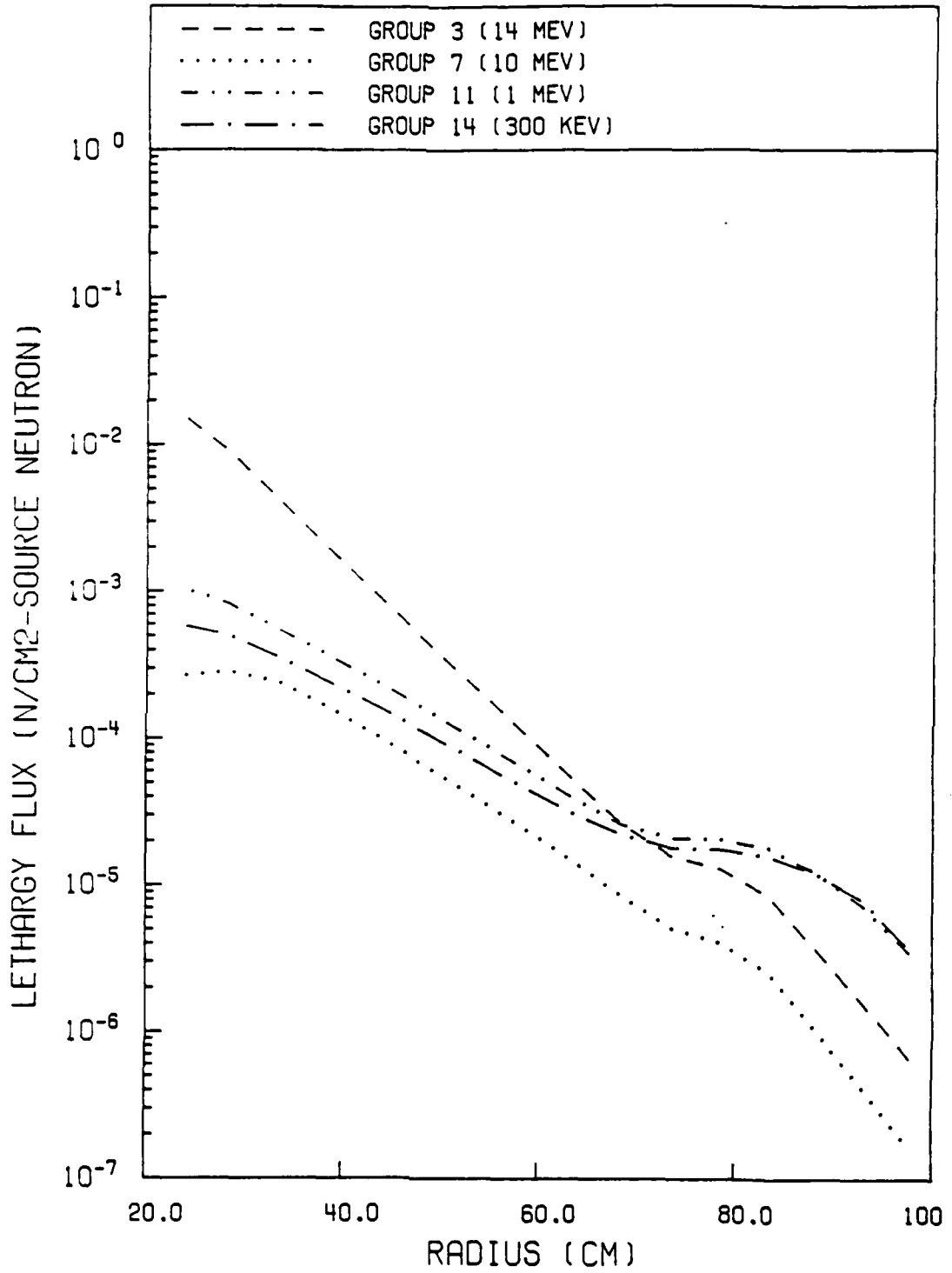


Figure VI.3.A. Radial Group-flux Profiles in Blanket HeC, R-Z.

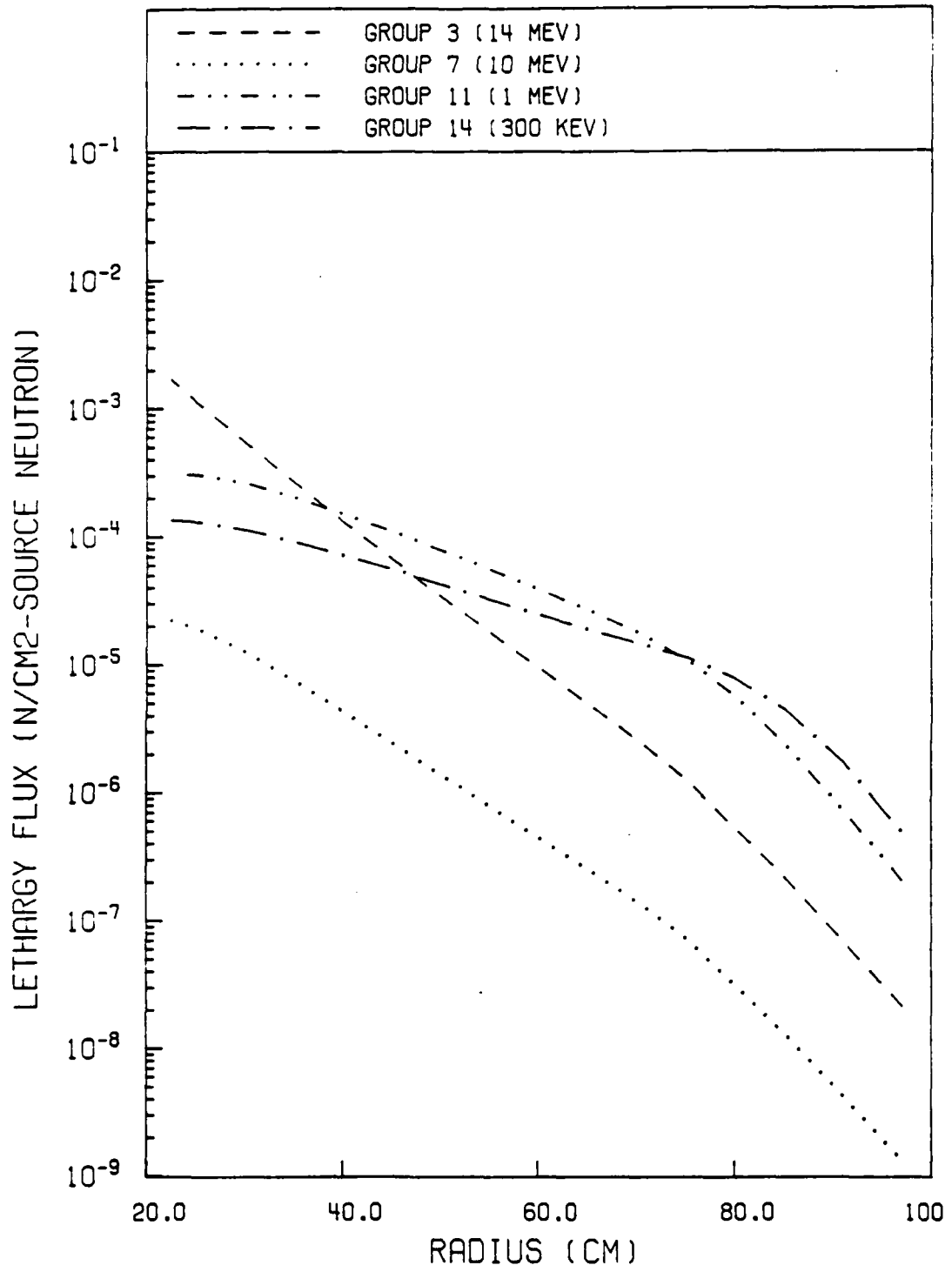


Figure VI.3.B. Radial Group-flux Profiles in Blanket LLC, R-Z.

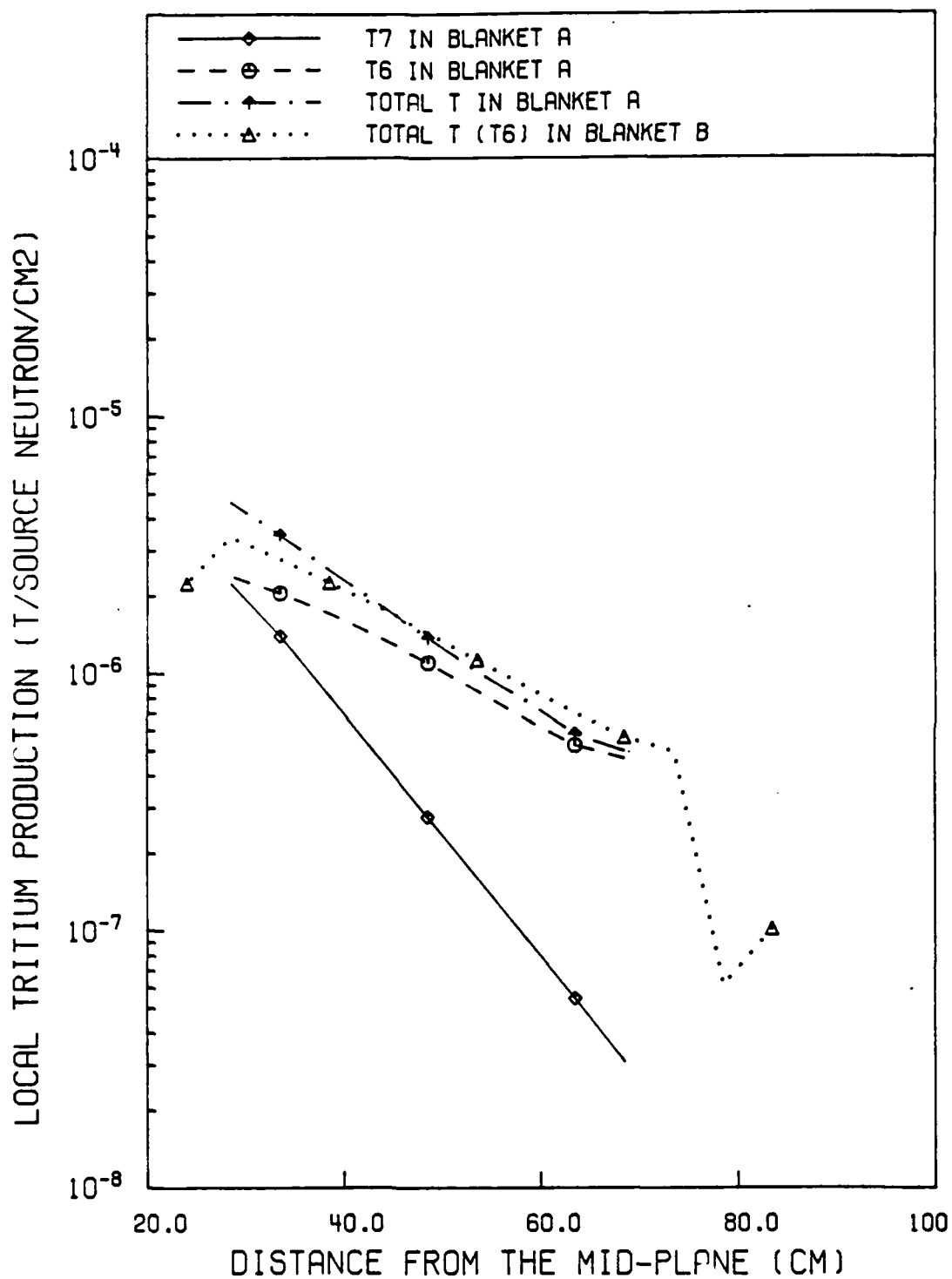


Figure VI.4. Radial Tritium Production at the Mid-plane, R-2.

## VI.2. Comparison of 1-D and 2-D R- $\theta$ Results

To determine the effects of the asymmetry of this design of the FRBF, a 2-D transport computation was performed. This section presents the results of the comparison of the 2-D asymmetric models to the 1-D symmetric models, both with isotropic distributed sources. The first figures, Figures VI.5.A and B, present the flux ratios for various groups at mid-breeder as they vary with azimuth. The flux ratio is defined as the value of flux obtained from the 1-D model divided by the value from the 2-D model. These figures demonstrate that in an arc of about 90° to 180° away from the asymmetry, the high-energy 2-D flux is within ~2% of the 1-D prediction. The lower-energy ratios deviate more from 1 in the Blanket LLC, which is an unexpected result. This may be due to a lack of capture of neutrons in the void region, to scattering of excess high-energy flux in the outer boundary of the void, to scattering in the vacuum wall, or some other effect. It also may be due to truncating the expansion of the scattering matrix at  $P_3$ , or to the negative source removal in DORT. This deviation will require further study to determine its cause and change the design to ameliorate it (see section VIII.2, Recommendations). Radial flux-ratio profiles are then shown in Figures VI.6.A and B for various groups at  $\theta=105^\circ$ , where the 2-D results are close to the 1-D results. These figures demonstrate that the relationship between the two predictions becomes closer

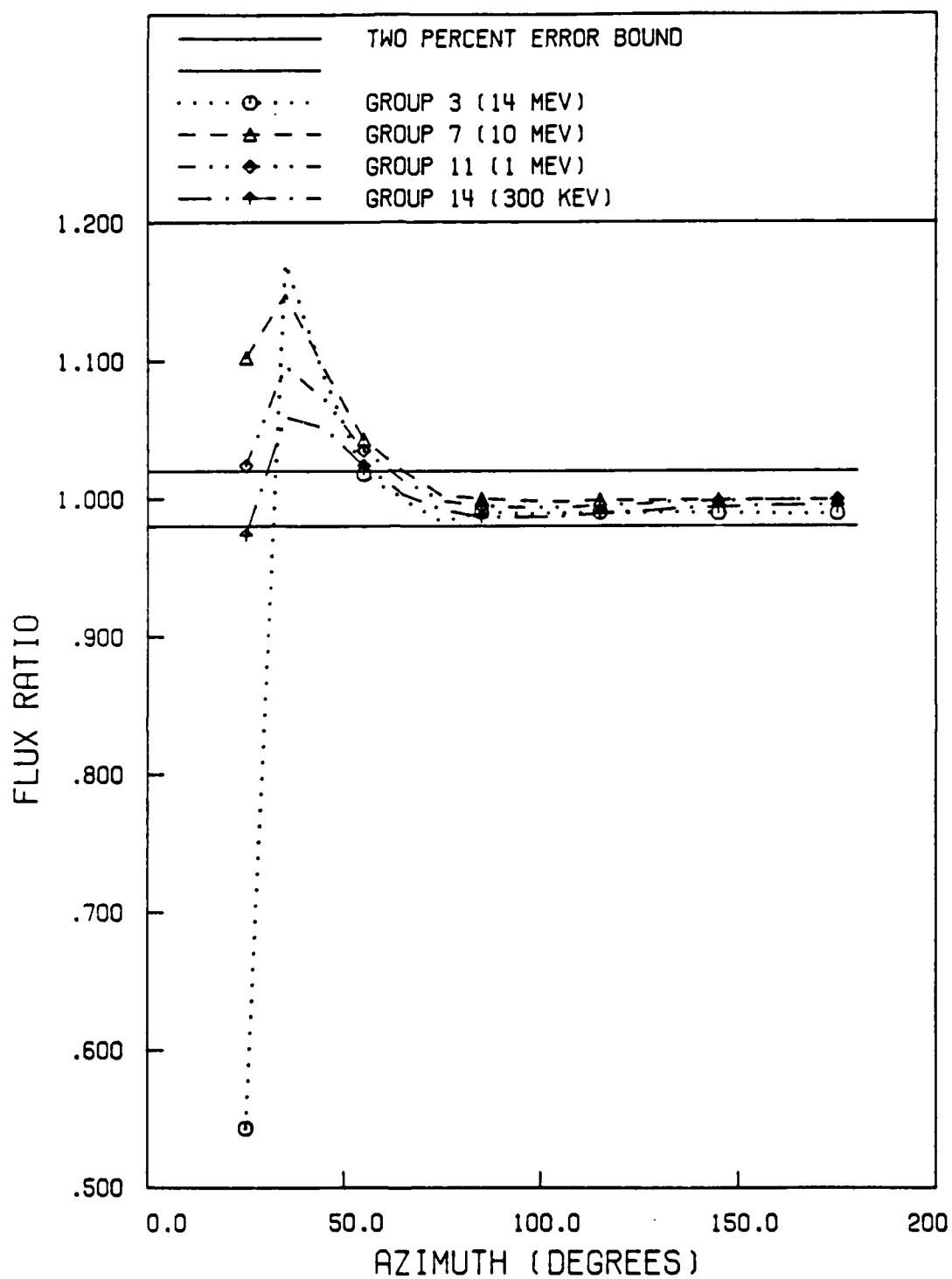


Figure VI.5.A. Azimuthal Group-flux Ratios in Blanket HeC, 1-D vs 2-D R- $\theta$ .

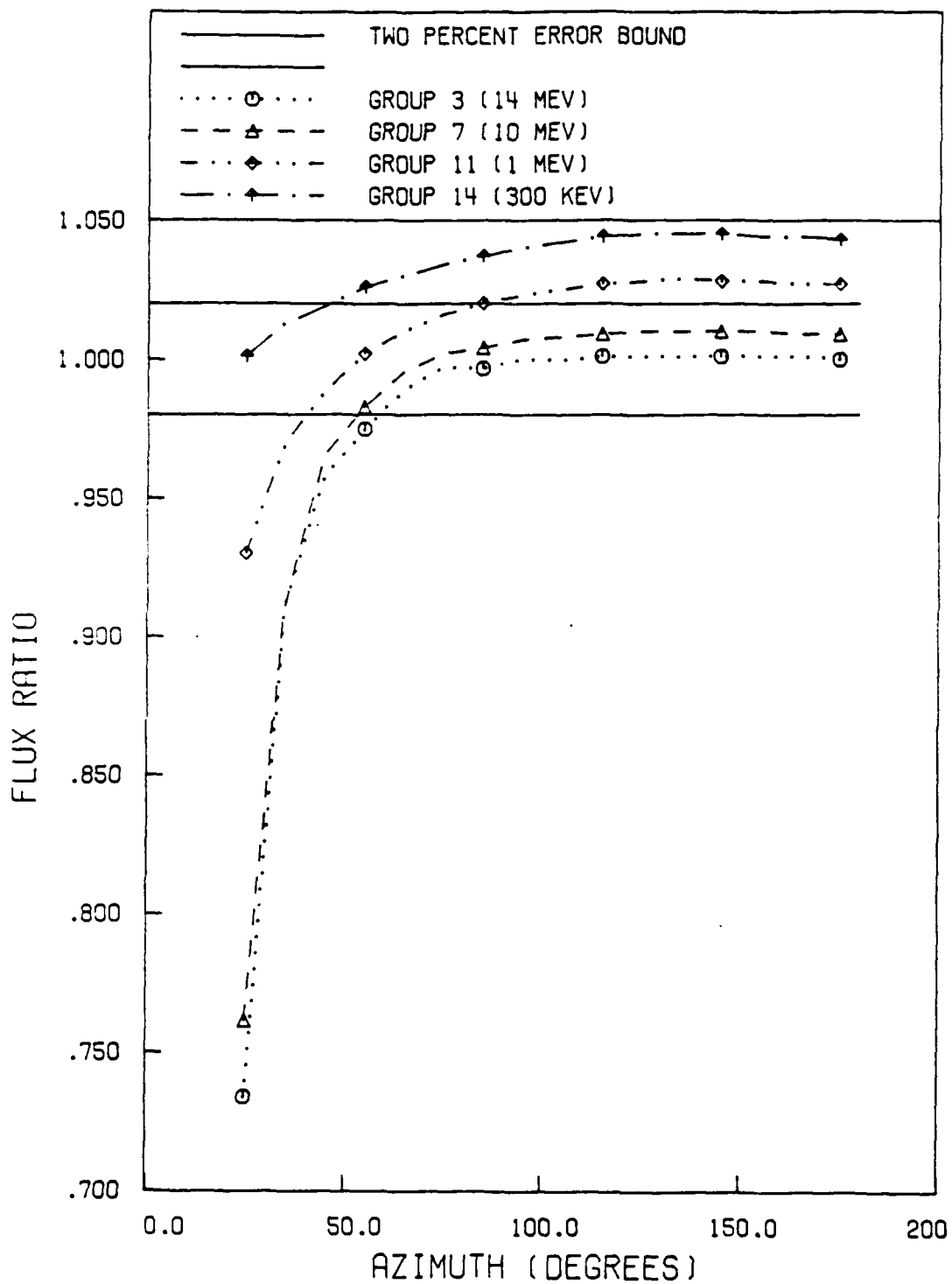


Figure VI.5.B. Azimuthal Group-flux Ratios in Blanket LLC, 1-D vs 2-D R- $\theta$ .

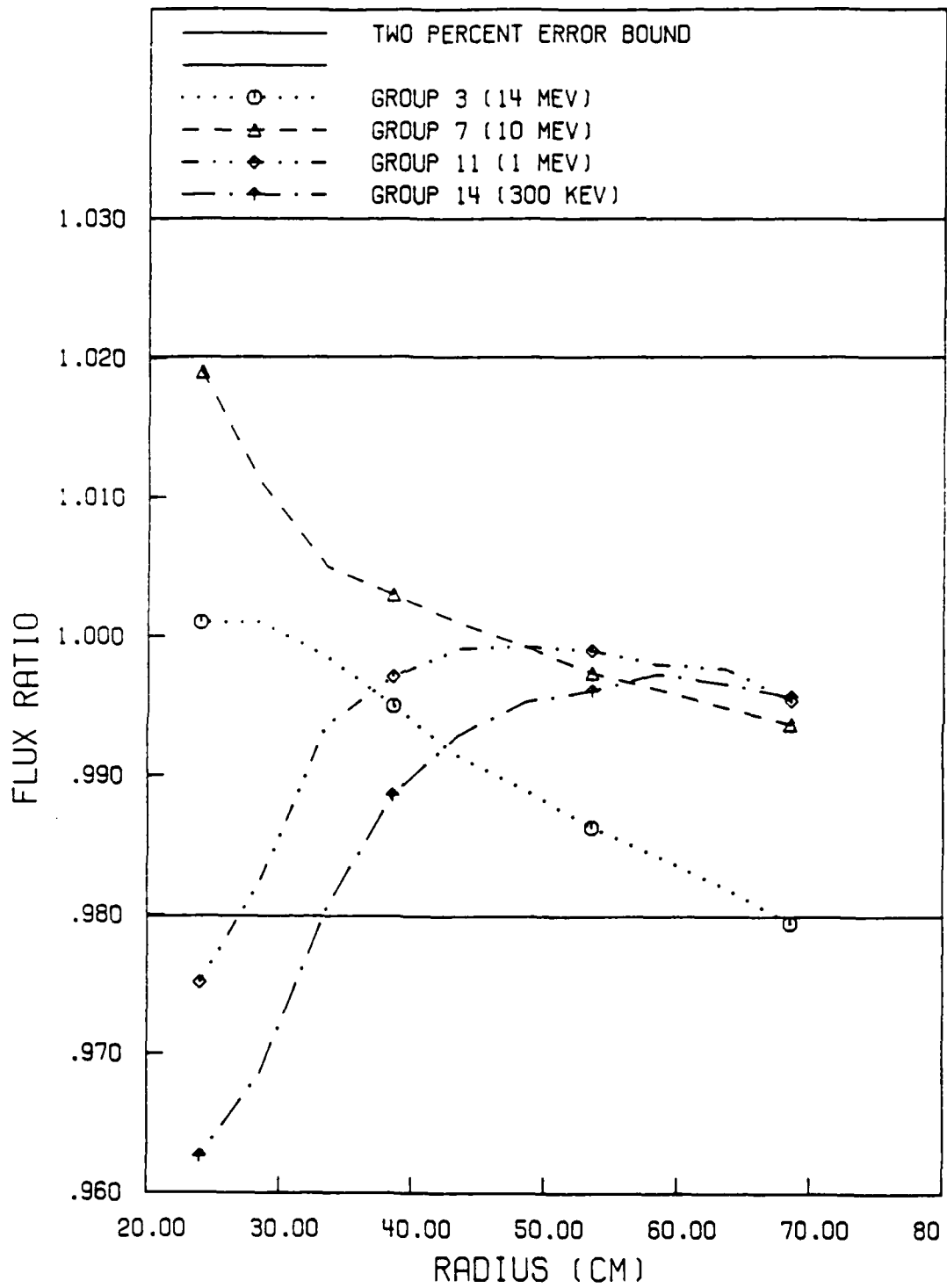


Figure VI.6.A. Radial Group-flux Ratios in Blanket HeC, 1-D vs 2-D R- $\theta$ .

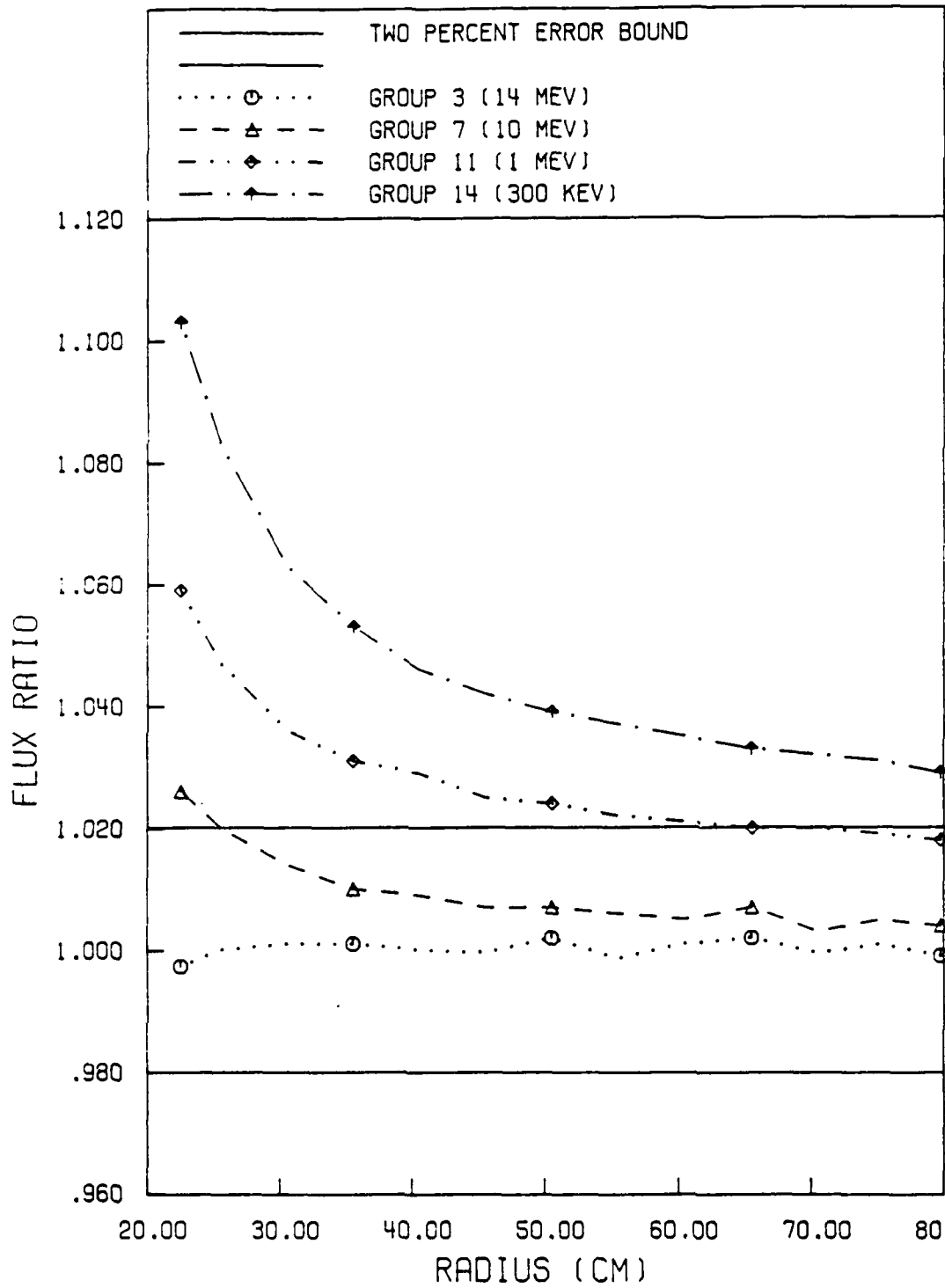


Figure VI.6.B. Radial Group-flux Ratios in Blanket LLC, 1-D vs 2-D R- $\theta$ .

to 1 as the neutron flux travels deeper into the blanket. The presence of the void region thus has a strong effect on the neutron source in the inner portion of the blanket.

Figures VI.7.A and B present the tritium production rates for various azimuthal segments of the blankets. Since tritium from  ${}^6\text{Li}(n,T)\alpha$  reactions occurs at lower energy, the effect of the deviation of the lower-energy neutron flux due to the asymmetry is clear in Figure VI.7.B. Figure VI.7.A shows that  $T_7$  is almost unaffected by the asymmetry, because the high-energy flux which produces T in the  ${}^7\text{Li}(n,n'T)\alpha$  reaction is not affected by the asymmetry. This is because the highest-energy neutrons travel radially outward until they are elastically scattered, inelastically scattered, or absorbed. Only the elastically scattered neutrons stay in the high energy groups, and the average angle of deflection in high energy is near zero. The average cosine of the scattering angle for iron, for instance, is 0.83 at 10 MeV. Thus, high-energy neutrons would have a very small chance of scattering  $90^\circ$  around the blanket, from the void region. The previous comparisons do not include the effects of the anisotropic source, which does have a slight effect on the flux distribution in the blanket.

2-D calculations with anisotropic sources demonstrated that the flux in any region generally varied as the source in groups 2 and 3 varied. However, these computations were not completed in a consistent manner, due to an

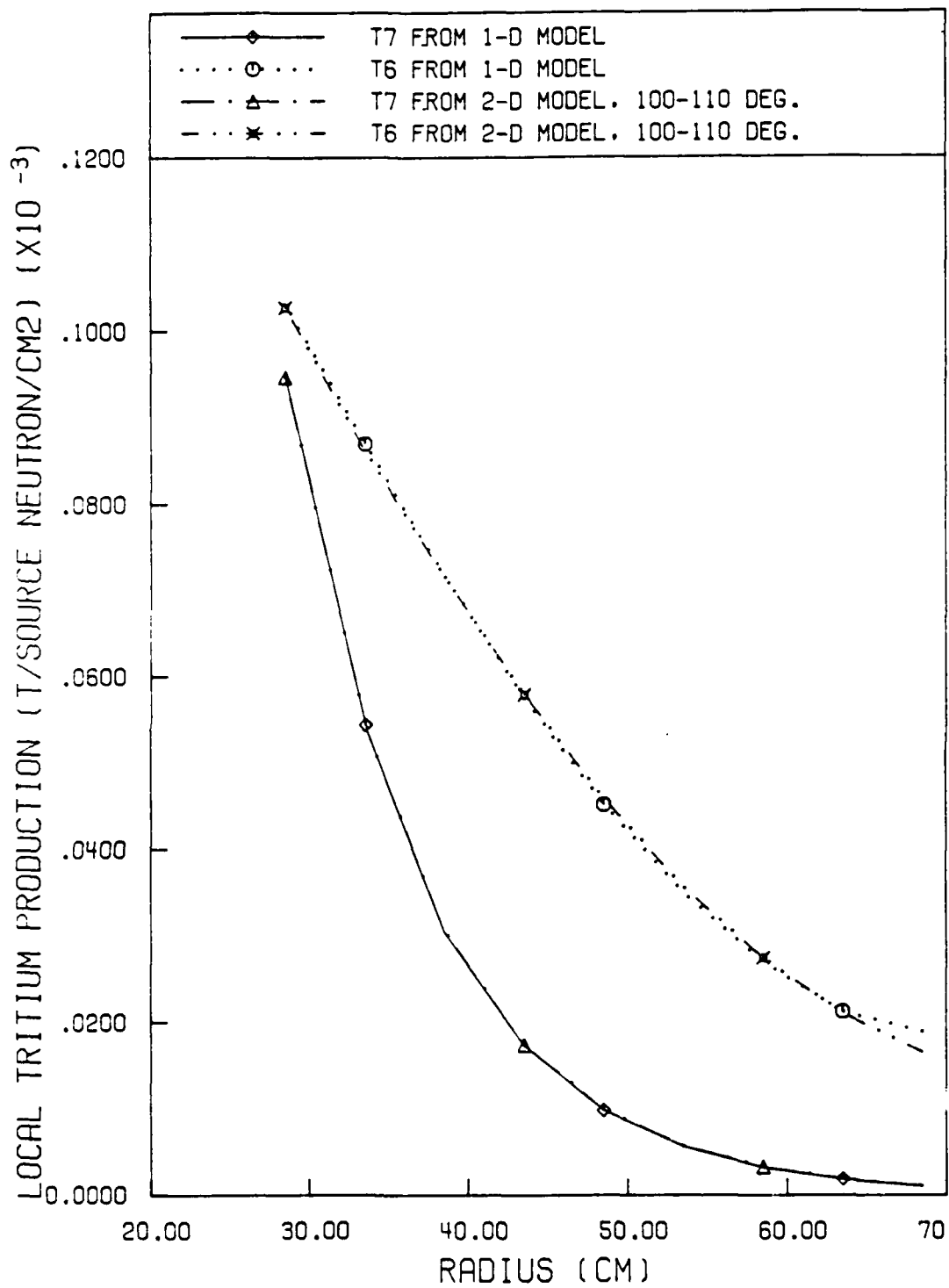


Figure VI.7.A. Radial Tritium Production in Blanket HeC, 1-D vs 2-D R- $\theta$ .

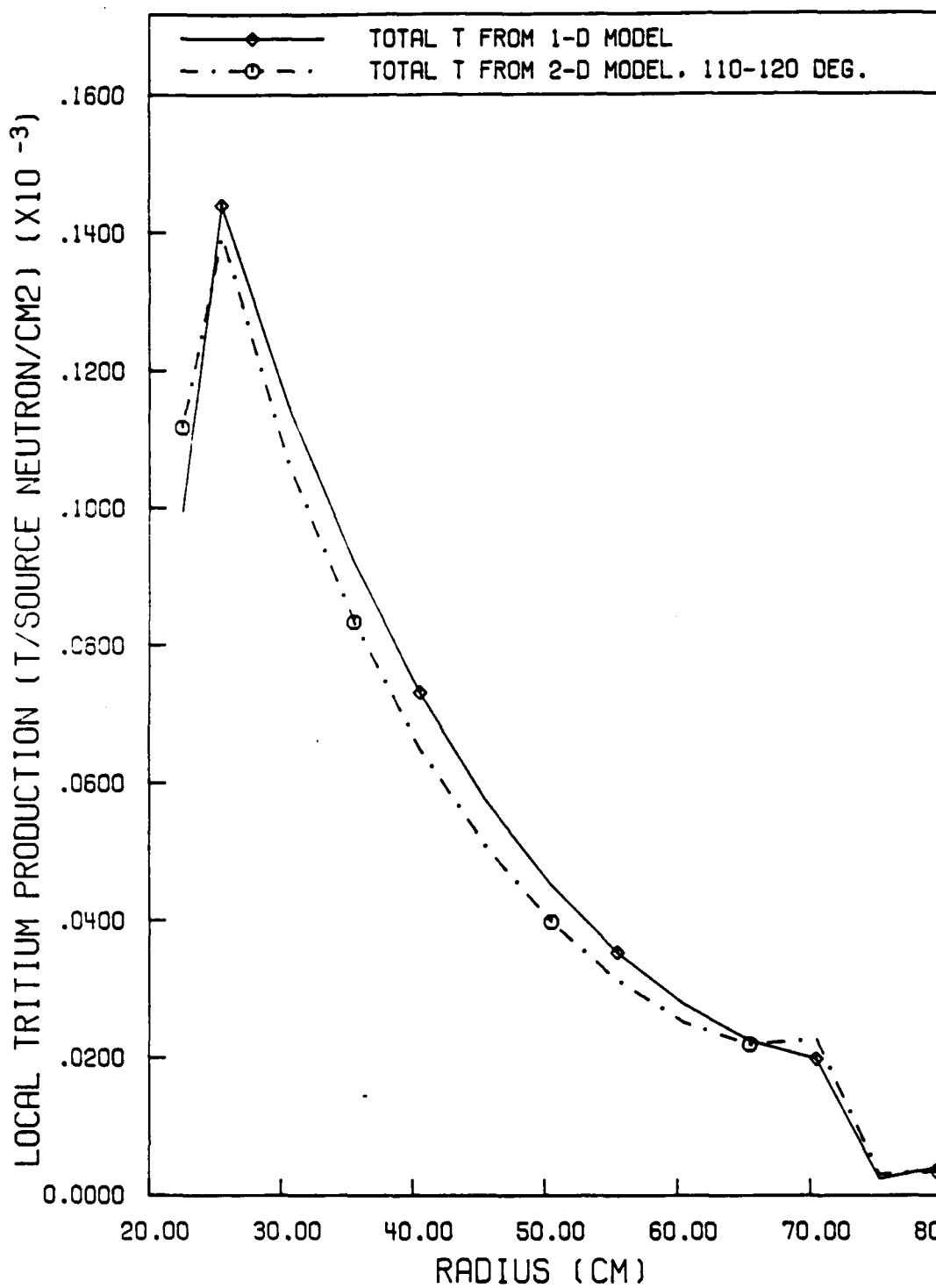


Figure VI.7.B. Radial Tritium Production in Blanket LLC, 1-D vs 2-D R- $\theta$ .

incompatibility between the DORT treatment of the quadrature and boundary flux input file in DORT. They did show that if the flux in group 3 was greater at an azimuth, the flux in the lower groups would also be greater (but not as strongly) at that azimuth. Thus, since the source strength varies by about  $\pm 2\%$  around  $90^\circ$  from the d-beam, the variation in flux due to anisotropy will be less than  $\pm 2\%$  in this region ( $60^\circ$ - $120^\circ$ ). Because this effect can be accounted for and is not affected by the assymetry, the 2-D comparisons just presented are adequate to demonstrate the range of deviations due to the design of the FRBF.

### VI.3. Central Source vs Plasma Source Results

Neutronics evaluations of the FRBF conceptual design with a plasma source were conducted to determine the differences between predictions based on FRBF measurements and actual conditions in a fusion reactor (plasma) test. Figures VI.8.A and B show the neutron spectra in the first wall and mid-breeder for the central (FRBF) source. Differences between these predictions and predictions with a plasma source are shown in Figures VI.9.A and B. The large deviation at about 14 MeV is due to the different source spectra in the two models. The deviation in the lower energies is not due to this spectral difference though, since the cross sections for the higher energy groups are nearly constant. Also, the previous discussion demonstrated

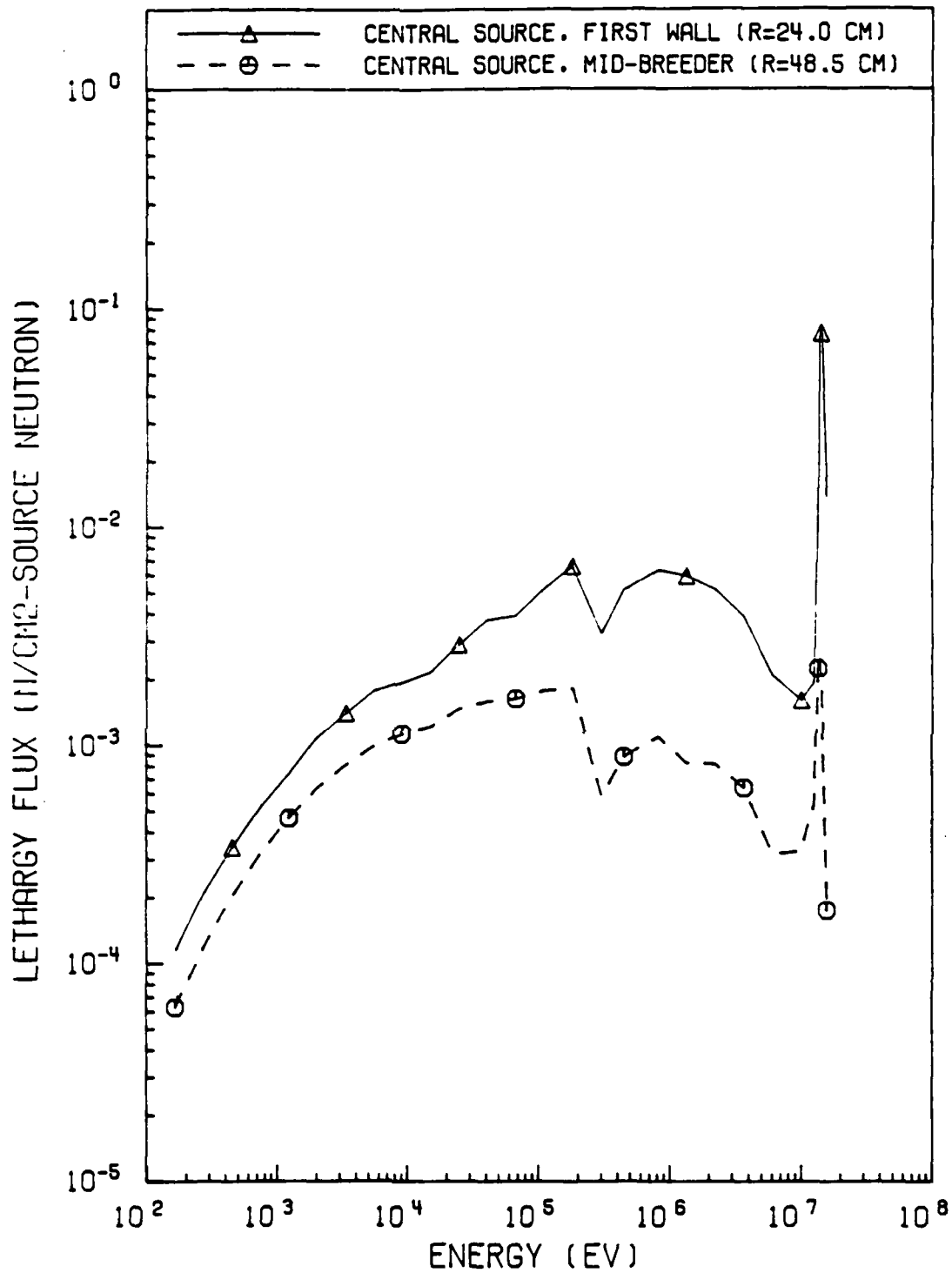


Figure VI.8.A. Central vs Plasma Source: Neutron Spectra in Blanket HeC.

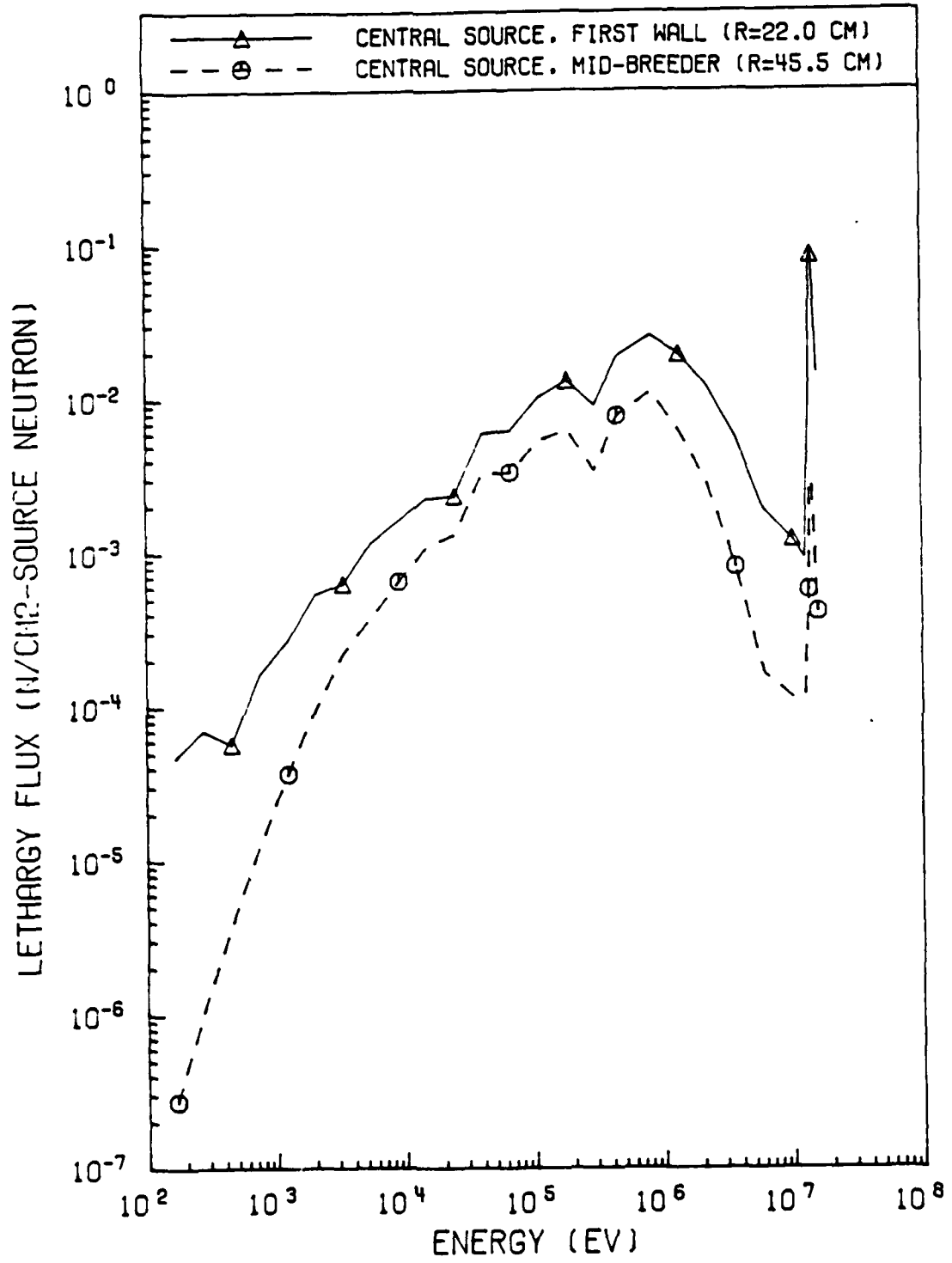


Figure VI.8.B. Central vs Plasma Source: Neutron Spectra in Blanket LLC.

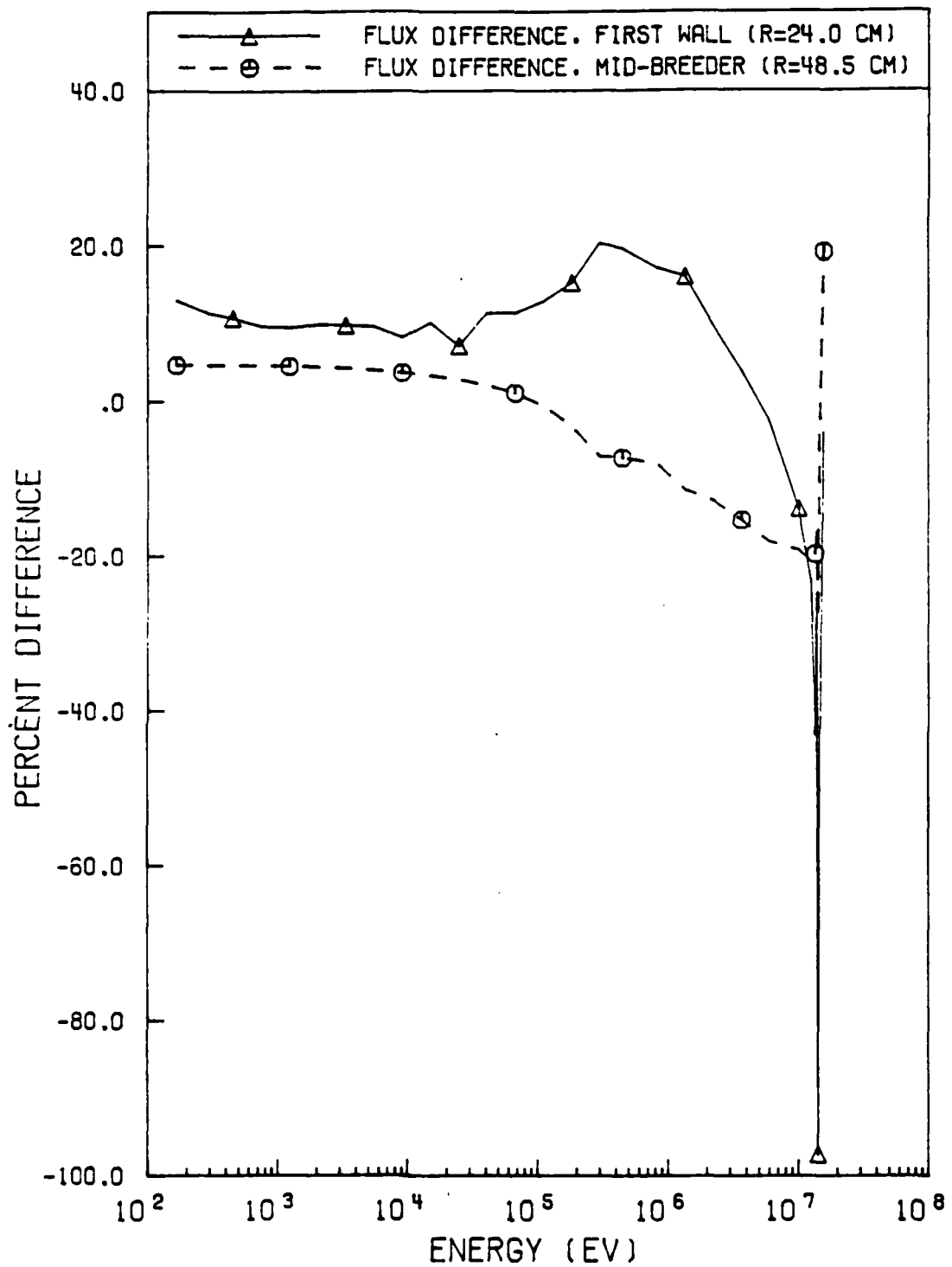


Figure VI.9.A. Central vs Plasma Source: Flux Differences in Blanket HeC.

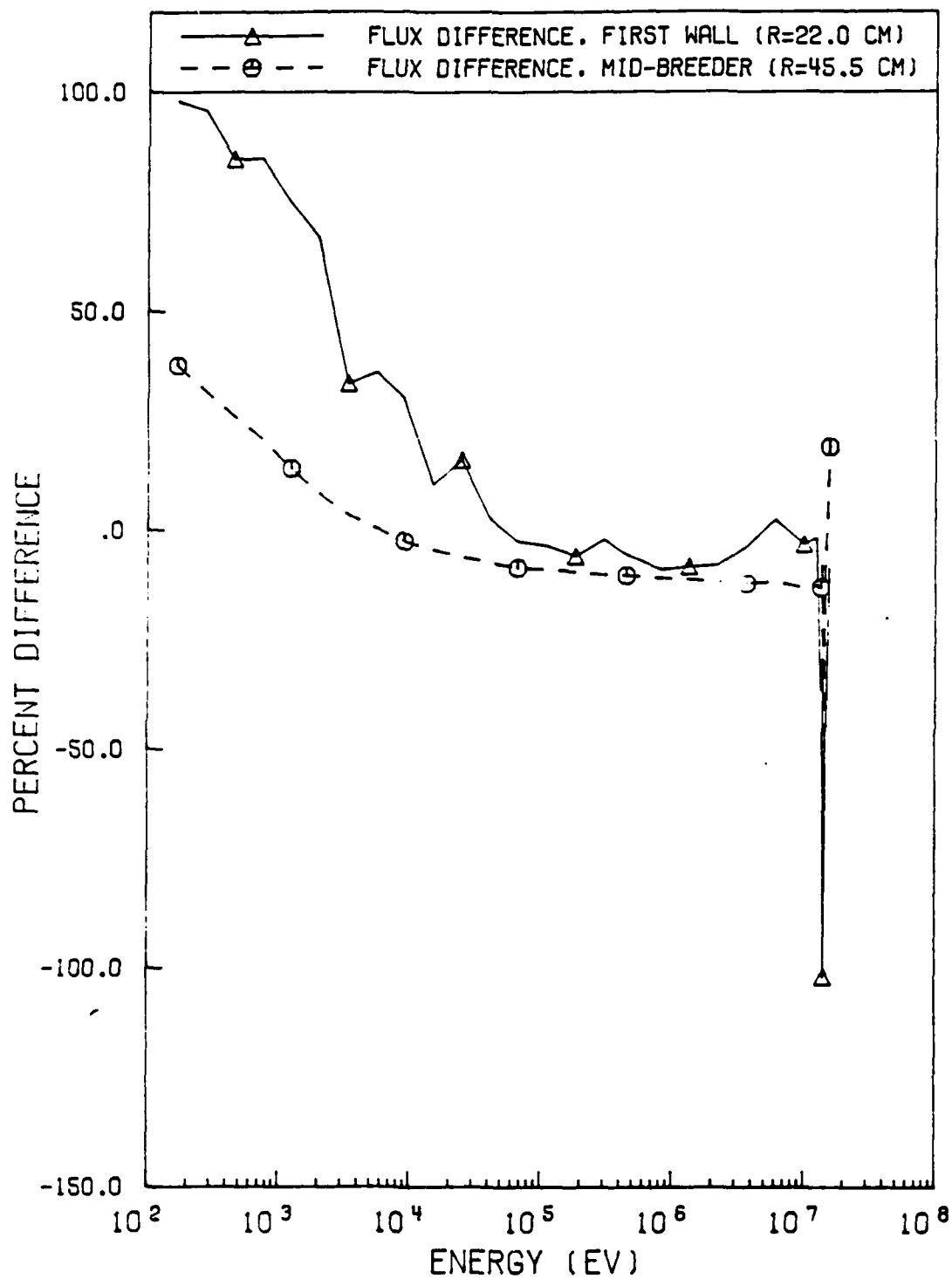


Figure VI.9.B. Central vs Plasma Source: Flux Differences in Blanket LLC.

that the inelastically scattered neutrons would have approximately the same energy, independent of the higher energy group. The deviation in neutron flux in the blanket, then, can only be caused by a difference in angular distribution of source neutrons with respect to the radial direction. The angular flux at the first wall due to the central source is very different from the fusion source, because neutrons from the central source must travel radially (perpendicular to the azimuthal direction). In contrast, neutrons leaving the plasma from the outer edge can exit tangentially to the plasma, thus striking the first wall at an angle far from perpendicular.

Figure VI.10.A and B next show the predicted radial tritium production profiles; again, the difference is due to the longer path length of some of the high-energy neutrons in the plasma model. Loss of neutrons by exponential attenuation due to inelastic scattering is significantly different in the two models, as is the production of lower-energy neutrons from this reaction. These comparisons clearly demonstrate that the neutronics conditions in a test system, even with an axially-distributed central source, cannot reproduce the conditions in a reactor (of any size) which contains a plasma. Thus, for any confidence in predicting tritium breeding, energy deposition, power density, and material damage in a fusion reactor design prior to actual testing; the neutronics methods must be

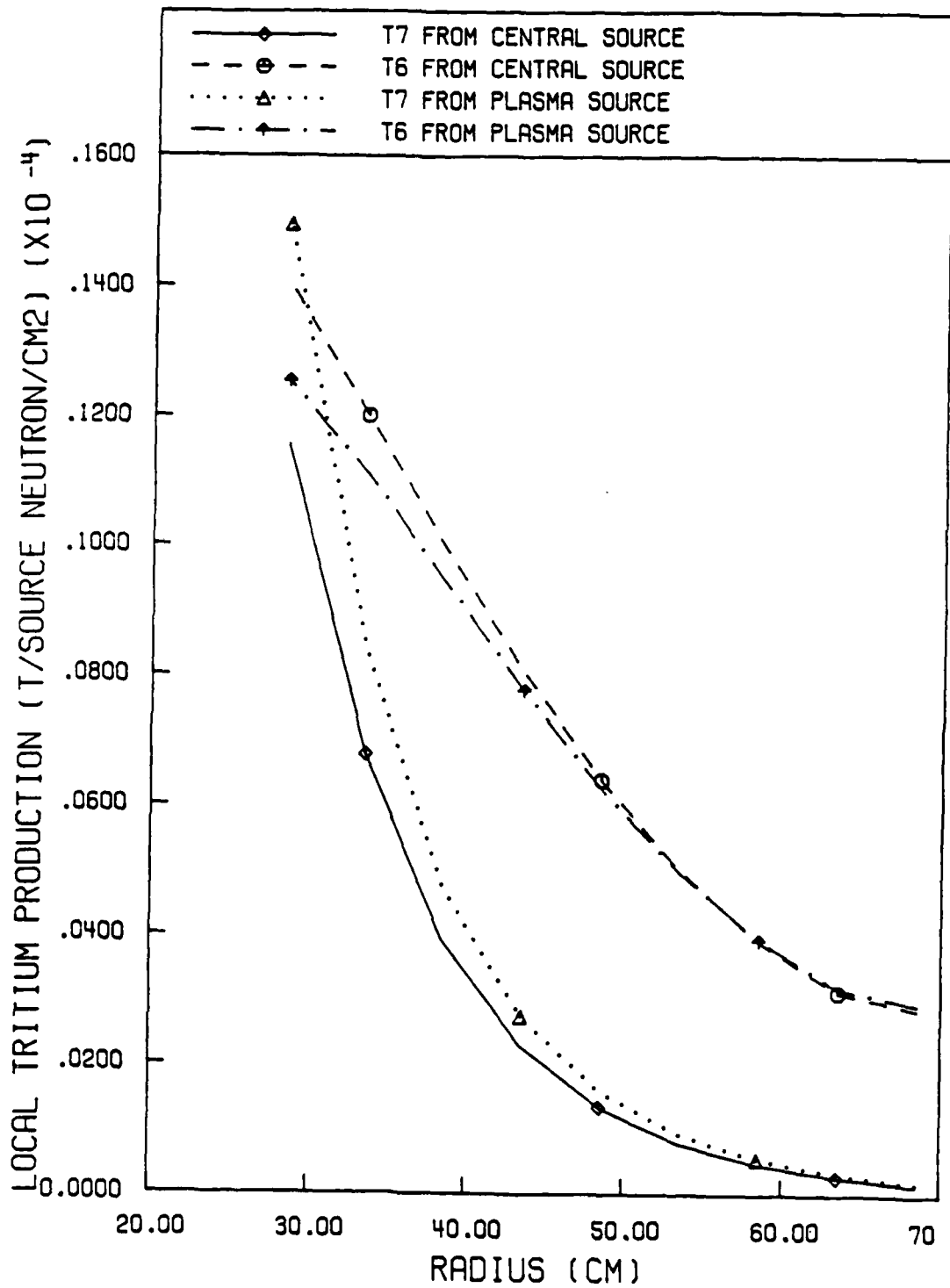


Figure VI.10.A. Central vs Plasma Source: Radial Tritium Production in Blanket HeC.

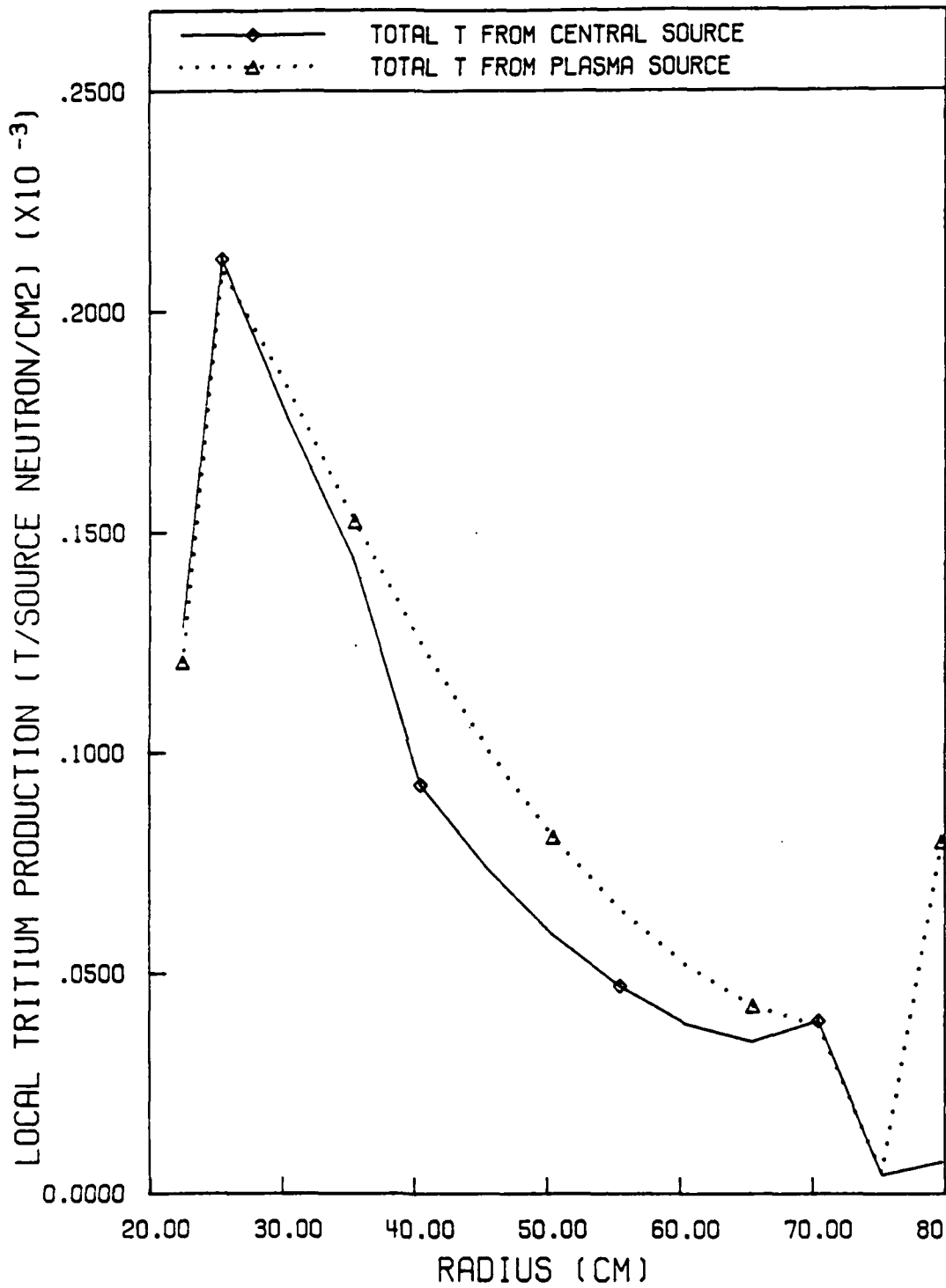


Figure VI.10.B. Central vs Plasma Source: Radial Tritium Production in Blanket LLC.

validated and the accuracy of data libraries must be confirmed.

The FRBF could be used for this validation of the neutronics methods and data libraries. The next chapter discusses the advantages of constructing an FRBF, including a discussion of constructing the facility at Purdue University. It also compares in several ways the FRBF with past and planned fusion reactor neutronics experiments.

## VII. ADVANTAGES OF THE FRBF

Results of the investigations of neutronics in the proposed FRBF design demonstrate that the facility can be used to perform accurate neutronics experiments, with only slight deviations due to asymmetry. If these deviations are predicted and considered when examining experimental results, they should not contribute significantly to deviations from neutronics computations. Thus, the construction of this facility should allow accurate representation in 2-D analyses for neutronics predictions of power distribution and tritium breeding. The major, very important, advantage is that 3-D analyses would not be required, because the design of the facility allows separation of the axial flux dependence in space and energy. This chapter describes some of the other advantages which the FRBF would have, compared to past and planned experiments. It also addresses additional advantages of constructing the facility at Purdue, and it describes other issues which should be considered. One of the major advantages of the FRBF would be flexibility for multiple experiments, and the low cost which this flexibility makes possible.

### VII.1. Flexibility for Multiple Experiments

One of the problems with past FRB experiments has been that the blanket assemblies were one-of-a-kind, or the blankets which were designed for flexibility had geometries which prevented accurate modeling (refer to Chapter II). The FRBF could eliminate these problems because it was conceived with flexibility as a design goal, as was the FBBF. By being constructed of concentric walls and an azimuthally and radially segmented shield, it offers the opportunity for varying configurations, materials, densities, etc. axially, radially, and/or azimuthally. The previously discussed results, for blankets having different compositions of similar isotopes, demonstrated that spectra and flux values were similar for the two models studied. This makes possible a further flexibility for experiments: it appears the two halves of the FRBF could be constructed of slightly different materials or configurations, and neutron transport, power distributions, and tritium breeding could be studied in each at about 60-120 degrees from the d-beam direction (the strong azimuthal variation seen in the flux near the void and SS wall would be much less pronounced near the interface between two similar, but different, blankets). Additionally, a segmented shield would permit removal of a section for installation and testing of a real fusion blanket module, such as the Lithium Blanket Module.<sup>30</sup> The composition of the rest of the FRBF blanket would reduce

flux variations at the boundaries of the test module. This designed-in flexibility is one of the reasons the FRBF could be used to conduct multiple tests at reduced cost.

The financial advantage of this flexible design is easily demonstrated. The original cost of the FBBF project, including design, fabrication and construction, and conducting the first experiment, was about 1/2 million dollars.<sup>42</sup> In contrast, the cost of the current project to re-design and replace the breeding blanket is about 25 thousand dollars; a factor of 20 less.<sup>43</sup> The projected cost for the most complicated blanket design is not expected to exceed 50 thousand dollars, or 1/10 the cost of the original facility. These costs do not include the cost of fuel for the facility, which is in the form of UO<sub>2</sub> fuel rods obtained on a loan basis. Thus, the above comparison includes only design, structural materials, and labor. It is still an illustrative comparison, which gives an impression of potential. Thus, the flexibility which will be designed and built into the FRBF can provide for neutron transport, tritium breeding, and power density investigations in a variety of blankets at a relatively low cost. The importance of this can be seen by reviewing recent literature related to the BCSS. The number of blanket design candidates has been reduced to only four due to the expenses involved in testing and analyzing them.

Constructing the FRBF at Purdue has another financial advantage; the laboratory which housed the FBBF has adequate space for installation of the FRBF and its electronic equipment. One of the shielding walls of the FBBF could be used to shield the FRBF, and an opposite (parallel) wall has only earth on the other side. Thus, only the construction of two shielding walls, the installation of the neutron generating and instrumentation system, and a new blanket are required to have created a new fusion reactor blanket testing facility. This new facility could then be used for conducting much needed differential and integral transport experiments on realistic blanket models. Another advantage of putting this new facility in the same building as the FBBF will be safety.

#### VII.2. Operational and Personnel Safety in the FRBF

Four major safety issues must be considered in the design of the FRBF on a university campus; they are: 1) radiation leakage, 2) tritium leakage, 3) experimental hazards, and 4) criticality. Only two of these issues are crucial for the FRBF--radiation and tritium leakage. The criticality issue does not exist here because no fissile fuel will be present; and the experimental hazards have been fully analyzed and safe techniques developed with work for the FBBF. Thus, radiation leakage and tritium leakage must be considered.

The mean-free-path of 14 MeV neutrons in most fusion reactor materials is about 10 cm.<sup>19</sup> Due to the greater penetration of these neutrons, more shielding and a thicker reflector may be required. The FBBF was designed for a maximum neutron production rate of  $\sim 10^{11}$  n/s. However, the design was based on a fission spectrum, not a fusion spectrum. Therefore, when the FRBF final design is completed, an evaluation of the blanket neutronics should include analysis of the leakage flux to demonstrate there is no need for extra shielding or reflector materials. However, because the blanket and shielding on the FRBF are thicker than the FBBF, and because fusion blankets are intentionally constructed of neutron absorbing materials (while the FBBF contains fissile materials), a significant difference in dose rates should not exist for equal source strengths.

The FBBF has been thoroughly analyzed for neutron and gamma-ray dose rates inside the experimental chamber, inside the laboratory, and in the areas above and around the facility.<sup>42</sup> Additionally, dose rate measurements have been made in these locations; the dose rate in the lecture halls above the facility is low enough to be not detectable. To estimate the dose rates from the proposed FRBF, only a comparison of neutron flux and spectrum at the outer edge of the reflectors is required. The ratios of dose rates will be approximately equal to the ratios of the leakage fluxes.

Special consideration should be given to shielding the gap provided for the neutron source d-beam system. The other safety issue, tritium leakage, is more difficult to estimate.

Tritium will be contained in a titanium-tritide ( $TiT^2$ ) coating on a copper target, in the center of a stainless steel vacuum tube. Tritium atoms migrate rather easily through most substances, and tritium atoms can be freed from the  $TiT$  matrix. High-energy deuterons, recoil alphas (from the d-T reaction), high-energy neutrons, and thermal effects all dislodge the tritium atoms from the matrix.<sup>39</sup> This tritium can be easily removed by the vacuum pump which is required for maintaining a vacuum in the d-beam tube. There are many techniques for pumping and trapping the hydrogen isotopes, such as sputter-ion pumps, cryogenic pumps, uranium getter pumps, and catalytic conversion methods. Preventing excess leakage of tritium should not be technically difficult. However, some tritium will escape from the system; this leakage should be estimated, at least to put a cap on the possible magnitude of concentration, and to compare this to standards.

Another potential hazard will exist when changing the tritiated targets. This will require opening the vacuum system; with the possible exposure of personnel to highly contaminated equipment. The target region should be constructed so that it can be removed as a sealed unit for

disposal, or for changing the target in a glovebox or other safe facility.

Another path for tritium loss is from the breeding blankets. They will produce tritium at a rate comparable to the neutron production rate ( $10^{11}$  n/sec). However, this tritium will most likely be contained in sealed systems, and some will be recovered for measurement. When these containers are opened, the possibility exists for larger quantities to escape in a short period of time. Safe experimental and operating procedures for handling these tritiated samples will have to be developed and followed.

Since all other safety concerns have been well addressed during the design, construction, and experimenting with the FBBF; and since the radiation and tritium leakage concerns have been evaluated above; it appears the FRBF can be operated safely in the basement of the Physics Building at Purdue University. The next item which needs addressed is the predicted precision of measurements in the FRBF.

### VII.3. Measurement Techniques and Accuracy

Most measurement methods and equipment will be the same as those used in the FBBF (see Chapter III). Much experience has been acquired, techniques have been thoroughly developed and tested, and confidence in results has been built. The statistical precision of the

measurements depends upon three parameters; measurement time, neutron flux, and precision of the neutron source prediction (because results will be expressed as an absolute ratio of measurement/source neutron). The design of the line source has a distinct benefit here, it permits long measurement times, on the order of weeks or months, without changes in source strength, and with relatively high neutron flux. Whereas most neutron generator targets have relatively short half-lives due to high local d-beam current and associated high temperatures; the stretched design of the FRBF source will reduce the local current and heating rate while allowing for cooling and recombination of tritium with the TiT matrix. The local heating rate can be reduced by a factor of 100 simply because the target is 100 cm long, and normal neutron generators have beams of about 1 cm<sup>2</sup>. This design will also permit removal of heat without excessive cooling structure or coolant, thus reducing the perturbation of the neutron-source spectrum. This should allow a target lifetime about two to three orders-of-magnitude greater than normal beam-target systems. By monitoring the recoil alphas and automatically adjusting the d-beam current to maintain a constant neutron production rate, measurements can be made over days, weeks, or even months. Thus, total fluence can be increased easily to reduce counting errors below one percent (one standard deviation). Then, the measurement results are mostly influenced by efficiencies and source-strength

determination. The alpha-recoil method has been developed for determining the strength of neutron generator sources. By using a bank of these detectors mounted vertically in line with the blanket axis, and shielded by the concrete wall of the blockhouse and by lead collimators, neutron source strength and axial shape may be precisely determined. The overall measurement statistics would then be on the order of one to two percent, which is much less than deviations between predictions and measurements in previous experiments.

With a source strength of  $10^{11}$  n/s, exposure of samples would be about  $10^6$  14 MeV n/s (integral flux is about 4 times this),  $\sim 10^6$  n/s in the inner blanket, and  $\sim 10^4$  n/s in the outer blanket or reflector. These values are based on the flux results from blanket HeC. These relatively high values of neutron flux, combined with a large volume available for experiments ( $\sim 60$  cm axially,  $\sim 60$  cm radially, and  $60$ - $90^\circ$  azimuthally), allows an increased capability and flexibility for measurements. Then, the use of multiple measurement techniques and long measurement times in a large experimental region could yield the same results for the FRBF that they have for the FBBF; identification of deficiencies in methods used to predict neutron and gamma-ray transport in blankets, and identification of the causes of those deficiencies and elimination of those causes. A few other advantages of constructing the FRBF at Purdue

University should be mentioned in this report.

#### VII.4. Other Issues

In addition to the experience with experimental techniques previously discussed, there are other advantages at Purdue. One of the major advantages of installing the FRBF at Purdue is its resources--the people and the facilities. Much experience has been gained among faculty, staff, and students at Purdue while designing, constructing, and experimenting in the FBBF. Benefits can be derived from this experience, which includes:

- Theory of fast-neutron reactions,
- Theory of cross section generation for transport predictions,
- Development and use of neutron and gamma measurement techniques,
- Development of a vectorized integral transport code,<sup>44</sup>
- Design, fabrication, acquisition, and installation of components and systems in the FBBF, and
- Analysis and comparison of fast reactor neutronics to measurements.

Another benefit is the physical resources, for instance, the Cyber 205 vector supercomputer is available for all faculty and students, and for all research projects. This experience and expertise could contribute significant improvements to the technology required for the future of fusion power.

## VIII. CONCLUSION

The FRBF is a conceptual design of a new fusion reactor blanket simulation facility unlike those used for past research. Deficiencies in the designs of past fusion reactor blanket neutronics experiments have largely been eliminated in the design of the FRBF. The neutronics evaluation conducted for this research indicates that the energy-dependence of flux can be separated from the axial dimension because of the use of an axially distributed, chopped-cosine source with a cylindrical geometry. Neutronics predictions will produce errors due to design of less than five percent, if based on 1-dimensional predictions. Actual analyses will include 2-dimensional treatments, which include geometric asymmetry and source anisotropy. Accurate treatments of neutronics in the frbf will not require 3-dimensional analyses, which are necessarily done in course space and energy. Then, the inaccuracies of transport predictions in this facility (C/E values) will contribute only a few percent to the deviations to be evaluated. The errors in predicting axial leakage will contribute the least to the overall deviations, due to the chopped-cosine source profile. Additionally, some of

these deviations can be reduced by reducing the volume of void in the blanket and by using the minimum wall thickness for vacuum enclosures. A capability to perform measurements for long periods and to use multiple measurement techniques improves the quality of data which can be obtained. Thus, the FRBF can produce C/E values which are more accurate than past comparisons between experiment and prediction. Following is a summary of this report.

#### VIII.1. Summary

The results of the few fusion reactor blanket simulation experiments performed to date have shown that improvements are needed in neutron transport codes and data files, in measurement techniques, but most critically in experiment design. The conceptual design of a new simulation facility, the FRBF, was developed. This facility has an axially distributed neutron source with a chopped-cosine shape. To determine if azimuthal asymmetry or neutron source anisotropy would severely affect predictions throughout the facility, neutronics in two blanket compositions were studied. The results of the neutronics analyses indicated that the design features of the facility and its source would not contribute in any significant way to inaccuracies in the prediction of results. Thus, any deviations between calculated and experimental values (C/E) can be interpreted in terms of inaccuracies of cross sections (such as

inelastic scattering) and deficiencies of computational methods (such as group constant generation and neutron transport codes). Arguments were then presented to demonstrate the advantages of constructing an FRBF-type facility at Purdue University. Its cost would be low because it could be built adjacent to the FBBF. The FRBF could be used to produce precise measurements of neutron fluxes in a variety of fusion reactor blanket materials and/or designs, at a relatively low cost. These measurements could then be compared to design predictions, with confidence that the facility would not contribute substantially to deviations. Thus, the FRBF could be used to validate neutronics methods and data libraries, and could contribute significantly to capabilities to predict tritium breeding rates and power densities in the first wall, blanket, shielding, magnets, and other components of proposed fusion reactor designs. Studies conducted in the FRBF could greatly enhance the expanding body of methodologies for the future of fusion technology. The following recommendations should be considered during the engineering design of this facility.

#### VIII.2. Recommendations

Further studies are required before construction of the FRBF. These include a determination of how to construct the blanket, analysis of designs of targets for the d-beam,

analysis of designs of accelerator and beam-sweeping systems, design of a vacuum system for the neutron generator, and a thorough analysis of shielding requirements. Some suggestions are:

1) Economical design of the blanket should stress maximum flexibility. It should provide for removal of large or small, axial, radial, or azimuthal segments. Excessive radially-directed channels should be avoided, as these will tend to promote neutron streaming.

2) The target support should have minimum structure and coolant. One method of construction might be to attach the TiT foil to a thin-walled copper tube in the center of the blanket. This could then be cooled by flowing air or another gas through it. If the tube is aligned such that the center of the target is at the center of the blanket, with the wall of the tube curving away from the beam, the support will contribute little disturbance of the azimuthal flux profile around the  $60^{\circ}$ - $120^{\circ}$  region. Also, safety should be a major consideration in the design of the neutron generating system, see Chapter VII.2 for a discussion.

3) The neutron generator and associated electronics (source-strength detectors, magnets, etc.) should be located outside the shielding wall of the facility. This will protect them from excessive neutron flux from the blanket, will reduce background counts in the detectors, and will reduce asymmetries in the FRBF room.

4) A zone in the center of the blanket for scattering

the source neutrons should be investigated. This could promote smoothing of the source anisotropy, reduce the energy slightly, to approximate the plasma source, and introduce some angular variation of the flux in the source region. The material in this zone must have an elastic cross section which is orders-of-magnitude greater than the inelastic cross section; otherwise, an unrealistic boundary source will be imposed on the first wall, and the scatterer will attenuate high-energy neutrons instead of just scattering them.

5) The flux variations found in the low-energy groups in the second model (Blanket LLC, LiPb-cooled) should be investigated. The source of the deviations should be determined, and a method for ameliorating the effect should be found.

LIST OF REFERENCES

## LIST OF REFERENCES

1. FINESSE Phase I Report, Technical Issues and Requirements of Experiments and Facilities for Fusion Nuclear Technology, Vol. I and II, UCLA-ENG-85-39, Univ. of California, Los Angeles (1985).
2. Leonard, B., "A Compendium of 14 MeV Neutron Source Experiments," Proc. of the Mag. Fus. Energy Blanket and Shield Workshop, Brookhaven National Laboratory, ERDA-76/117/1, 66 (1975).
3. Maynard, C., "Integral Experiments for CTR Nuclear Data," Symposium on Neutron Cross Sections from 10-40 MeV, Brookhaven National Laboratory, BNL-NCS-50681, 377 (1977).
4. Green, L., "Review of Integral Fusion Blanket Experiments," Proc. of the Fourth Topol. Mtg. on the Tech. of Cont. Nucl. Fus., CONF-801011, 395 (1981).
5. Woodruff, G., Atom. Kern. 44, 60 (1984).
6. Muir, D., and M. Wymann, "Neutronic Analysis of a Tritium-Production Integral Experiment," Tech. of Cont. Therm. Fus. Exp. and the Engr. Aspects of Fus. Reactors, Austin, TX, Nov 1982, CONF 72111, 910 (1984).
7. Bachmann, H., U. Fritscher, F. Kappler, D. Rusch, H. Werle, and H. Wiese, Nucl. Sci. Engr. 67, 74 (1978).
8. Fritscher, U., F. Kappler, and D. Rusch, Nucl. Inst. Meth. Phys. Res. 153, 563 (1978).
9. Kappler, F., D. Rusch, A. Werle, and H. Wiese, "Determination of Neutron Spectra in a Lithium Sphere," Proc. Eighth Symp. on Fus. Tech., Netherlands, June 1974.
10. Herzing, R., L. Kuypers, P. Cloth, D. Filges, R. Hecker, and N. Kirch, Nucl. Sci. Engr. 60, 169 (1976).
11. Cloth, P., D. Filges, H. Geiser, R. Herzing, G. Stocklin, and R. Wolfle, "Studies of the Space Dependent Tritium Production and the Fast Flux Distribution in a Lithium Blanket Experiment," Proc. Eighth Symp. on Fus. Tech., Netherlands, June 1974.

12. Herzing, R., L. Kuijpers, P. Cloth, D. Filges, R. Hecker, and N. Kirch, Nucl. Sci. Engr. 60, 169 (1976).
13. Seki, Y., H. Maekawa, M. Moriyama, T. Hiraoka, and J. Hirota, "Analysis of Fission Ratio Distribution in Spherical Lithium Metal Assembly with Graphite Reflector," JAERI-M 6220, Aug 1975.
14. Maekawa, H., and Y. Seki, J. Nucl. Sci. Tech. 14, 97 (1977).
15. Seki, Y., and H. Maekawa, J. Nucl. Sci. Tech. 14, 210 (1977).
16. Seki, Y., D. Muir, and H. Maekawa, J. Nucl. Sci. Tech. 14, 680 (1977).
17. Itoh, S., Y. Seki, and H. Maekawa, "Measurements and Calculations of Fast Neutron Spectra in a Graphite-Reflected Lithium Assembly," Tech. Cont. Nucl. Fus., CONF 780508-P1, 385 (1978).
18. Maekawa, H., Y. Oyama, J. Kusano, and T. Nakamura, J. Nucl. Sci. Tech. 16, 377 (1979).
19. Hemmendinger, A., C. Ragan, and J. Wallace, Nucl. Sci. Engr. 70, 274 (1979).
20. Yamamoto, J., A. Takahashi, M. Ebisuya, and K. Sumita, J. Nucl. Sci. Tech. 17, 255 (1980).
21. Iguchi, T., T. Nishitani, J. Takagi, M. Nakazawa and A. Sekiguchi, "Neutron Spectra and Tritium Production Rate Measurements in the One Dimensional LiF Slab Geometry as a Fusion Reactor Blanket Benchmark Experiment," Proc. Fourth Topol. Mtg. Tech. of Cont. Nucl. Fus., CONF-801011, 387 (1981).
22. Perkins, L., N. Evans, M. Scott, B. Underwood, Nucl. Sci. Engr. 78, 30 (1981).
23. Santoro, R., R. Alsmiller, J. Barnes, and G. Chapman, J. Fus. Energy 2, 237 (1982).
24. Profio, A., G. Shani, and G. Dissanaiké, Nucl. Sci. Engr. 78, 178 (1981).
25. Maekawa, H., Y. Oyama, T. Suzuki, Y. Ikeda, and T. Nakamura. Nucl. Tech./Fus. 4, 1165 (1983).
26. Oyama, Y., and H. Maekawa, "Measurements of Angle-Dependent Neutron Spectra from Lithium-Oxide Slab Assemblies by Time-of-Flight Method," JAERI-M 83-195, Nov 1983.

27. Haldy, P., A. Kumar, K. Gmur, R. Fruh, J. Ligou, J. Schneeberger, Atom. Kern. 44, 65 (1983).
28. Sitaraman, S., and G. Woodruff, Trans. ANS 43, 197 (1982).
29. Sahin, S., and A. Kumar, Fusion Tech. 6, 97 (1984).
30. Jassby, D., J. File, P. Bertone, D. Graumann, R. Creedon, B. Engholm, E. Hager, J. Lindgren, L. Yang, Y. Harker, and F. Tsang, J. Fus. Energy 4, 57 (1985).
31. Ott, K., F. Clikeman, and G. Harms, Nucl. Sci. Engr. 88, 1 (1984).
32. Santoro, R., J. Barnes, J. Drischler, R. Alsmiller, "Multigroup Energy-Angle Distributions for Neutrons from the  $T(d,n)^4\text{He}$  Reaction ( $E_d = 100-400$  KeV)," ORNL/TM-9251, July 1984. Contains tables for correlations for d-beams of various energies and a listing of the program used to generate the data. Due to errors in the program, the probability listed for the forward 20-degree cone is about 6% less than the correct probability.
33. Aparcedo, E., "Conceptual Design of a 14 MeV Neutron Source Arrangement with an Average Cosine Shape," M.S. Research Report, Purdue University, West Lafayette, IN, April 1983.
34. Santoro, R. R., ORNL, personal communication (Sep. 1985).
35. Landolt, R. R., Purdue, personal communication (Sep. 1985).
36. Rhoades, W. A., and R. L. Childs, "An Updated Version of the DOT One- and Two-dimensional Neutron/Photon Transport Code, ORNL-5851, ORNL, (1982).
37. Alcouffe, R., F. Brinkley, D. Marr, and R. O'Dell, "User's Guide for TWODANT: A Code Package for Two-Dimensional, Diffusion-Accelerated, Neutral-Particle Transport, LA-10049-M, LANL (1984).
38. Little, W. W., and R. W. Hardie, "2DB User's Manual - Revision I," BNWL-831 REV1, BNL, Richland, WA (1969).
39. Barschall, H. H., et al., Neutron Sources for Basic Physics and Applications, Ed S. Cierjacks, Pergamon Press, NY (1983).

40. Roussin, R. W., "VITAMIN-E: A Coupled 174 Neutron, 38 Gamma-Ray Multigroup Cross-Section Library for Deriving Applications-Dependent Working Libraries for Radiation Transport Calculations," Draft ORNL/RSIC report, also DLC-113, ORNL (1984).
41. Kidman, R. B., and R. E. MacFarlane, "LIB-IV, A Library of Group Constants for Nuclear Reactor Calculations," LA-6260-MS, LANL, Los Alamos, NM (1976).
42. Clikeman, F. M., Ed., "Fast Breeder Blanket Facility," Electric Power Research Institute, EPRI NP-1947 (1981).
43. Clikeman, F. M., Purdue, personal communication (Dec. 1985).
44. Koch, K. R., "A Direct Integration Multiple Collision Integral Transport Analysis Method for High Energy Fusion Neutronics," Ph.D. Thesis, Purdue University, West Lafayette, IN, August 1985.

**APPENDICES**

Appendix A. Tables.

Table A.1. Material Compositions for Blanket HeC.

Element	Materials					
	1a 1st Wall	2a Breeder	3a Plenum	4a Shield	5a Air	6a Source
Fe	1.234E-2*	5.484E-3	1.028E-2	5.745E-2	---	---
Cr	1.787E-3	7.944E-4	1.490E-3	1.600E-2	---	---
Ni	6.885E-6	3.060E-6	5.734E-6	1.179E-2	---	---
Mo	8.424E-5	3.744E-5	7.020E-5	---	---	---
Mn	7.362E-5	3.272E-5	6.135E-5	---	---	---
Si	7.200E-5	3.200E-5	6.000E-5	---	---	---
C	1.345E-4	5.984E-5	1.122E-4	---	---	---
<sup>7</sup> Li	---	5.456E-2	---	---	---	---
<sup>6</sup> Li	---	4.373E-3	---	---	---	---
O	---	2.946E-2	---	---	9.740E-6	---
N	---	---	---	---	3.640E-5	---
Cu	---	---	---	---	---	8.450E-2

\*Read 1.234e-2 as  $1.234 \cdot 10^{-10}$  atom/barn-cm.

Table A.2. Material Compositions for Blanket LLC.

Element	Materials					
	1a 1st Wall	2a Breeder	3a Reflector	4a Shield	5a Air	6a Source
Fe	2.749E-2*	4.124E-3	4.949E-2	6.258E-2	---	---
Cr	6.370E-3	9.555E-4	1.147E-2	1.863E-3	---	---
Ni	6.450E-3	9.675E-4	1.161E-2	1.422E-3	---	---
Si	4.214E-4	6.320E-5	7.584E-4	3.524E-4	---	---
C	9.855E-5	1.478E-5	1.774E-4	2.078E-3	---	---
Mo	4.934E-4	7.401E-5	8.881E-4	---	---	---
Pb	1.378E-2	2.549E-2	2.756E-3	---	---	---
Ti	1.463E-4	2.274E-5	2.669E-4	---	---	---
<sup>7</sup> Li	2.823E-4	5.222E-4	5.645E-5	---	---	---
<sup>6</sup> Li	2.540E-3	4.699E-3	5.081E-4	---	---	---
Mn	---	---	---	1.907E-2	---	---
H	---	---	---	6.700E-3	---	---
O	---	---	---	3.350E-3	9.740E-6	---
N	---	---	---	---	3.640E-5	---
Cu	---	---	---	---	---	8.450E-2

\*Read 2.749e-2 as 2.749·10<sup>-10</sup> atom/barn-cm.

Table A.3. Fifty-group Structure (ORNL).

Group	Energy (MeV)	Lethargy	Spectrum	FRBF Spectrum
1	1.568e+7*	-5.00e-1	3.124e-1	1.069e-2
2	1.492e+7	-4.00e-1	2.135e+0	1.563e+0
3	1.455e+7	-3.75e-1	6.420e+0	2.763e+0
4	1.419e+7	-3.50e-1	8.325e+0	2.665e+0
5	1.384e+7	-3.25e-1	4.787e-1	2.476e+0
6	1.350e+7	-3.00e-1	1.409e+0	5.220e-1
7	1.252e+7	-2.25e-1	9.205e-4	0.000
8	1.221e+7	-2.00e-1	3.682e-3	0.000
9	1.105e+7	-1.00e-1	3.682e-3	0.000
10	1.000e+7	0.00e+0	4.882e-3	0.000
11	9.048e+6	1.00e-1	1.234e-3	0.000
12	8.187e+6	2.00e-1	1.234e-2	0.000
13	7.408e+6	3.00e-1	1.801e-2	0.000
14	6.703e+6	4.00e-1	2.500e-2	0.000
15	6.065e+6	5.00e-1	3.315e-2	0.000
16	5.488e+6	6.00e-1	4.221e-2	0.000
17	4.966e+6	7.00e-1	5.129e-2	0.000
18	4.493e+6	8.00e-1	6.143e-2	0.000
19	4.066e+6	9.00e-1	7.069e-2	0.000
20	3.679e+6	1.00e+0	7.912e-2	0.000
21	3.329e+6	1.10e+0	8.368e-2	0.000
22	3.012e+6	1.20e+0	9.220e-2	0.000
23	2.725e+6	1.30e+0	9.643e-2	0.000
24	2.466e+6	1.40e+0	9.900e-2	0.000
25	2.231e+6	1.50e+0	9.994e-2	0.000
26	2.019e+6	1.60e+0	1.000e-1	0.000
27	1.827e+6	1.70e+0	1.000e-1	0.000
28	1.653e+6	1.80e+0	1.000e-1	0.000
29	1.496e+6	1.90e+0	1.000e-1	0.000
30	1.353e+6	2.00e+0	2.000e-1	0.000
31	1.108e+6	2.20e+0	4.000e-1	0.000
32	7.427e+5	2.60e+0	3.000e-1	0.000
33	5.502e+5	2.90e+0	3.000e-1	0.000
34	4.076e+5	3.20e+0	3.000e-1	0.000
35	3.020e+5	3.50e+0	2.500e-2	0.000

\*Read 1.568e+7 as  $1.568 \cdot 10^{10}$ .

Table A.3, Continued.

Group	Energy (MeV)	Lethargy	Spectrum	FRBF Spectrum
36	2.945e+5	3.53e+0	7.500e-2	0.000
37	2.732e+5	3.60e+0	1.000e-1	0.000
38	2.472e+5	3.70e+0	1.000e-1	0.000
39	2.237e+5	3.80e+0	1.000e-1	0.000
40	2.042e+5	3.90e+0	1.000e-1	0.000
41	1.832e+5	4.00e+0	1.000e-1	0.000
42	1.657e+5	4.10e+0	1.000e-1	0.000
43	1.500e+5	4.20e+0	8.000e-1	0.000
44	6.738e+4	5.00e+0	1.000e-1	0.000
45	2.479e+4	6.00e+0	2.000e+0	0.000
46	3.355e+3	8.00e+0	2.000e+0	0.000
47	4.540e+2	1.00e+1	2.000e+0	0.000
48	6.142e+1	1.20e+1	2.000e+0	0.000
49	8.315e+0	1.40e+1	3.581e+3	0.000
50	1.000e-1	1.84e+1	3.161e+4	0.000

Table A.4. Forty-one-group Structure (Purdue).

Group	Energy (MeV)	Lethargy	Spectrum	FRBF Spectrum
1	1.568e+7*	-5.00e-1	2.447e+0	1.561e+0
2	1.455e+7	-3.75e-1	6.420e+0	2.763e+0
3	1.419e+7	-3.50e-1	8.325e+0	2.665e+0
4	1.384e+7	-3.25e-1	2.787e-1	2.476e+0
5	1.350e+7	-3.00e-1	1.409e+0	5.220e-1
6	1.252e+7	-2.25e-1	8.285e-3	0.000
7	1.000e+7	0.00e+0	6.822e-2	0.000
8	6.065e+6	5.00e-1	2.593e-1	0.000
9	3.679e+6	1.00e+0	2.531e-1	0.000
10	2.231e+6	1.50e+0	5.000e-1	0.000
11	1.353e+6	2.00e+0	5.000e-1	0.000
12	8.208e+5	2.50e+0	6.000e-1	0.000
13	4.505e+5	3.10e+0	4.000e-1	0.000
14	3.020e+5	3.50e+0	5.000e-1	0.000
15	1.832e+5	4.00e+0	5.000e-1	0.000
16	1.111e+5	4.50e+0	5.000e-1	0.000
17	6.738e+4	5.00e+0	5.000e-1	0.000
18	4.087e+4	5.50e+0	5.000e-1	0.000
19	2.479e+4	6.00e+0	5.000e-1	0.000
20	1.503e+4	6.50e+0	5.000e-1	0.000
21	9.119e+3	7.00e+0	5.000e-1	0.000
22	5.531e+3	7.50e+0	5.000e-1	0.000
23	3.355e+3	8.00e+0	5.000e-1	0.000
24	2.035e+3	8.50e+0	5.000e-1	0.000
25	1.234e+3	9.00e+0	5.000e-1	0.000
26	7.485e+2	9.50e+0	5.000e-1	0.000
27	4.540e+2	1.00e+1	5.000e-1	0.000
28	2.754e+2	1.05e+1	5.000e-1	0.000
29	1.670e+2	1.10e+1	5.000e-1	0.000
30	1.013e+1	1.15e+1	5.000e-1	0.000
31	6.144e+1	1.20e+1	5.000e-1	0.000
32	3.727e+1	1.25e+1	5.000e-1	0.000
33	2.260e+1	1.30e+1	5.000e-1	0.000
34	1.371e+1	1.35e+1	5.000e-1	0.000
35	8.315e+0	1.40e+1	5.000e-1	0.000
36	5.043e+0	1.45e+1	5.000e-1	0.000
37	3.059e+0	1.50e+1	5.000e-1	0.000
38	1.855e+0	1.55e+1	5.000e-1	0.000
39	1.125e+0	1.60e+1	5.000e-1	0.000
40	6.826e-1	1.65e+1	5.000e-1	0.000
41	4.140e+0	1.70e+1	3.519e+4	0.000

\*Read 1.568e+7 as 1.568 · 10<sup>10</sup>.

### Appendix B. Angle-energy Correlation Code

The following program reads  $dE/dx$  data for Ti and T and neutron-production cross sections for the  $T(d,n)^4He$  reaction. It then computes the combined energy loss rates for TiT and does a numerical integration of the slowing down equation. It uses an angle-energy relation based upon reaction kinematics to produce a table of energy group vs emission angle of d-T-generated neutrons. It also predicts the neutron yield per ampere of d-beam current. This code is derived from ORNL/TM-9251; however, the integration method has been changed to better approximate the results in the forward and backward directions.

```

program angen3
dimension cdedx(300), sig(300), tdedx(300), ed(300)
dimension en(300,40), ea(300,40), prob(300,40)
dimension egrd(7), angs(17), sprob(7,17), lang(17)
dimension theta(37), dedx(300), sumr(17)

c
real md, mt, mn, ma, mr
data nou,ntty /6,6/
data md, mt, mn, ma /2.014102,3.016030,1.008665,4.002603/

c
data q, den, xn, tden /17.589,8.47e-02,1.75,4.280/
data pi, fac, ati, at /3.14159,1000.,48.,3./
data krts, nang /1, 36/

c
input energy, cross section, and de/dx for Ti and T
energy values must be equally spaced
ehi below is energy of deuteron beam

c
read #, ehi
write #, ehi
npts = 1
do 10 i=1,200
    read (5,98990) ed(i), sig(i), cdedx(i), tdedx(i)
    if (ed(i).ge.ehi) go to 11

c
npts = npts + 1
if (ed(npts).gt.ehi) then ehi=ed(npts)
dele=ed(2)-ed(1)
print #, 'npts=',npts, ' ed(',npts,') = ',ed(npts)

c
number of angles and intervals for output
dimension of angs is one greater than nnang

c
data nnang /16/
data angs /0.,20.,30.,40.,50.,60.,70.,80.,90.,
1 100.,110.,120.,130.,140.,150.,160.,180./

c
number of energy groups and intervals for output
dimension of egrd is one greater than neni

```

```

data nentr /7/
nen1 = nentr - 1
data egrd /12.52,13.50,13.84,14.19,14.55,14.92,15.68/

c
fti=ati/(ati+at*xn)
ft=at*xn/(ati+at*xn)
write (nou, 99989)
print *, 'fti = ',fti, ' ft = ',ft
c calculate combined stopping power in kev/gm/cm**2
c then change to MeV/cm
do 50 i=1,npts
dedx(i)=fac*(cdedx(i)*fti+tdedx(i)*ft)
dedx(i)=dedx(i)*tden

50 continue
c
sump=0.
sumf=0.
summ=0.
sumt=0.
c set up angles in radians
c
c
theta(1) = 2.5*pi/180.
deth = 2.*theta(1)
do 80 i=2,nang
theta(i) = theta(i-1)+deth
80 continue
c
c set up angle/energy probabilities
c i is angle index, j is energy index
c
mr = 1./((md+mt)/(ma+mn))
nptm1=npts - 1
do 100 i=1,nang
do 90 j=1,nptm1
eda=ed(j)-dele/2.
siga=(sig(j)+sig(j+1))/2
dedxa=(dedx(j)+dedx(j+1))/2
et = eda+q

```

```

a = mr*md*ma*eda/et
b = mr*md*mn*eda/et
c = mr*mt*mn*(1.+md*q/mt/et)
d = mr*mt*ma*(1.+md*q/mt/et)
if (b.gt.d) write (nou,99995) b, d, i, j
x = cos(theta(i))
x2 = cos(theta(i)+deth/2.)
x1 = cos(theta(i)-deth/2.)
y = sin(theta(i))
y2 = sin(theta(i)+deth/2.)
y1 = sin(theta(i)-deth/2.)
en(j, i) = et*b*(x+sqrt(d/b-y**2))*2
ea(j, i) = et-en(j, i)
denom = et*sqrt(a*c)*sqrt(d/b-y**2)
sf = en(j, i)/denom
prob(j, i) = sf*sig/dedx*dele*(x1-x2)
        continue
90      continue
100
c
c calculate reaction integral
c using Weddle's rule
c
c in=((npts-1)/6)
c in=npts-in#6
do 110 j=2+in,npts-5,6
    sumf = sumf+
        5.*sig(j)/dedx(j) +
        1.*sig(j+1)/dedx(j+1) +
        6.*sig(j+2)/dedx(j+2) +
        1.*sig(j+3)/dedx(j+3) +
        5.*sig(j+4)/dedx(j+4) +
        2.*sig(j+5)/dedx(j+5)
110      continue
sumf=(sumf+sig(1)/dedx(1)-sig(npts)/dedx(npts))*3.*dele/10.
        #den*4.*pi*6.25e+15
write (nou, 99989)
print #, '4pi yield per milliamp deuterons = ', sumf
c
c normalize angle/energy probabilities to 1
c i is angle index, j is energy index

```

```

c
do 130 i = 1, nang
  do 120 j = 1, nptm1
    sump = sump+prob(j, i)
  continue
120 continue
130 do 300 i=1, nang
  do 140 j=1, nptm1
    prob(j, i) = prob(j, i)/sump
    summ = summ+prob(j, i)
  continue
140 continue
300 do 160 i=1, nang
  theta(i) = theta(i)*180./pi
  theta is now in degrees
c
  if (krts.eq.1) goto 160
  write (nou, 99994) (ed(j), en(j, i), ea(j, i), prob(j, i), j=1, nptm1)
  continue
160
c
c
c
c
  sum probabilities into output angle bins
  ith = 1
  do 240 ic=1, nnang
    do 180 i=1, nen1
      sprob(i, ic) = 0.
    continue
  sumr(ic) = 0.
  do 220 n=ith, nang
    if (theta(n).lt.angs(ic)) goto 220
    if (theta(n).gt.angs(ic) .and.
      theta(n).lt.angs(ic+1)) goto 190
    goto 230
  continue
180 do 210 j=1, nen1
  continue
190 do 200 i=1, nptm1
  do 210 j=1, nen1
    do 200 i=1, nptm1
      if (en(i, n).ge.egr(j) .and. en(i, n).le.egr(j+1))
        sprob(j, ic) = sprob(j, ic)+prob(i, n)
    continue
  continue
200

```

```

210          continue
220          continue
230          continue
240          continue
          ihi = ehi*1000.
          write (nou,99993) ihi
          write (nou,99992)
          np1 = nnang+1
          do 250 ic=1,np1
             iangs(ic) = angs(ic)
250          continue
          write (nou,99991)
          nangd2=nnang/2
          write (nou,99919) (iangs(ic),iangs(ic+1),ic=1,nangd2)
          do 260 k1=1,nen1
             write (nou,99990) egrd(k1), egrd(k1+1),
                (sprob(k1,k2),k2=1,nangd2)
          *
260          continue
          nangd2p1=nangd2+1
          write (nou,99919) (iangs(ic),iangs(ic+1),ic=nangd2p1,nnang)
          do 265 k1=1,nen1
             write (nou,99990) egrd(k1), egrd(k1+1),
                (sprob(k1,k2),k2=nangd2p1,nnang)
          *
265          continue
          do 280 ic=1,nnang
             do 270 is=1,nen1
                sumr(ic) = sumr(ic)+sprob(is,ic)
             continue
             sumt = sumt + sumr(ic)
270          continue
280          write (nou,99988) (sumr(k1),k1=1,nnang)
          print *, 'sum of probabilities is ',sumt
          write (nou,99987)
          stop
          format (1h , 15h b .gt. d b = , f10.5, 5h d = , f10.5,
             3x, 13, 3x, i3)
          format (3(f10.5, 2x), e15.6)
          format (//59x, 18hdeuteron energy = , i3, 4h KeV)
          format (x, 12henergy range, 42x, 26hprobability by angle inter,
             9hval (deg))
          *
99995
          *
99994
99993
99992
          *

```

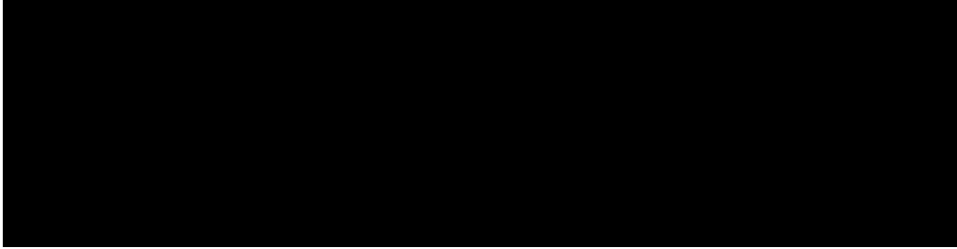
```
99991 format (5x, 5h(MeV))
99919 format (14x, 5hangle, 2x, 10(i3, 1h-, i3, 4x))
99990 format (/x,Opf6.2,1h-,f5.2, 5x, 1p10e11.3)
99989 format (/)
99988 format (/5x, 12htotal prob. ,x, 1p10e11.3./)
99987 format (/8x, 20h normal termination ,/)
99980 format (5e13.3)
99979 format (/5x,7hneutron,7x,7hcross ,4x,9h(de/dx)Ti,4x,
*      8h(de/dx)T,5x,10h(de/dx)TiT)
99978 format (4x,7h energy,7x,7hsection)
99977 format (4x,7h (MeV),/)
98990 format (x,4e14.4)
end
```

VITA

## VITA

**Name:** Denis E. Beller

PII Redacted



**Education:** BSChE, University of Colorado, May 1976  
MSNE, USAF Inst. of Technology, March 1981  
Ph.D., Purdue University, May 1986

**Memberships:** Tau Beta Pi, American Nuclear  
Society, AFIT Association of Graduates